Effectiveness of Recycled Plastic Pin for Improving Bearing Capacity of Embankment over Soft Soil

by

MD AZIJUL ISLAM

DISSERTATION

Presented to the Faculty of the Graduate School of

The University of Texas at Arlington

In Partial Fulfillment for the

Requirements of the Degree of

DOCTOR OF PHILOSOPHY

THE UNIVERSITY OF TEXAS AT ARLINGTON

AUGUST 2021

ACKNOWLEDGEMENTS

I would like to express my sincere gratitude to my supervising professor, Dr. Sahadat Hossain, for his constant guidance, support, and encouragement throughout this research. He generously shared his experience and knowledge with me and provided the motivation and "push" that I needed to complete my research and dissertation. His patience, constructive comments and valuable suggestions helped me to present myself as a good researcher. I am grateful for the opportunity to work under him and for having the freedom to work at my own pace. I could asked for a better advisor.

I want to extend my gratitude to Dr. Xinbao Yu, Dr. Seyed Mohsen Shahandashti, and Dr. Muhammad N. Huda for devoting their time as committee members and for their constructive feedbacks and suggestions. I am honored and grateful to have such incredible teachers at The University of Texas at Arlington.

I would also like to thank the Texas Department of Transportation (TxDOT) for funding this research. A special thanks goes to the Hunter Ferrell Landfill in Irving for their immense help with the field activities.

I would like to specially thank all the SWIS members for their support during my studies. The fieldworks would not have been possible without the invaluable support of Dr. Prabesh Bhandari and Ms. Faria Fahim Badhon. I am very thankful to the unwavering support and assistance of Dr. Nur Basit Zaman, Arif Mohammad Aziz, Md Aminul Islam, Dr. Anuja Sapkota, Dr. Jobair Bin Alam and Dr. Asif Ahmed. It has truly been a life-changing experience to be a part of this team.

Finally, and most importantly, I would like to wholeheartedly thank my wife Ms. Tahsina Islam for her constant cooperation, patience, sacrifice and unconditional support throughout my studies.

Furthermore, I wish to acknowledge my parents and brother. Their unwavering trust, support, love and encouragement helped me to fulfill my dream to pursue a doctoral degree. No words can describe my gratitude towards them. I am grateful towards all my friends here in Arlington who made this journey worthwhile. Thanks to almighty Allah for granting me with the strength, and patience that I needed throughout my research work.

August 9, 2021

ABSTRACT

EFFECTIVENESS OF RECYCLED PLASTIC PIN FOR IMPROVING BEARING CAPACITY OF EMBANKMENT OVER SOFT SOIL

Md Azijul Islam

The University of Texas at Arlington, 2021

Supervising Professor: Dr. MD Sahadat Hossain

Construction of embankment over soft foundation soils is incredibly a challenging task due to the risk of bearing failure and excessive settlement of foundation soil. Most of the available conventional methods for addressing these problems are either expensive or time-consuming or both. Therefore, research has been striving to develop a sustainable alternative to the current conventional methods. A noble approach to improve the soft foundation soil could be the use of Recycled Plastic Pins (RPP) in combination with geosynthetics. The load transfer efficiency of a geosynthetic-reinforced and RPP supported embankment is influenced by interactions among embankment fill, geosynthetics, and foundation soil.

The objective of this study is to investigate the effectiveness of Recycled Plastic Pins (RPP) for controlling ground settlement of soft foundation soil. Two field test sections (6 m × 7.5 m) were constructed over soft soil; one was left unreinforced to use it as a control section, and the other section was reinforced with RPPs. A Load Transfer Platform (LTP), composed of Recycled Crushed Concrete Aggregate (RCCA), sandwiched between two geogrid layers, was placed above the RPPs for transferring load from embankment onto the RPPs. Vertical pressures, settlements, and pore water pressures were monitored. After 260 days, a maximum settlement of 52 mm was observed for the control section, whereas, for the reinforced section, it was 23 mm. Excess pore

pressure dissipated faster in the control section. The measured data indicated that the RPP supported a significant percentage of the embankment load. The in-situ measurements have proven the effectiveness of RPPs in combination with LTP in reducing settlement.

In the analytical study, an integrated method based on force equilibrium, soil arching, and stress distribution is developed to calculate differential settlement and stresses on RPPs and adjacent soil in between RPPs. The load transfer mechanism accounted for soil arching and tensioned membrane effects were comprehensively studied. The proposed analytical method was validated with measured results from a field study. Furthermore, the method was also compared with other field study and design methods. A parametric study is also conducted to observe the effects of influential factors such as RPP size, spacing, tensile stiffness of geosynthetics, and friction angle of aggregates used in LTP. The results indicate that more efficiency of load transfer can be achieved with larger size and closer spacing of RPPs. The tensile stiffness of geosynthetic also has a greater influence on the load transfer mechanism.

Furthermore, a numerical investigation was conducted using finite element software PLAXIS 2D. The model was calibrated against the field measured data in the context of settlement and pressure variations. The performance of the RPP supported embankment was evaluated with maximum consolidation settlement, differential settlement, and soil arching effect. An extensive parametric study was performed to evaluate the effect of RPP size, and spacing, load transfer platform, stiffness of geosynthetics, and shear strength of embankment fill. The present method can be applied for any embankment construction over soft soil, bridge approaches, and widening of a highway where the foundation soil is unsuitable for regular construction.

TABLE OF CONTENTS

LIST OF ILLUSTRATIONS

LIST OF TABLES

CHAPTER 1

INTRODUCTION

1.1 Background

In the past few decades, embankments have become more frequently used to support highways and railways; however, the number of sites with suitable soil conditions has declined (Zhunag and Cui 2016). Therefore, more and more embankments have been built on land which was previously unsuitable. Construction of embankments on soft foundations often encounters possible bearing capacity failure, excessive settlement, and slope instability (Xu et al. 2016). Construction time and time required for settlement stabilization are also important challenges for construction over soft foundations. Certain techniques must be used for improving the soil foundation to enhance the stability of the embankment and eliminate the problems associated with bearing failure and settlement (Han and Gabr 2002). The conventional approaches for improving soft soil condition are expensive and time-consuming. Therefore, studies have been striving to develop a sustainable alternative to the current conventional methods. Furthermore, there are some strict requirements regarding total and differential settlement (often less than 25 mm) for the highway embankments or the approach embankments near bridges. Due to these strict requirements, piles are often used to support embankments.

The use of piles in conjunction with geosynthetics is an effective improvement technique for soft soil conditions. The benefits associated with the use of pile-supported earth platforms are rapid construction without preloading, small lateral deformation, and easily controlled settlements (Han and Gabr 2002). Different types of piles can be used, such as concrete piles, drilled shafts, vibro-

concrete columns, controlled modulus columns, rammed aggregate pier, sand compaction pile, micropile, and Recycled Plastic Pins (RPP). Chen et al. (2010) reported three case studies of pile-supported embankments in the eastern coastal region of China. Y-shaped cast-in-place piles were used for the improvement of the pavement section. The differential settlement, earth pressure, and pore water pressure were monitored to evaluate the efficacy of the pile-supported embankment technology. Hong et al. (2014) examined the behavior of embankments with pile-supported beam foundations at full scale. It was concluded that end-bearing piles with beam groups at smaller center-to-center distance could considerably reduce settlements of piled embankments. Zhao et al. (2019) conducted a case study of a widened highway embankment project which was supported by prestressed tubular concrete (PTC) piles and geogrids. The instrumentation data indicated that a large portion of the embankment loads were supported by PTC piles. Among the available methods of ground improvement, RPP is a new technological innovation. RPP was first used as a slope stabilization technique on highways in Missouri and Iowa (Hossain et al. 2017). Now a days, Many other states in USA are using RPP to stabilize slopes because it is cost-effective (Khan et al. 2016; Hossain et al. 2017).

RPP is manufactured primarily from recycled plastics. Some other materials like polymers, sawdust, and fly ash can also be used with recycled plastics (Chen et al. 2007). RPPs are made of lightweight material and are less susceptible to chemical and biological degradation than other structural elements. Typically, RPP is composed of 55 - 70% high-density polyethylene (HDPE), 5 - 10% low-density polyethylene, and a small percentage of polystyrene and polypropylene (McLaren 1995). Moreover, additives, including fiberglass and wood fibers, are added during the manufacturing process to improve the modulus of elasticity of RPP (Breslin et al. 1998). Approximately 600 mineral water/soda bottles are used for one 3 m long (10 cm × 10 cm) RPP

(Hossain et al. 2017). Compressive strengths of recycled plastic members ranged from 11 MPa to 21 MPa with no cross-sectional area correction, tested at a nominal strain rate of 0.006 mm/mm/min (Bowders et al. 2003). The compression moduli determined at 1% percent strain varied from 552 MPa to 1310 MPa (Bowders et al. 2003).

As an added benefit, geosynthetics over piles also enhance load transfer efficiency and reduce the total as well as differential settlement of structures (Abdullah and Edil 2007; Han and Gabr 2002). For the purpose of transferring the load to more competent soil deposits, a geosynthetic-reinforced load transfer platform (LTP) can be constructed immediately above the piles. The platform is typically made of ballast, gravel, or hydraulically bound fine-grained soil. Geosynthetics are often placed on this platform. The function of geosynthetic reinforcement in LTP is to retransmit the surcharge load apportioned to the subsoil to the piles and to reduce the lateral spreading of the embankment (Abdullah and Edil 2007). Due to soil arching mobilized by pile embankments, major embankment loads can be transferred to a more rigid layer below soft ground through LTP and piles (Oh and Shin 2007; Watchman et al. 2010; Filz et al. 2012;). Several researchers have studied load transfer platforms theoretically and numerically (Han and Gabr 2002; Michalowski et al. 2018; Zhang et al. 2020). Han and Gabr (2002) conducted a numerical study in order to investigate the influences of Geogrid Reinforced Pile Supported (GRPS) embankment design parameters on the performance of embankments. The authors observed that maximum tensile force in geosynthetics and stress concentration ratio (SCR) increase with the height of embankment fill, the tensile stiffness of geosynthetics, and the elastic modulus of pile material. Demir et al. (2013) investigated the effectiveness of geogrid reinforced soil footings using large scale field tests. It was found that the compacted granular fills with two layers of geogrid improved the bearing capacity of the foundation, approximately 130% and 70% at large and low settlements,

respectively. An experimental study was conducted by Briancon and Simon (2012) using pile-supported embankments on soft soil. The authors found significant improvement in the load transfer mechanism for a granular platform with geosynthetics. In comparison with using only one geotextile layer, the two geogrid layers provide a more uniform stress distribution on top of the platform.

1.2 PROBLEM STATEMENT

Embankments over soft soil are prone to settlement and bearing capacity failure. Embankments built on soft foundation soil can be subject to significant stresses. These stresses can result in potential bearing failure, excessive settlement, and local or global stability problems (Liu et al. 2007). Differential settlement, which is fairly frequent in foundation cases involving soft soils, makes the failure much more dangerous (Han and Gabr 2002). In Texas, problematic soil is predominant because of soft clay and a high groundwater table. Texas Department of Transportation (TxDOT) faces significant construction, repair and maintenance challenges every year. Traditionally, bearing capacity is improved in the following ways: removal and replacement of the unsuitable materials, lime or cement stabilization, jet grouting, dynamic compaction, geopier, sand compaction pile, stone column, micropile, pile supported embankment etc. However, in most of the cases the conventional techniques are costly and time consuming.

Therefore, an innovative and cost-effective solution of controlling excessive settlement of embankment over soft soil is needed. A possible solution could be the use of RPPs in combination with LTP. RPPs have proven to be an effective measure for the stabilization of shallow slope failure (Khan et al. 2015). In addition, tests conducted on RPP showed that it has considerable load carrying capacity (Bowders et al. 2003). In combination of geosynthetics as load transfer platform,

RPPs might prove to be efficient in supporting structures, resulting in the reduction of significant part of total and differential settlement. RPP is a lightweight material, which is less susceptible to chemical and biological attack, resistant to moisture, required almost no maintenance. Apart from the structural benefits, the use of RPP reduces the waste volume entering the landfill and provides additional market for recycled plastic (Loehr et al. 2000).

Even though RPP has been used for many years for slope stabilization projects, is often reported in the literature, the lack of widely accepted design procedure remains one of the biggest barriers limiting its wide use such as for improving bearing capacity of soft soil. Furthermore, the mechanism of load transfer depends on multiple factors, such as embankment height, the elastic modulus of piles, stiffness of geosynthetics, etc. The influence of the aforementioned factors is intertwined and complex, especially for RPP supported embankments. There are very limited literatures for investigating the behavior and performance of RPP supported embankments (Zaman 2019). It is necessary for engineers to understand the behavior of RPP supported embankment to carry out safe and economical design and construction. Moreover, it is important to evaluate the effect of different parameters such as the length, spacing and size of RPP for effective application in reducing settlement of foundation soil.

1.3 Research Objective

The main objective of the current study is to evaluate the effect of RPP to improve the soft foundation soil for embankment construction. As a part of this research objective, settlement and bearing capacity will be evaluated for RPP supported embankment. The specific tasks to achieve the objective of the study include:

1. Site Investigation and selection for field scale test section location.

2. Development of preliminary design for the test sections.
3. Field installation of RPPs and construction of test sections.
4. Instrumentation of the test sections for performance evaluation.
5. Regular performance monitoring of the constructed test sections.
6. Analysis of the field data for evaluating the effectiveness of using RPPs.
7. Development of a design methodology for embankment construction with RPP over soft soil.

1.4 Dissertation Organization

Chapter 1 describes the background, problem statement, and objectives of the research. It's the total dissertation "in a nutshell". Chapter 1 is followed by an extensive literature review presented in Chapter 2. The rest of the dissertation is divided into three papers. The first paper describes a field scale study of the performance evaluation of RPP supported embankment. It entails the real time monitoring of settlement and pressure variations of reinforced section and control section. The second paper focuses on the development of an analytical solution for the RPP supported embankment over soft soil. The final paper covers the in-situ findings in the numerical environment. It explains the influence of different design parameters with an extensive parametric study. These papers are followed by a summary and conclusions.

CHAPTER 2

LITERATURE REVIEW

2.1 Introduction

Engineers often have trouble with structures constructed over soils that do not have enough bearing and shearing capacity. Construction of structures on sites with problematic soil conditions is not recommended most of the time. Sometimes, the only option is to replace soil with adequate fill material despite its high cost. There are several methods available for improving the bearing capacity of embankment foundation soils. The present chapter provides comprehensive analysis of the literature that addresses the problem associated with soft foundation soils and the conventional improvement techniques.

2.2 Background

In many parts of the world, highways and runways are built over soft soils, which can pose a significant problem to civil engineers. Generally, to construct highways or runways on soft soils, the soft soil is removed and replaced with a stronger material, such as crushed rock. As a result of the high cost of replacing soft soils, related administrations often evaluate alternative construction methods (Ozdemir, 2016).

It is extremely important to understand the site soil conditions before constructing any type of structure such as buildings, bridges, highways, or dams. Construction sites usually do not have perfect soil conditions for supporting this kind of structure. According to a TxDOT memorandum (2013), for sites with problematic foundation soils, it is sometimes more cost-effective to provide a ground improvement plan to allow the safe use of structure rather than altering the type of the

structure. Ground improvement plans can vary from the simple remove and re-compact or replace material to the complex, i.e, the use of geopiers, stone columns or geogrid reinforced pads.

Various techniques have been reported in the literature, some of which have even been patented, with the possibility of using a blend of several techniques at an individual site. This study aims to increase the bearing capacity of soils significantly. This can be accomplished by modifying the soil properties such as cohesion (c), stiffness, or unit weight (γ). Usually an increase in unit weight (or density) is accompanied by an increase in either c or both (assuming the soil is cohesive). According to Bowles (1988), compaction always can reduce the void ration and increase the density, thus reduces long-term settlements. In general, particle packing reduces "immediate" settlements by increasing stress-strain modulus.

2.3 Characteristics of soft soil

In general, soft clays are sedimentary deposits that have been deposited recently, usually by rivers, lakes, or seas. Deposits of this type often have bedding and laminations, intercalated with sand and silt seams, and are subjected to repeated drying and wetting near the surface.

2.3.1 Geotechnical characteristics of soft soil

A soft clay is a fine-grained soil characterized by a moderate to high clay fraction and high plasticity. They have a high compressibility and a low shear strength (generally less than 25 Kpa). Typical characteristics of soft clay are as follows:

(i) Predominantly fined grained i.e., more than 50% of soil passing through #200 sieve

(ii) High liquid limit & plastic limit values

(iii) High natural moisture content and even higher than the liquid limit

(iv) Low material permeability but the overall permeability can be more

(v) Low shear strength which usually varies with depth. Two types of soft soil can be classified according to their undrained strength:

- Very soft clay (undrained strength less than 12 kPa)
- Soft clay (undrained strength less than 25 kPa)

(vi) Highly compressible, organic content increases the compressibility

2.3.2 Shear strength characteristics

Normal consolidated clays have an almost linear increase in shear strength with depth. Skempton (1953) proposed the following formula for the relationship between the ratio of undrained shear strength to overburden pressure and the effective overburden pressure:

$$\frac{S_u}{\sigma_o} = 0.11 + 0.0037\, I_p \qquad (2.1)$$

Where, S_u = Undrained shear strength of soil; σ_o = Effective overburden pressure, I_p = Plasticity Index.

2.3.3 Problems associated with soft clay

It is well known that soft clays are problematic soils. Soft soil can be defined as a special type of soil which is susceptible to failure or cause excessive settlement when superstructure is constructed over it. There are three common characteristics of soft clays: high compressibility, poor bearing capacity, and a long consolidation time. Ground water table plays an important role for the lows shear strength of the soft clay. Above the ground water table, soil get moist due to the capillary action. Thus, the unsaturated condition of the soil above ground water table need to be investigated for understanding the behavior of all the soil layers (Ahmed and Islam 2020). There are several

issues to be addressed when studying soft clays, from field investigation to their modeling behavior. Soft soil can be classified into two categories:

(i) Saturated clays and fine silts (alluvium), Maine clays

(ii) Loose sand (especially when under water table)

2.4 Modes of failure of embankment constructed over soft/weak soil

Embankments generally fail by one of the following mechanisms:

a) Bearing Capacity Failure: Based on the failure of bearing capacity, collapse height (H_{max}) of the embankment is calculated (Figure 2.1a).

b) Rotational Failure: If the embankment height is less than H_{Max}, rotation failure occurs. The failure occurs along an arc that passes through the foundation soil and embankment (Figure 2.1b).

c) Sliding Failure: Sliding failure occurs when slope portion ABC slides laterally as a rigid body due to active pressure acting on it. Failure occurs when $P_1 > P_2$ (Figure 2.1c).

d) Lateral Spreading Failure: In this failure, soil wedge A B' C slides along B' C due to the active pressure P_1' acting on the face A' B'. Failure occur when $P_1' > P_2'$ (Figure 2.1d).

e) Foundation Soil Squeezing Failure: In layered soft soils, a layer with a lower strength can form a preferential horizontal sliding plane. This mechanism may be favored where stiff crest overlies soft soil or where the thickness of soft soil is small. The failure will occur when total resisting force acting on the block is less than the disturbing force i.e. $F_p + T_1 + T_2 < F_a$ (Figure 2.1e).

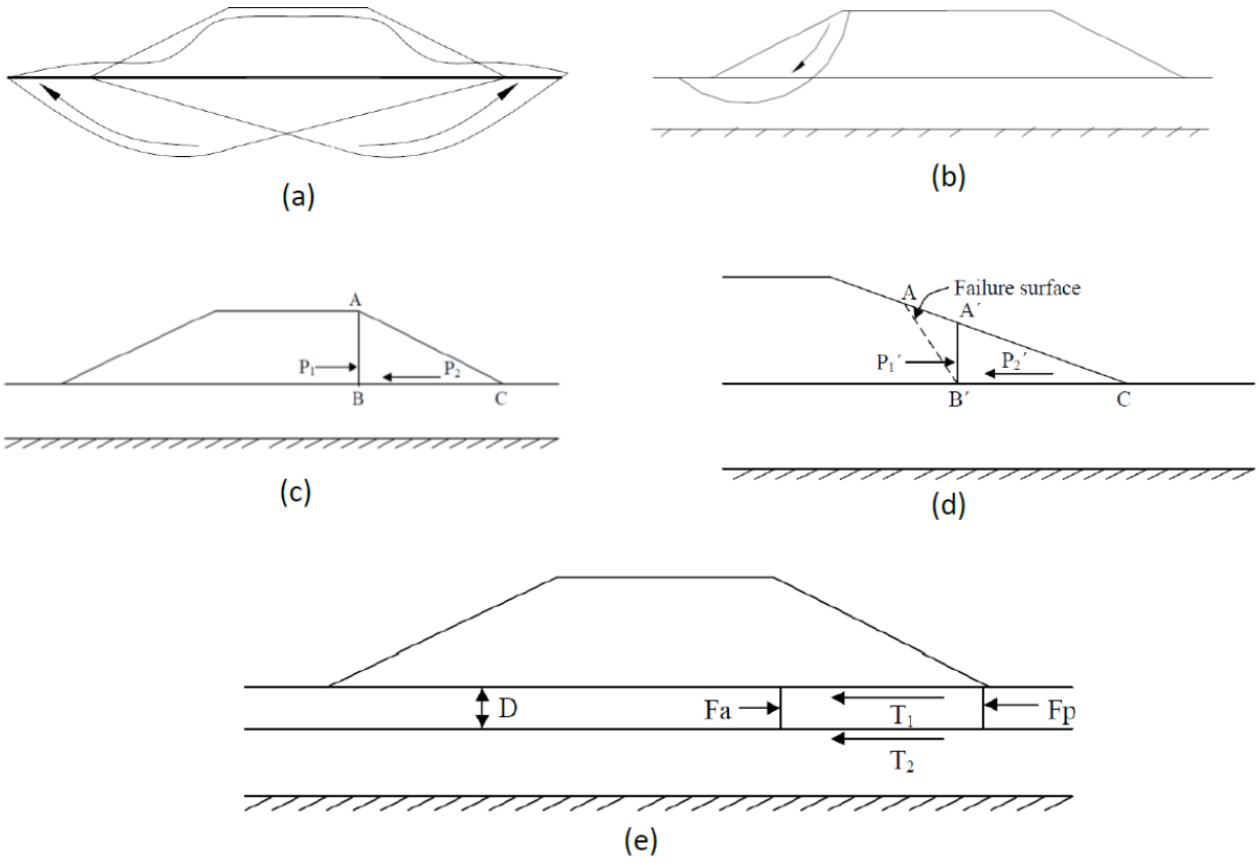

Figure 2.1: Modes of embankment failure: (a) Bearing capacity failure; (b) rotational failure; (c) sliding failure; (d) spreading failure; (e) foundation soil squeezing failure (Zaman, 2019)

2.4.1 Bearing capacity failure

A lot of earth dams and highway embankments are constructed on soft clay. The stability of an embankment built on soft clays is often identified as a problem related to bearing capacity. Vertical loads acting on the foundation surface are combined with an outward shear stress generated by horizontal stresses in the embankment fill. A shear stress in the outward direction reduces the bearing capacity of the foundation soil. A base reinforcement can enhance stability by increasing the inward shear stress on the foundation surface. The soil is displaced sideways from beneath the

embankment at the onset of failure, but the embankment itself does not spread due to the reinforcement.

In many dams and embankments, the materials used for construction are brittle enough to develop tension cracks across their height. As an alternative, they are constructed from granular materials. Typically, for a foundation, the slip circle will be almost vertical through any granular mass, so it seems reasonable that the granular mass' shear strength can be ignored.

2.4.2 Settlement of foundation soil

Applied stresses can result in changes in the volume of foundation soils. Depending on the type of soil and the applied loads, the magnitude and rate of deformation may differ. According to Terzaghi, consolidation is the result of soil reacting to loads applied to it. Consolidation tests on undisturbed samples can provide the soil parameters required for settlement prediction. In soft clay, there are three types of settlements that occur; immediate settlement, consolidation settlement, and secondary compression.

2.4.2.1 Immediate settlement

Often called undrained settlement, initial settlement occurs as a result of initially applied loads causing shear strains. Settlements occur at constant volume when clay is saturated as a result of strains from below the loaded area. For embankment over soft clay, the immediate settlement occurs with the placement of embankment load and as such of no further consequence.

2.4.2.2 Consolidation settlement

In the event of consolidation settlement, the water drains from the ground due to hydraulic gradient caused by excess pore pressure. The stress is transferred simultaneously to the soil skeleton, which

is compressed. Shear deformations are also involved in this time-dependent process, resulting in further settlement. According to Terzaghi's theory, the settlement rate for primary consolidation in one dimension can be calculated over time. The process of computing settlements and related aspects is detailed in the stage construction method as well.

2.4.2.3 Secondary settlement

The major component of the secondary compression (also known as drained creep) occurs essentially after complete dissipation of excess pore water pressures and at practically constant effective stress. As of today, no consensus has emerged on the best method of separating primary and secondary components of consolidation. The primary consolidation and secondary compression should be considered separately, even though they are occurring simultaneously. In order to estimate secondary settlements, it is necessary to examine the stress strain time relationship of the clay.

2.5 Review of existing bearing capacity improvement methods

Soft clay ground has been treated using a variety of methods. These methods include in-situ earth reinforcement and piles of various materials, including over excavation and replacement, geosynthetic reinforcement, preloading, grouting, DCM (Deep-Cement Mixing) or sand column; timber or concrete piles; micro piles, cast-in-situ piles (Figure 2.2). These improvement methods all have their advantages and disadvantages. Different types of bearing capacity improvement methods are briefly discussed here.

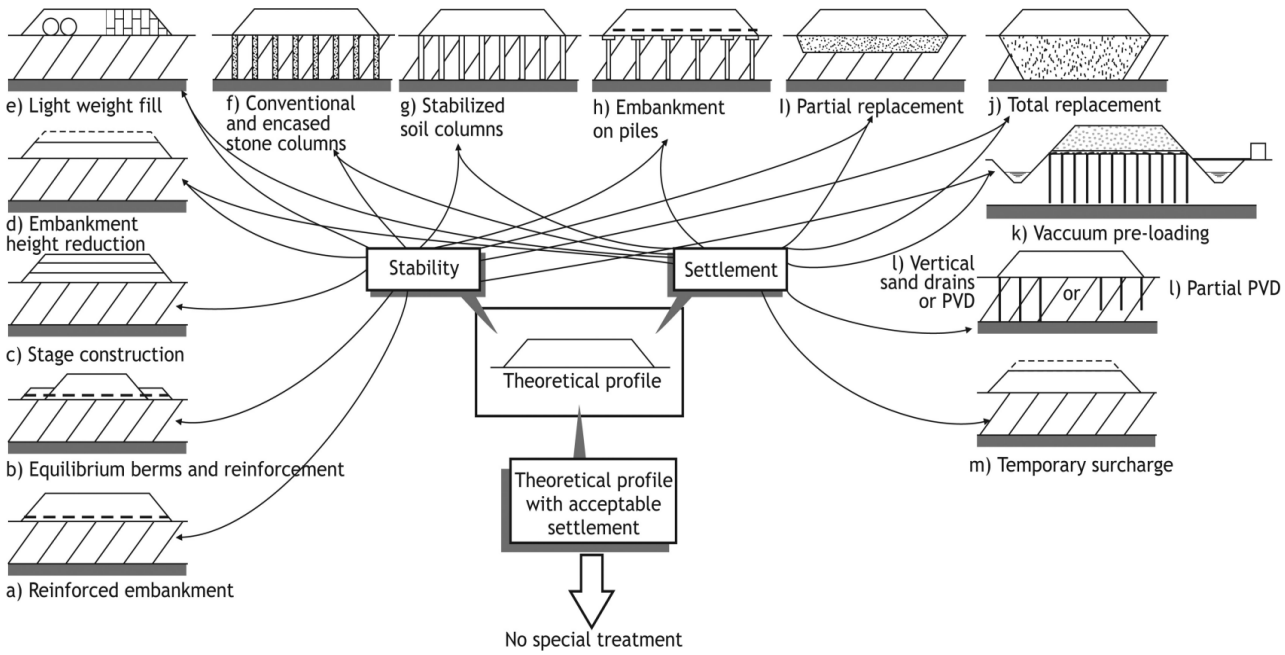

Figure 2.2: Construction methods of embankments on soft soils (Leroueil, 1997)

2.5.1 Over-excavation or replacement method

A popular method for improving soil condition is to replace it with a better material. A lightweight fill can limit or prevent the increase in load on soft soils as a result of replacing heavy fill. Likewise, this method has old roots, e.g., excavation of bad soil in peat areas and replacement with bales of horticultural peat. Geofoam, also known as expanded polystyrene (EPS), is fast becoming the preferred lightweight fill material. It is very light, only 15 to 30 kg/m^3. It is usually used in large blocks, thus can be easily trimmed on site. The use of these materials is also seen in embankment construction (Figure 2.3). It ensures fast construction without causing major disruptions to neighboring structures. Vertical walls can be achieved where space is limited by applying a facing. However, the chemical resistance of geofoam is weak. It needs to be protected against chemical spills (Barends, 2011).

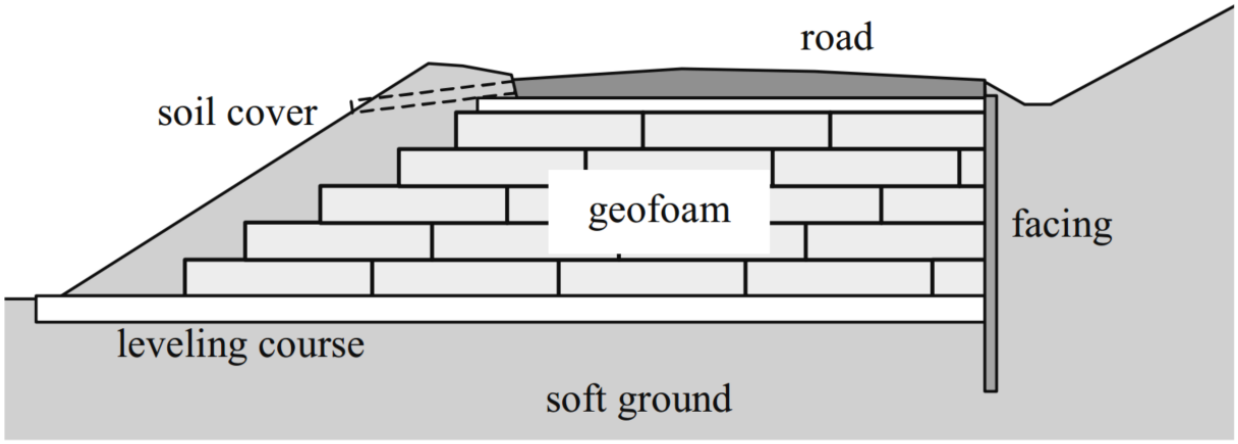

Figure 2.3: Lightweight fill (geofoam) application in an embankment slope (Barends, 2011)

2.5.2 Lime stabilization

Stabilizing soil with additives is sometimes necessary, especially for fine-grained soil (Das, 2015). With the right proportions of lime, soils can be altered or stabilized. The targets of applying lime are to (a) modify the soil, (b) accelerate the construction process and (c) enhancing the shear strength and durability of soil layer. Zhou, Yin, & Ming (2002) conducted an experimental study to evaluate the suitability of lime for the improvement of weak fly ash ground. A series of unconfined and confined compression tests were carried out in the laboratory and field to observe the improvement with time. Based on the laboratory test results, lime mixing ratios of 10 and 20% were chosen to construct in situ lime and fly ash mixed testing columns (called Lime-FA columns or piles). Load test results conducted on this column group is shown in Figure 2.4. It was found that the addition of lime does not affect bearing capacity when the axial load is below 100 KPa.

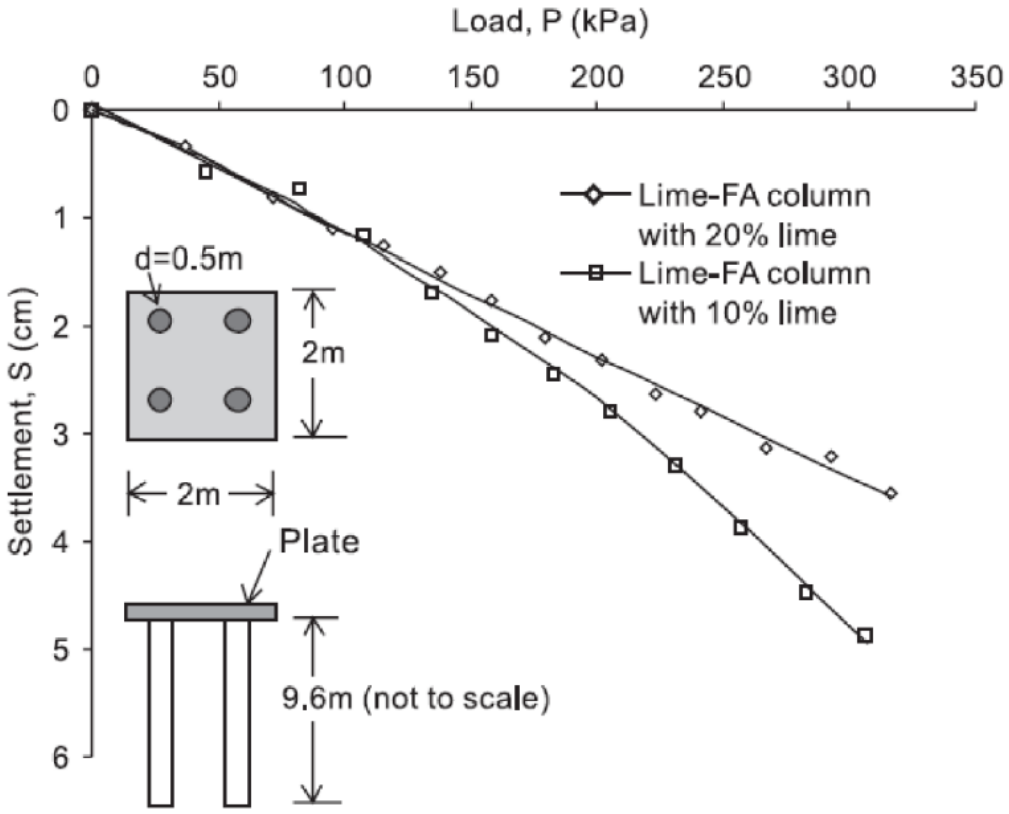

Figure 2.4: Load vs settlement curves from field plate loading tests on a set of four Lime-FA columns (Zhou et al. 2002)

Der (2011) specifies three ways to stabilize lime on the field:

(i) After mixing with the proper amount of lime at the site and adding moisture, the in-situ material or borrowed material can be compacted.

(ii) Lime and water can be mixed into the soil at a plant, then hauled back to the site for compaction.

(iii) Injecting lime slurry to a depth of four to five meters can be done under pressure.

2.5.3 Cement stabilization

The cement stabilization consists of mixing it with soils and other materials in order to make them stronger and more durable. Using this process, it is possible to build road pavements with materials

that would otherwise be unsuitable for use. It is economically and environmentally beneficial to use stabilized soils in place of natural aggregate. While there are other stabilizing agents, cement and lime are obviously the most important (Sherwood, 1993).

2.5.4 Jet grouting

Stabilization of soil can be achieved by injecting cement slurry with very high nozzle pressure into the soil, forming a solidified concrete matrix. The injected cement grout fills the voids without changing the original structure or volume of the soil, leading to a densification of the soil matrix. A jet grouted soil is able to stabilize itself due to the hardening of the grouted fluid that forms like cemented columns within the ground, improving its bearing capacity. The method is typically used to underpin foundations, control water, support excavation, and to seal the bottom of excavated areas. It is possible to implement jet grouting in three basic ways: using a single rod, double rod or triple rod system to reach the design depth. The method is suitable for soils that are easily erodible, such as gravelly soil and clean sand, but is unsuitable for clay that is difficult to erode.

2.5.5 Dynamic compaction

A well-established soil improvement technique, dynamic compaction, provides a high energy impact by densifying loose fill of cohesionless soil by dynamic loading. The process of densifying or solidifying can be applied to the entire mass of soft soil. In this process, a heavy mass of 10-40 tons is dropped on to the ground at predetermined grid points from a height varying between 10-25 m (Chow et al. 1992). According to Das (2011), compaction levels were determined by:

(i) The weight of the hammer

(ii) The height of the drop

(iii) The spacing between the hammer's drop locations

2.5.6 Vertical drainage

Ground improvement can also be achieved by artificially draining soft soils and consolidating under applied overburden. During the construction of embankments or sand fills on marshy areas (polders), wick drains are often used to provide such enhanced drainage, especially in areas with soft soil. In some cases, the method is called Prefabricated Vertical Drains (PVD). Drains are constructed from a polypropylene core with grooves (castle board or fish-bone) and a filter fabric wrapped around it. A mandrel presses them into the soil at intervals of one to three meters. Excess pore water in the soft layers flows through the filter fabric into the grooves where it is carried upward to the surface under less pressure. Thereafter, it is drained into ditches, canals, etc. As a result, the soil consolidates and settles more quickly (Barends, 2011).

Drainage can also occur downward to a layer of sand that drains. The possibility exists in the Netherlands where the Pleistocene sands underlying the soft Holocene deposits usually have potential heads equal to or even lower than the surface ditch levels. However, In the Pleistocene, however, pore water is usually connected to seawater and can be silty. If potential head in the Pleistocene can equal or surpass the polder levels, the drainage system is generally terminated 1 to 1.5m above the Pleistocene in order to prevent the flow of silty water upward (Figure 2.5).

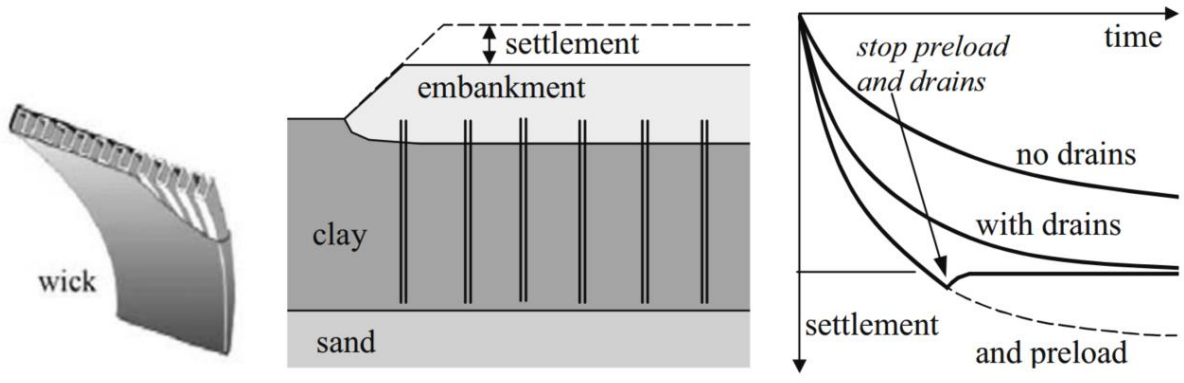

Figure 2.5: Vertical drainage applied for widening a highroad on soft soil (Barends, 2011)

2.5.7 Geopier

The Rammed Aggregate Pier (RAP) system is an alternative to concrete foundations for the support of settlement-sensitive structures (Geopier, Tensar). The Geopier ground improvement system is used for improving soils from good to poor, including soft to stiff clay and silt; loose to dense sand; organic silt and peat; variable, uncontrolled fill; and soils below the ground water. There are five methods that have been used in different projects. Vertical ramming results in high density and strength RAP elements aiding in superior bearing capacity and settling control.

2.5.8 Sand compaction pile

The sand compaction pile (SCP) is one of convenient method for eliminating liquefaction, improving ground stability, reducing settlement etc. To improve soft foundation soil, well-compacted sand piles with and without confinement are placed in the ground. Nazir and Azzam (2010) conducted laboratory model tests to study the improvement of soft clay layer with/without confinement of partially replaced sand piles. Their research focused on improving the bearing capacity and controlling settlement of soils by using sand piles.

2.5.9 Stone column

Enhanced load bearing capacity of clay layers can be achieved by using the stone column method. The stone column is composed of crushed coarse aggregates of different sizes, and the ratio of the different sizes of stones will be decided according to design criteria. By either top-feeding or bottom-feeding compacted granular columns, the soil is densified and reinforced. The top feed method uses water jets to remove soft material, stabilize the probe holes, and ensure that the stone backfill reaches the tip of the vibrator. A bottom-feed vibration-replacement method is a dry operation where the vibrator remains in the ground during construction.

Load capacity of the stone columns is offered by the confinement of the surrounding soil. In very soft soils this lateral confinement may not be adequate and the formation of the stone column itself may be doubtful (Murugesan and Rajagopal, 2009). Using suitable geosynthetic to protect the stone columns is one of the most ideal methods for improving their performance.

2.5.10 Micropile

Micropiles are used to provide structural support which is a deep foundation element constructed using high-strength, small diameter steel casing and/threaded bar. Micropiles are also known as minipiles, pin piles, needle piles and root piles. This technique has been used to support most types of structures and has the advantage of installing in a restricted access and low headroom interiors which allow facility upgrades with limited disruption to normal operations. Both open ended and closed ended piles can be used for the ground improvement techniques (Islam et al. 2021c)

2.5.11 Pile supported embankment

Embankment supported by piles is a popular technique for improving foundation stability and reducing structural deformation (Ariema and Butler, 1990). The pile mattress (Figure 2.6) is a type of load relief structure. Through a system of mats and piles, much of the loading is transferred to deep-seated bearing layers, reducing the ground pressure. The mat consists of geotextile or geogrid reinforcement (chicken-foot design) that takes the load off the pile heads after settling. It is possible to use a reinforced soil mattress as an alternative to mats since it is capable of transferring load using arching. The load relief structures require the use of many aspects of geotechnical engineering: pile behavior (end-bearing and/or friction), settlements, horizontal deformation, arching, geogrid strength and flexibility, durability and safety factors. Recent years have seen

geosynthetics being used in conjunction with piles or columns as a way of supporting embankments over soft clay foundations (Han and Collin, 2005).

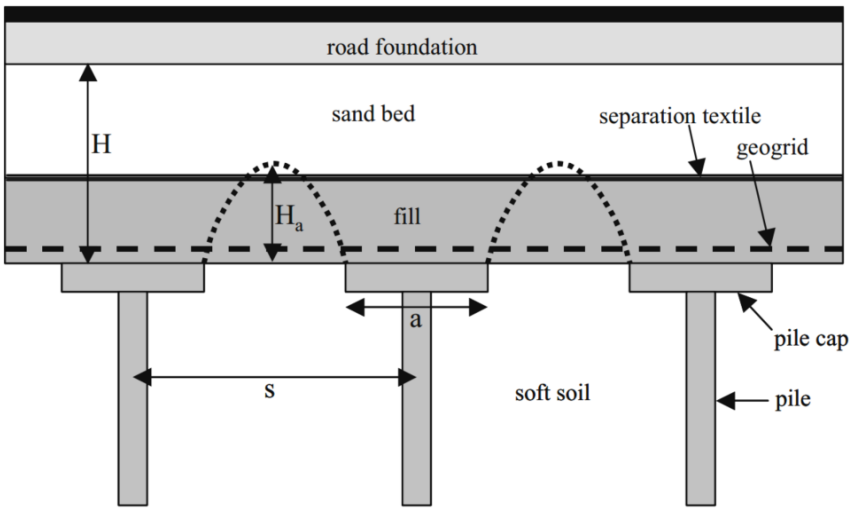

Figure 2.6: Pile supported embankment (Barends, 2011)

Several researchers studied pile support embankments without and with geosynthetic reinforcement. The former is referred as conventional pile-supported embankment while the latter is known as geosynthetic-reinforced pile supported embankment. An geosynthetic-reinforced embankment can either be designed to be built over piles or on a columnar system. According to a study conducted by Hewlett and Randolph (1988), it is estimated that the pile covering as much as 10% of the area beneath the embankment may carry more than 60% of weight of the embankment due to arching action in the fill. A single geosynthetic reinforcement layer acts as a tensioned member while a multilayer system behaves similar to a stiffened platform (like a plate) which is due to the interlocking of geosynthetic reinforcement with the soil (Han & Gabr, 2002). This type of ground improvement engineering technique has been practiced for nearly two decades (Collin, Watson, & Han, 2005).

The use of geogrid-reinforced embankments can be cost-effective and effective for road engineering because of their structural stability and economy (Lai et al., 2014). Geogrid transfers load from piles to geogrid by arching. However, there are still several issues with the application of such embankments. For instance, intolerant post-construction settlement and local instability reduce the pavement's lifetime and require more frequent maintenance. (Zheng et al., 2009, Zhang et al., 2013). In the case of GRPS embankments constructed on compressible soils, these problems are more severe and seem closely related to the inability to mobilize the soil arching effect, which has been proven to be a key factor in load transfer.

2.5.11.1 Numerical study on pile supported embankment

Han and Gabr (2002) performed numerical study to explore pile-soil-geosynthetic(s) interactions by considering three major influence factors: the height of the fill, the tensile stiffness of geosynthetic, and the elastic modulus of pile material. Numerical study was conducted using the FLAC (Fast Lagrangian Analysis of Continua) program where the piles are typically arranged in square or triangular patterns in practice (Figure 2.7). The results of the numerical study established that inclusion of geosynthetic in earth platforms can reduce the total and differential settlements above the pile heads, and at the ground surfaces, promote efficient load transfer from the soil to the piles and reduce the possibility of soil yielding above the pile heads. Analysis data indicated that the soil arching ratio decreases with an increase in the height of embankment fill, an increase in the elastic modulus of the pile material, and a decrease in the tensile stiffness of geosynthetic. The study results also indicate that the stress concentration ratio and maximum tension in geosynthetic increase with increasing the height of embankment fill, increasing the stiffness of

geosynthetic, and increasing the elastic modulus of the pile material. There is a maximum tension near the edge of geosynthetic piles due to the distribution of tension.

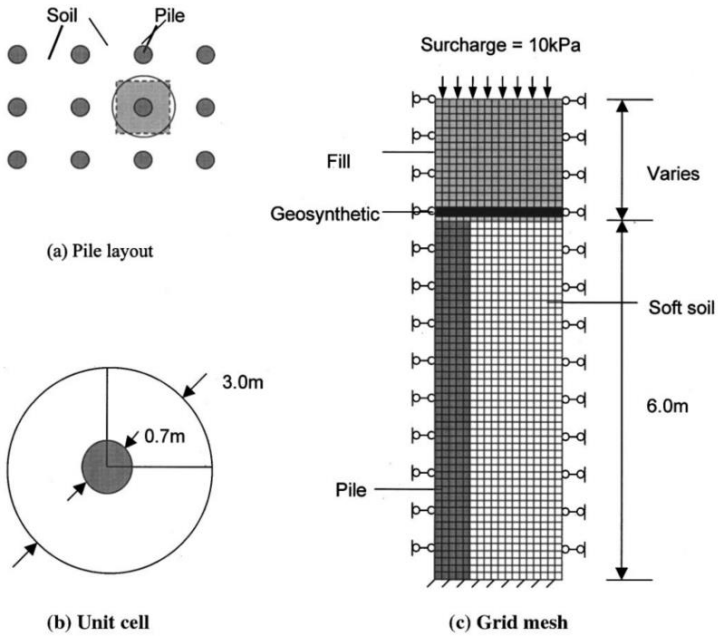

Figure 2.7: Finite difference modeling of geosynthetic-reinforced and pile-supported earth platform system (Han & Gabr, 2002)

2.5.11.2 Field model study on pile supported embankment

Oh and Shin (2007) conducted several pilot scale tests at the Geotechnical Experimentation Site of the University of Incheon, Rep. of Korea. he cross-section and plan view of the pilot scale field test site is presented in Figure 2.8. Five different test conditions were constructed at the site, with different pile spacing and reinforcement conditions. The test site measured 13 m×3 m×1.6 m (depth). It was initially filled with marine clay obtained from the Bay of Incheon. Following the placement of the piles, settlement plates were installed on the clay layer. Over the pile cap and marine clay, a layer of biaxial geogrid was applied. A three-stage embankment construction was used to impose a surcharge on the clay-pile-geogrid system (Figure 2.8). Embankments were 2.7 meters high in the end.

Figure 2.9 shows the variations in height of the embankment and settlement of the clay layer over time for the five test sections. It can be observed that with clear spacing/pile dia (D/b) = 3.0, the settlement is reduced by about 40% or more due to reinforcement. Also the efficiency of the system decreases with the increase of D/b ratio. Figure 2.10 shows the variation of the vertical stress variation (q_b) above the geogrid with embankment filling. Using these measured vertical stresses, the arching ratios (ρ) were calculated. The results are shown in Figure 2.10 and Figure 2.11. The ratio decreased from about 0.75 at an embankment height of 0.7 m to about 0.4 when the embankment height was 2.7 m. The stress is transferred from the arching to the pile head as a result of arching. In turn it reduces the settlement when geogrids are in use. In soft ground, geosynthetic reinforcement helps to reduce differential settlement by affecting soil arching. Also, the most effective load transfer and vertical stress reduction at the mid span between piles occurs when the pile cap spacing index D/b is 3.0.

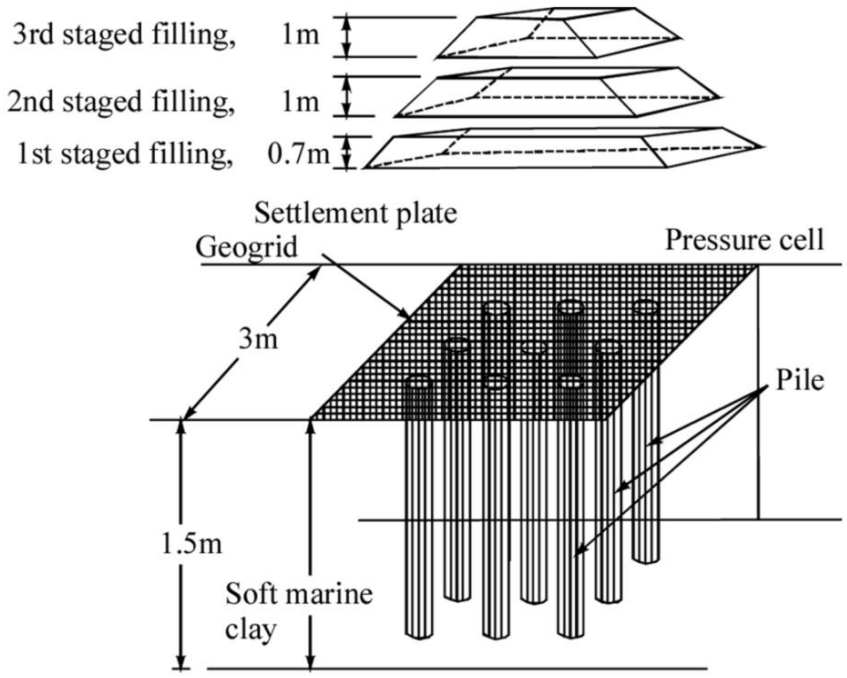

Figure 2.8: Schematic diagram of staged embankment construction (Oh & Shin, 2007)

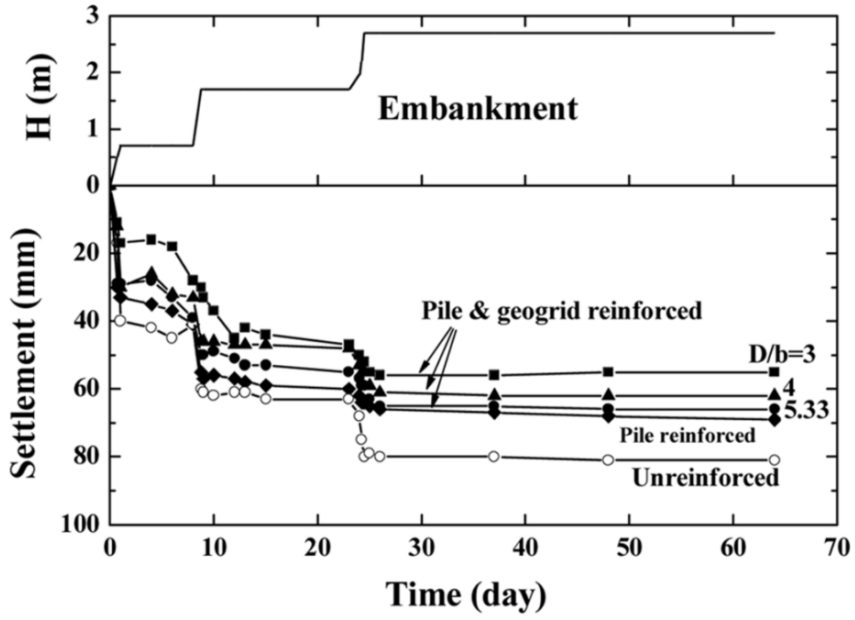

(a)

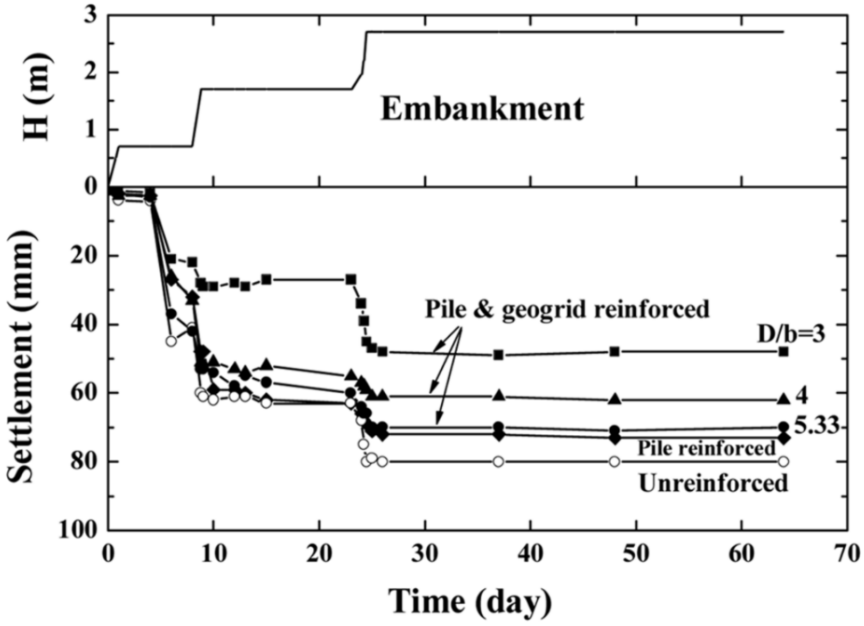

(b)

Figure 2.9: Variation of settlement with time: (a) Midspan in the horizontal direction; and (b) midspan in the diagonal direction (Oh & Shin, 2007)

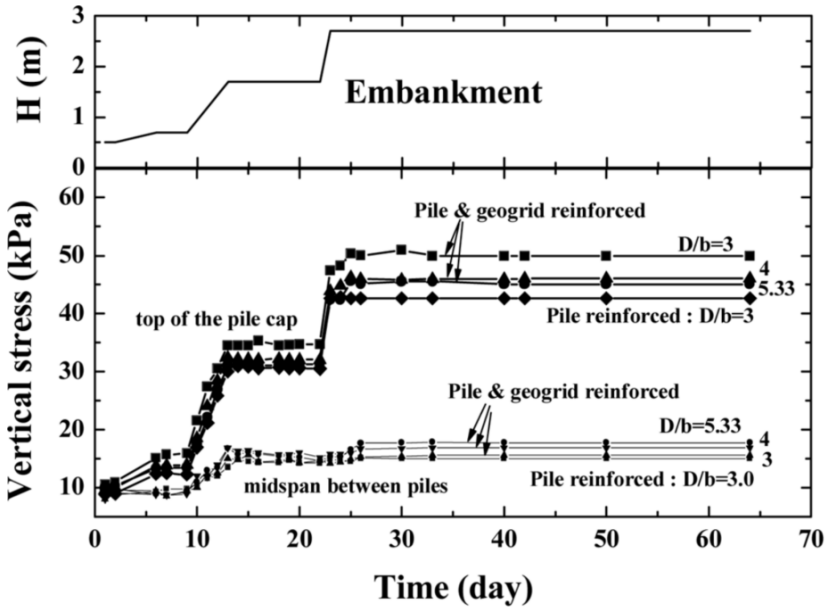

Figure 2.10: Vertical stress (q_b) variation with embankment filling by field model tests (Oh & Shin, 2007)

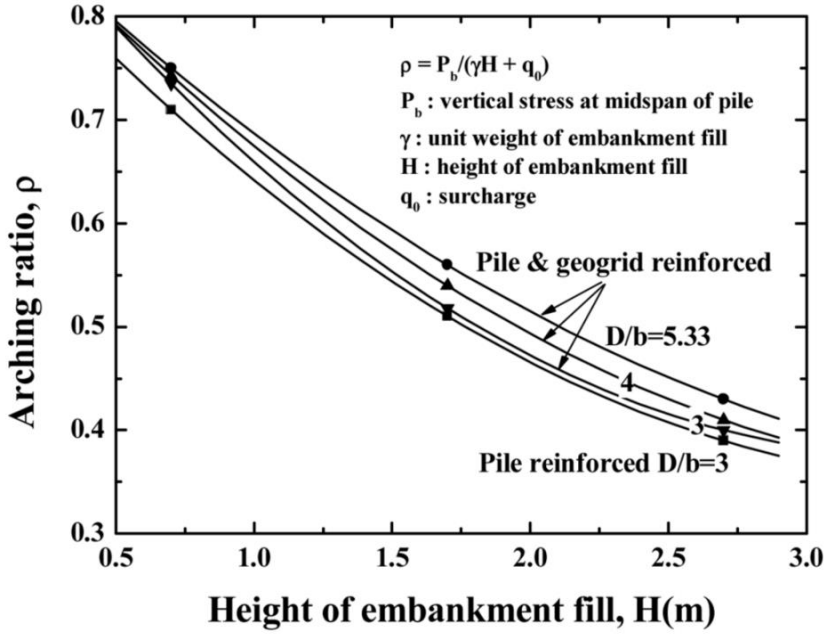

Figure 2.11: Variation of arching ratio with embankment filling by field model tests (Oh & Shin, 2007)

2.5.11.3 Laboratory study on pile supported embankment

Hewlett and Randolph (1988) conducted some experimental program using a grid of piles to support the embankment in the vicinity of the structure. Several small scale experiments were conducted with dry sand and analyzed the settlement behavior of piled embankments. Hewlett and Randolph (1988) concluded that closely spaced smaller piles are more effective than widely spaced larger pile (Figure 2.12). Furthermore, piles give direct support to the embankment by means of arching action between adjacent pile caps. Use of a membrane over the pile caps will provide support and prevent lateral spreading of the embankment.

(a) (b)

Figure 2.12: Photographs of model tests on dry sand, (a) widely spaced large pile with large settlement, (b) closely spaced small piles with small settlement (Hewlett & Randolph, 1988)

2.5.11.4 Case study on pile supported embankment

Michalowski et al. (2018) conducted a case study of a new section of a freeway was constructed as part of the European route E372 in the eastern region of Poland. One portion of the embankment was over organic clay with a thickness up to 9.5 m. Controlled modulus columns were used in the column supported embankment, with a total of 13,670 columns along a 750-m section of an

expressway. This case study suggests that proper transfer of embankment loads to the columns should be assured. Serviceability failure is likely to be caused by disruption of load transfer from embankments to columns at culvert locations.

Some other techniques for ground improvement method are also available. Use of vegetation in slopes is getting popular day by day as a sustainable slope stabilization method (Badhon et al. 2021a; Islam et al. 2021). Due to the inclusion of roots, the soil shear strength increases, eventually the factor of safety of slope increases (Islam et al. 2020; Badhon et al. 2021b). These techniques can be applied to the slope of the embankment for improving the global stability of embankment. However, for improving the bearing capacity of foundation soil, vegetation technology is inappropriate.

2.6 Soil arching of pile supported embankment

The soil arching phenomenon is a common occurrence in geotechnical engineering. Differences in movement between the subsoil and supports cause soil arching. Pile embankments are often designed with soil arching as a primary method, in which piles serve as supports. During deformation of a piled embankment, loads are transferred from the soil to the piles, which results in soil arching.

The interactions among pile (caps), foundation soil, fill, and geosynthetic can be schematically portrayed as shown in Figure 2.13. Under the influence of fill weight, W_1, the embankment fill mass between pile caps has a tendency to move downward, due to the presence of soft foundation soil. This movement is partially restrained by shear resistance, τ, from the fill above the pile caps. The shear resistance reduces the pressure acting on the geosynthetic but increases the load applied

onto the pile caps. This load transfer mechanism was termed the ‘‘soil arching effect’’ by Terzaghi (1943). The degree of soil arching was defined as follows (Han & Gabr, 2002):

$$\rho = \frac{\rho_b}{\gamma H + q_0} \tag{2.2}$$

Where ρ = soil arching ratio; ρ = 0 represents the complete soil arching while ρ = 1 represents no soil arching; pb5applied pressure on the top of the trapdoor in Terzaghi or McNulty’s studies (geosynthetic for this study); γ = unit weight of the embankment fill; H = height of embankment; and q_0 = uniform surcharge on the embankment.

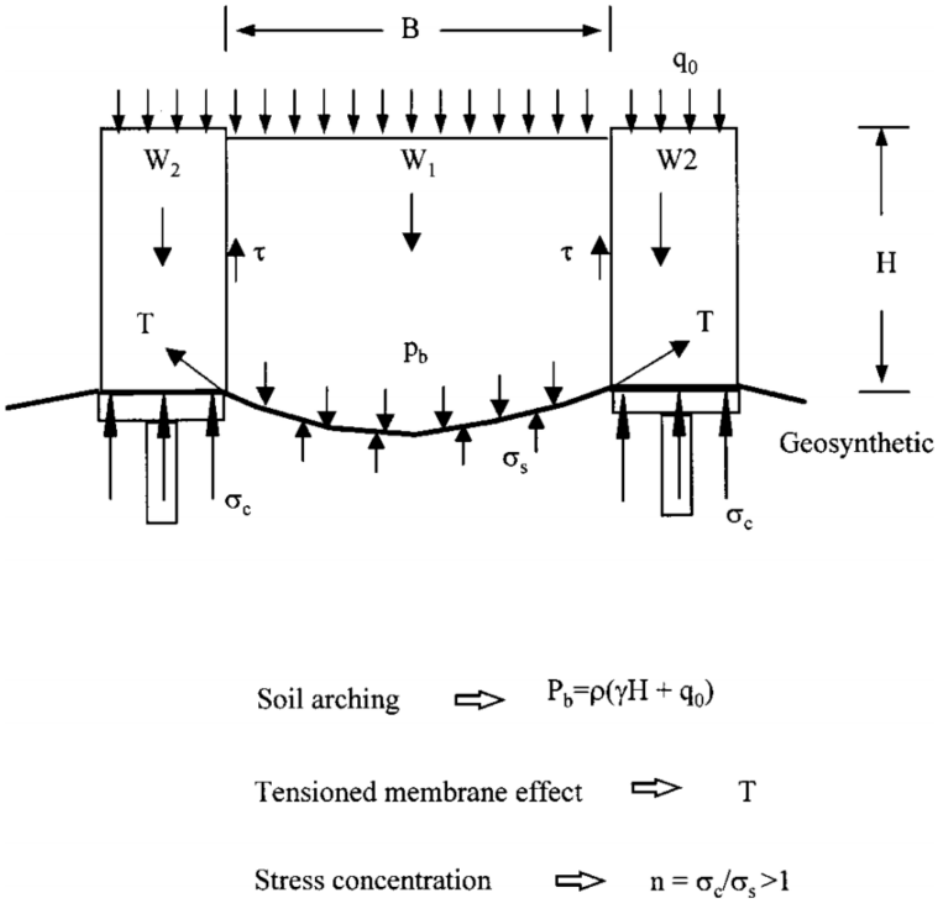

Figure 2.13: Load transfer mechanisms of geosynthetic-reinforced pile supported earth platforms (Han & Gabr, 2002)

2.6.1 Experimental study on soil arching

Rui et al. (2019) conducted fourteen unreinforced and eight geosynthetic reinforced model tests using 2D multitrapdoor test setup with analogical soil. Particle Image Velocity (PIV) was used to measure the displacement of analogical soil above trapdoors. Based on the same conditions, basal geosynthetic reinforcement determined that the three deformation patterns developed into two concentric elliptical arches. Furthermore, Due to the higher deflection in the lower tensile stiff geosynthetic than the higher tensile stiff geosynthetic, the soil arching was greater.

2.6.2 Analytical study on soil arching

Load transfer to piles is greatly influenced by the arching effect of soil fill. Soil arching can occur without any use of load transfer platform of pile caps. A yielding mass of soil transfers pressure to adjoining stationary parts by means of the arching effect, defined by Terzaghi (1943). Terzaghi (1936) experimented with the pressure on a narrow strip of a trap door by lowering the trap door slightly while increasing the pressure on the adjacent portions of the platform by adding sand above the platform. A phenomenon known as shear stresses was found between the yielding (moving) sand mass underneath and the adjacent stationary sand mass, which prevented the mass from falling below the yielding trap door. In other words, the pressure exerted on the trapdoor was instead transferred to the adjacent stationary platform, a phenomenon Terzaghi called ‘soil arching’.

Arching effect in granular free-draining soil is studied by (Hewlett & Randolph, 1988). The effect is analyzed considering the limiting equilibrium of stresses in a curved region of sand between adjacent piles. The case of most relevance for embankment piling is for arching above a grid of piles, where the form of "sand vault" suggested by the model tests is as shown in Figure 2.14 (a).

The vault is comprised of a series of domes, the crown of each dome being approximately hemispherical, its radius equal to half the diagonal spacing of the pile grid. The ensuing analysis considers the equilibrium of this system of vaulting. Figure 2.14 (b) shows a section through a piled embankment. The stress field that is analyzed is indicated. The principal element of the stress field is the semi-circular zones of arched sand. These "arches of sand" shed the uniform overburden of the embankment onto the pile caps. Although the arches of sand lie within a continuum, their action is similar to that of masonry arches as found in cathedrals.

The analysis leads to lower bound on the efficacy of the pile support, which is the proportion of embankment loading taken directly by the piles. Also it implies that the pile spacing should not be greater than about half of the embankment height for this condition to hold. Geotextile laid over the pile caps will increase the efficiency of the support. Finally, possible design approach was recommended considering the approach road of bridges where settlement of embankments needs to be minimized (Figure 2.14c).

Analytical study for calculating load carried by the pile and subsoil based on the displacement compatibility principle is conducted by Liu et al. (2017). A unit cell concept was utilized to study the load transfer mechanism of GRPS embankment. Figure 2.15 shows an axisymmetric cylindrical unit cell model in plan view, which consists of one capped pile and the tributary soft soil, bridging layer, geosynthetic and embankment fill from its influence area. It is assumed that the z axis starts at the top of the pile cap and is positive in the downward direction. For piles laid out in a square array with center- to-center spacing, s, the area of the unit cell, A_{tot}, is equal to s^2 or $\pi\, d_{uc}^2/4$, where d_{uc} is the equivalent diameter of the unit model. The model is capable of analyzing both square and circular pile caps usually used in practical engineering.

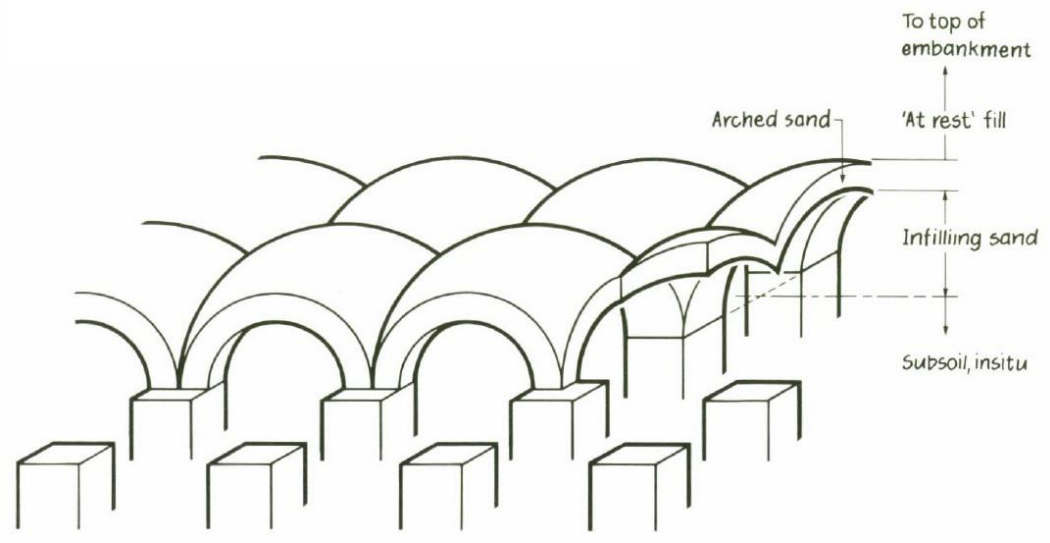
To top of embankment
Arched sand
'At rest' fill
Infilling sand
Subsoil, insitu

(a)

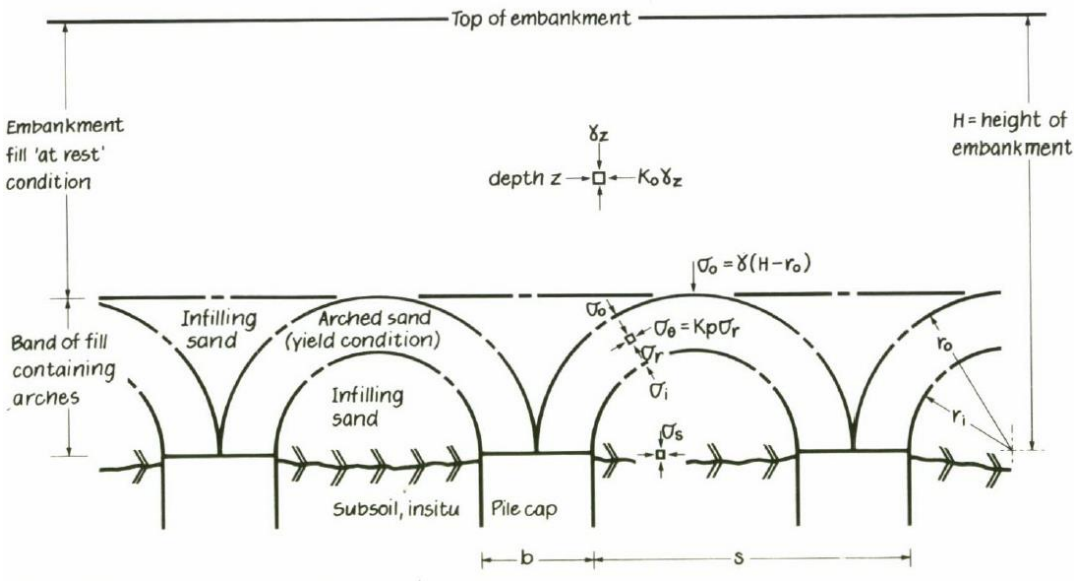
Top of embankment
Embankment fill 'at rest' condition
H = height of embankment
γz
depth z
Kₒγz
σₒ = γ(H − rₒ)
Band of fill containing arches
Infilling sand
Arched sand (yield condition)
Infilling sand
σₒ
σθ = Kpσr
σr
σi
σs
rₒ
rᵢ
Subsoil, insitu
Pile cap
b
s

(b)

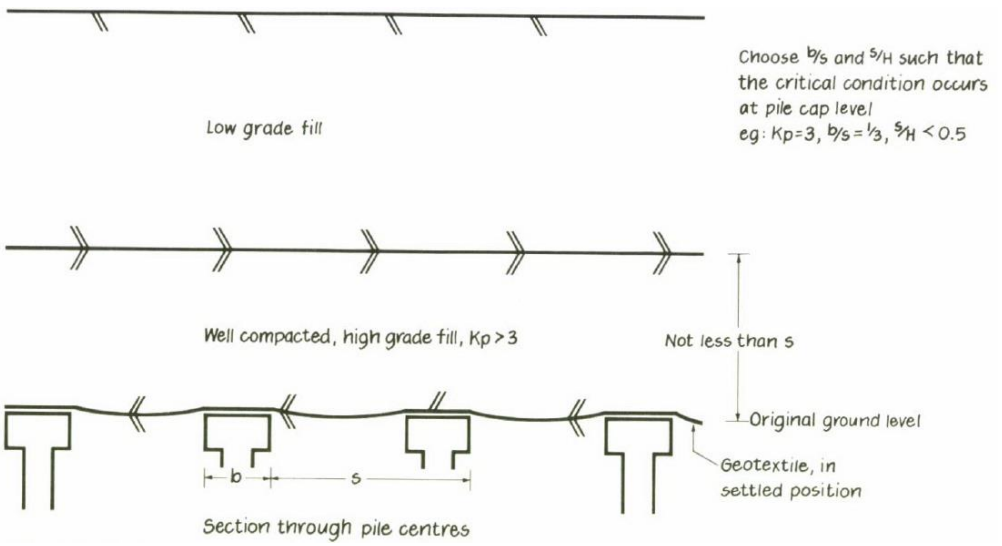

(c)

Figure 2.14: Analysis of arching effect: (a) isometric view of a grid of pile caps and a series of domes forming a vault spanning between them, (b) section through a piled embankment (c) Design recommendations (Hewlett & Randolph, 1988)

For the square pile cap shown in Figure 2.15 (a), the cap area, A_c, is equal to b_c^2 or $\pi\, d_{uc}^2/4$, where b_c is the width of a pile cap and d_c is the equivalent diameter of the pile cap. The area replacement ratio for pile cap, mc, is equal to A_c/A_{tot}. The length, the crosssectional area, the diameter, and the area replacement ratio of the pile are expressed as L, A_p, d_p, and m_p, respectively, where m_p is equal to A_p/A_{tot}.

For determining the stress reduction ratio, the stress concentration ratio, and the differential settlement at the embankment base, an iterative method based on the developed method was presented. The results implied that cohesion plays a greater role in transferring loads from soft subsoil to rigid piles than internal friction angle in embankment fill. The mobilization coefficient of shear strength indicates that the soft subsoil is being loaded more by the piles. The cohesion of embankment fill plays a more critical role in transferring load from soft subsoil to rigid piles via

shear stress than internal friction angle. Thus, when designing an embankment, the cohesion of the fill should be considered.

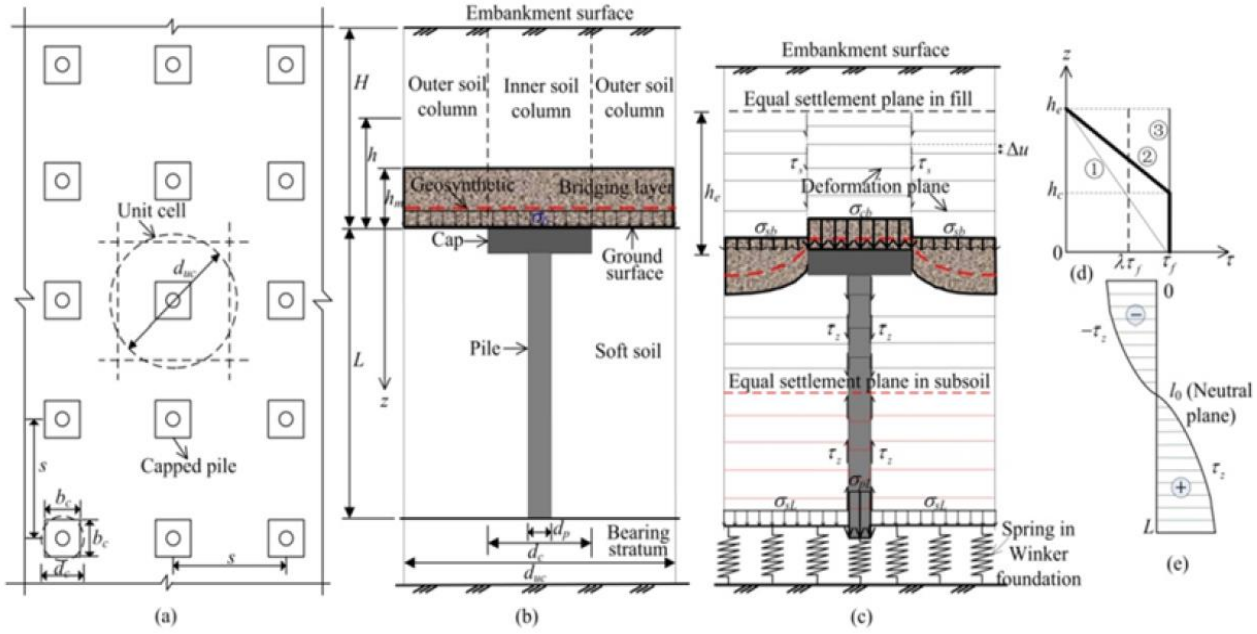

Figure 2.15: Analytical model for GPRS Embankment: (a) Axisymmetric Unit Cell for a Square Pile Grid: (b) Unit Cell in Profile View Before Settlement, (c) Simplified Cross-section after Settlement, (d) Distribution of Shear Stress within Embankment, (e) Distribution of Skin Friction Along the Pile (Liu et al., 2017)

Serviceability behavior and deformation that often govern the suitability of their design is very important for geosynthetic reinforced column supported embankment. While the deformation dependent development of arching stresses is at odds with these limit equilibrium models, the limit equilibrium models may be suitable for LTP design, provided that the value of arching stress is representative, and on the safe side, of the ultimate stress acting on the geogrid layers through its design life. This arching stress/deformation compatibility issue is highlighted in Figure 2.16, where

the transition from initial conditions, to the so-called “ultimate” long-term condition in an LTP is shown (King et al. 2017).

Additionally, the thickness of soft soil, its compressibility, and consolidation rate vary significantly along the length of the Geosynthetic Reinforced Column Supported Embankment (GRCSE). Based on the different settlement rates between unit cells, further differential settlement occurs. The use of the GRCSE method to describe the development of arching and its relationship with the serviceability, working and ultimate conditions is shown in Figure 2.17. During the critical period of differential and total settlement, the embankment's LTP must be in a serviceable condition, which may take over a decade if sub-soil settlement is controlled by creep settlement (King et al., 2017).

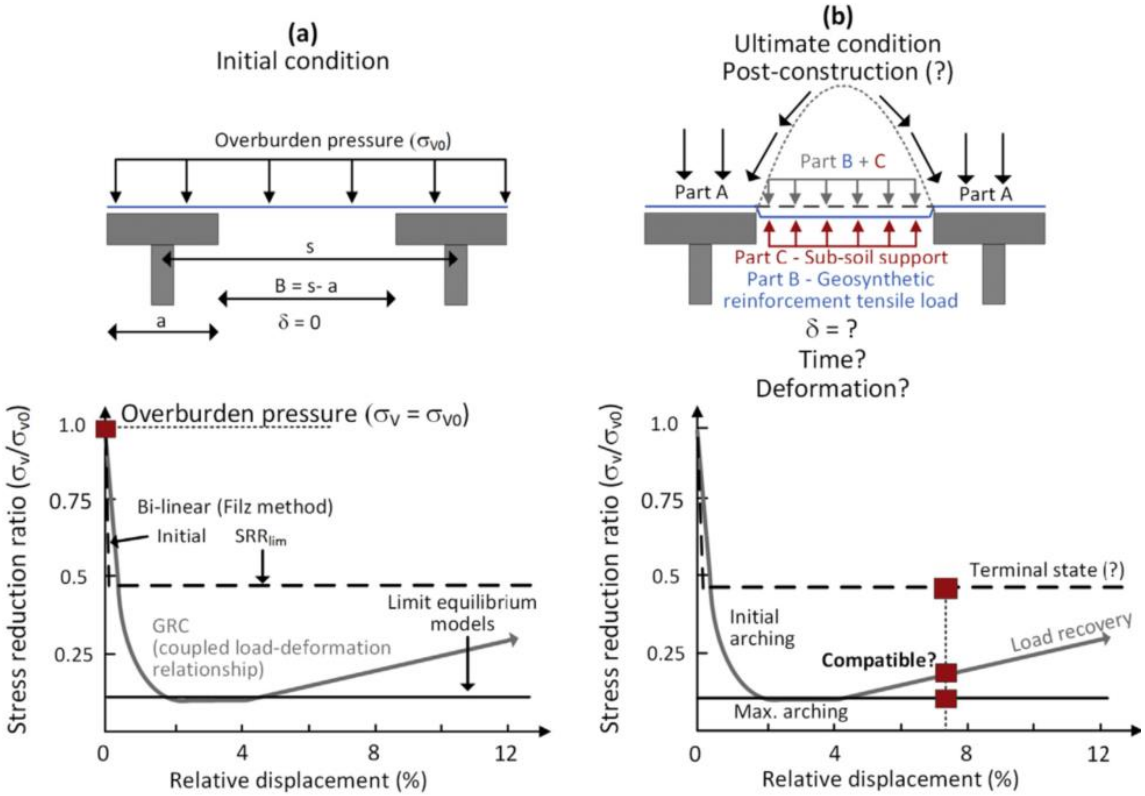

Figure 2.16: (a) initial condition with no sub-soil settlement; (b) long-term ultimate limit state design condition in GRCSE (King et al., 2017)

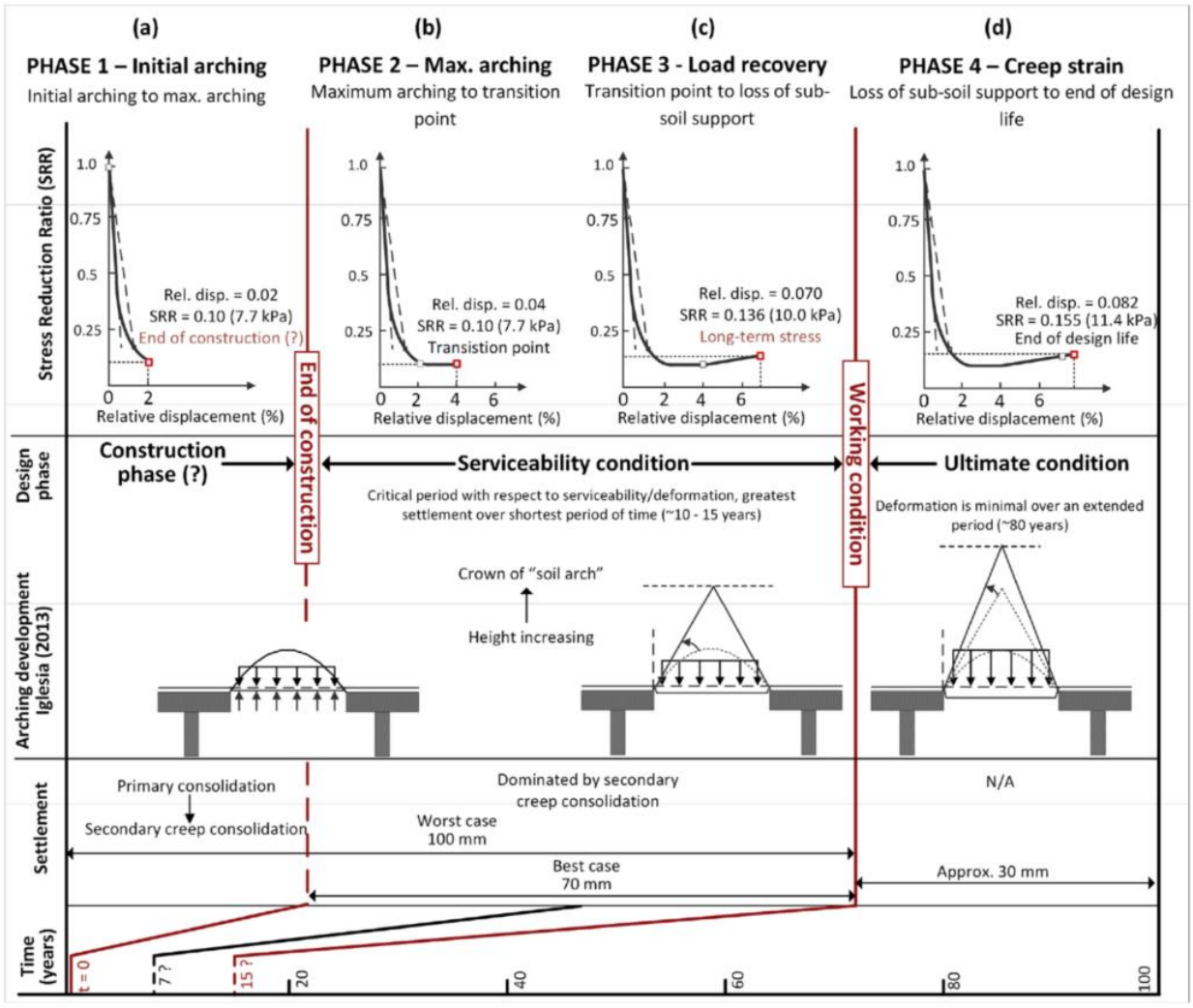

Figure 2.17: Ground reaction curve design approach (a) Initial arching (b) Maximum arching (c) Load recovery and (d) Creep strain (King et al., 2017)

2.6.3 Numerical study on soil arching

2-D numerical analysis was conducted by Oh and Shin (2007) using FLAC 2D. Based on the difference in stiffness between piles and soft ground, the mechanisms of load transfer can be combined with embankment soil arching and geogrid tension. Figure 2.18 presents the finite difference mesh that was used by Oh and Shin (2007).

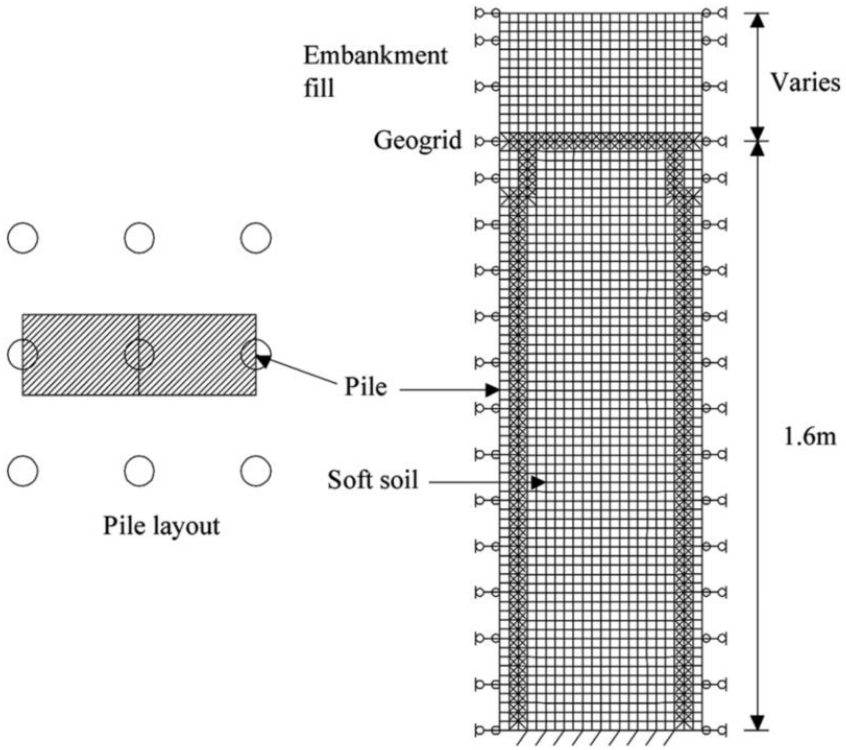

Figure 2.18: Finite difference mesh of geogrid reinforced pile embankment

Using the numerical results of analyses of pile heads at the pile cap and the midspan of the pile, Figure 2.19 shows a vertical stress variation with height of embankment fill. There is a greater vertical stress in geogrid reinforced cases (D/b = 3) than in other reinforced cases at the location of the pile cap.

An analysis of settlement data indicated that the higher vertical stress at this location was associated with a significant transfer of load from the soil mass to the pile, indicating that the geogrid reinforcement enabled load transfer. At the midspan location, however, the only pile reinforced case occurred at a minimum value of vertical stress because of the arching effect, which is fully developed without interference from the geogrid reinforcement. Regarding pile spacing (D/b), the vertical stress at the cap increases as the D/b decreases while it decreases at the midspan as the D/b decreases.

It is possible to explain this phenomenon by the arching ratio variation and the pile spacing (D/b), as demonstrated in Figure 2.20. The arching effect of the pile only reinforced case (D/b = 3.0) is higher than pile and geogrid reinforced cases, and the arching effect of pile and geogrid reinforced cases increases with decreased pile spacing until D/b = 3.0. Therefore, the pile and geogrid reinforced with D/b = 3.0 is most efficient for generation of soil arching and reduces the differential settlement by interaction between geogrid reinforcement and pile. A geogrid embedded horizontally and a pile can interact under an embankment and any surface loading in two different ways: (a) geogrid tension and elongation at the midspan between piles without load transfer by geogrid reinforcement by means of the small surcharge loading, and (b) load transfer from soil mass to the pile cap by geogrid reinforcement by means of large surcharge loading. Geogrid reinforcement and pile load transfers are affected by pressures that occur at midspan and by pile spacing (D/b).

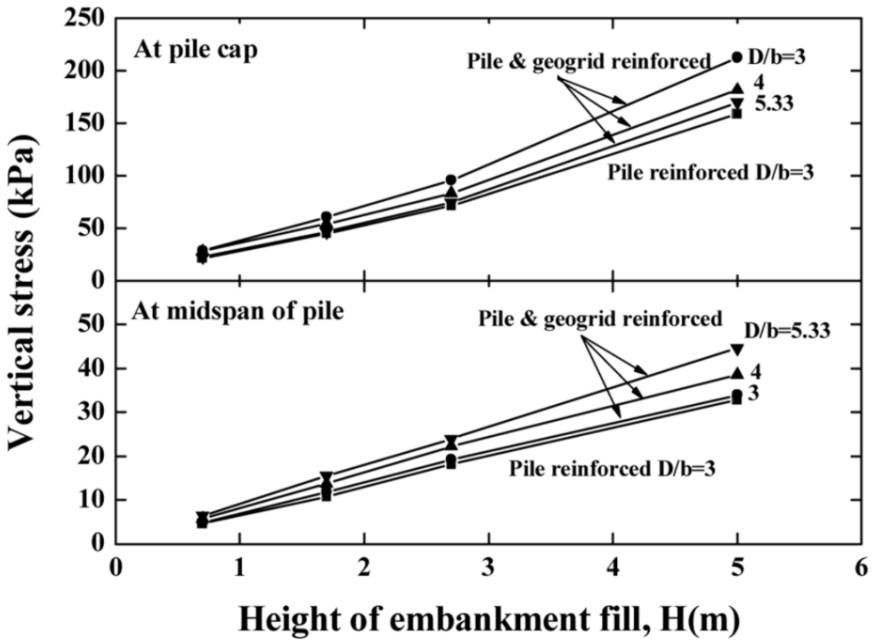

Figure 2.19: Vertical stress variation with reinforced method and position from numerical analysis (Oh & Shin, 2007)

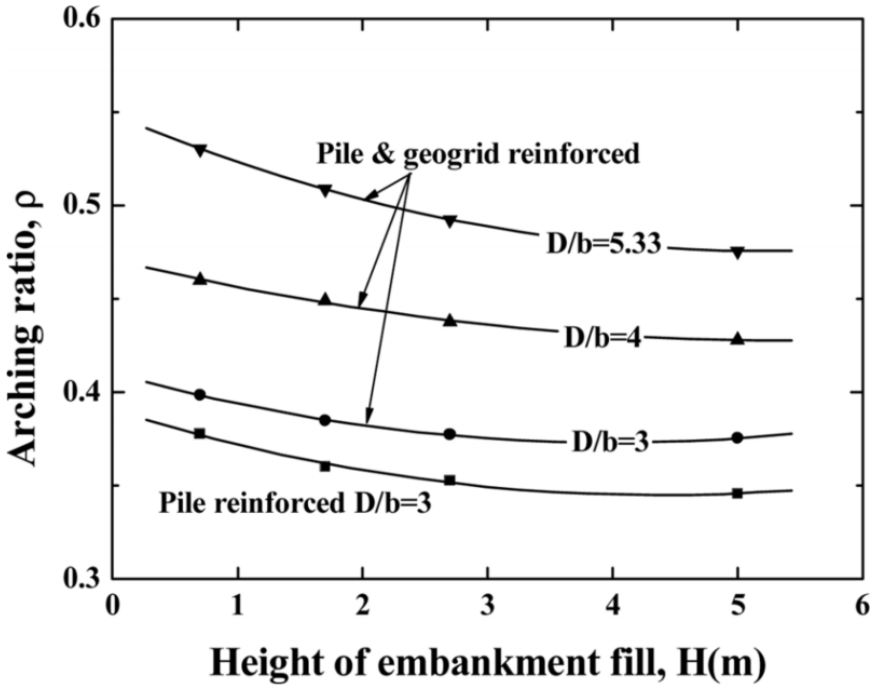

Figure 2.20: Arching ratio with embankment height from numerical analysis (Oh & Shin, 2007)

A series of 3-D numerical analyses was performed by Ye et al. (2020) on the behavior of GRPS embankments with different numbers of geosynthetic layers. It was found that, with the addition of geosynthetic reinforcement, the soil arching effect was minimized, however, overall load carried by the piles was increased. In a three layer load transfer platform, the lower layer significantly affected load transfer compared to middle and upper layers. However, on top of the gravel cushion, almost all of the layers mitigated differential settlement.

2.7 Load transfer platform

An embankment supported by columns is a useful product for constructing roads on soft, fine-grained soils. At the base of an embankment, normally a load transfer platform (LTP) is used to minimize differential settlement and stabilize the embankment and to even out settlement differentials.

2.7.1 Existing literature on load transfer platform

Abdullah and Edil (2007) conducted a study on a field test embankment over ground to investigate the performance of different types of LTPs supported on rammed aggregate piers (geopiers). Based on the recommended designs for LTP, there were three types constructed: a geosynthetic-reinforced LTP with two layers of geogrid (catenary LTP), a geosynthetic reinforced LTP with three or more layers of geogrid (beam LTP), and a reinforced concrete LTP (Figure 2.21). All LTP sections showed relatively low differential settlement between geopiers and matrix soil, but the beam LTP showed the smallest one. Even though geosynthetic-reinforced LTPs may vary depending on the region, beam LTPs are less costly than geosynthetic-reinforced LTPs and provide better performance.

A field study was conducted by Michalowski et al. (2018) with controlled modulus columns. The columns were equipped with a load transfer platform for facilitating the loads from the embankment. The platform included a 0.3 m sand layer placed over a woven geotextile and an upper 0.4 m geogrid-reinforced layer of sand. There are three levels of reinforcement for the uniaxial geogrid: top and bottom transverse layers and a middle layer placed in the longitudinal direction (Figure 2.22).

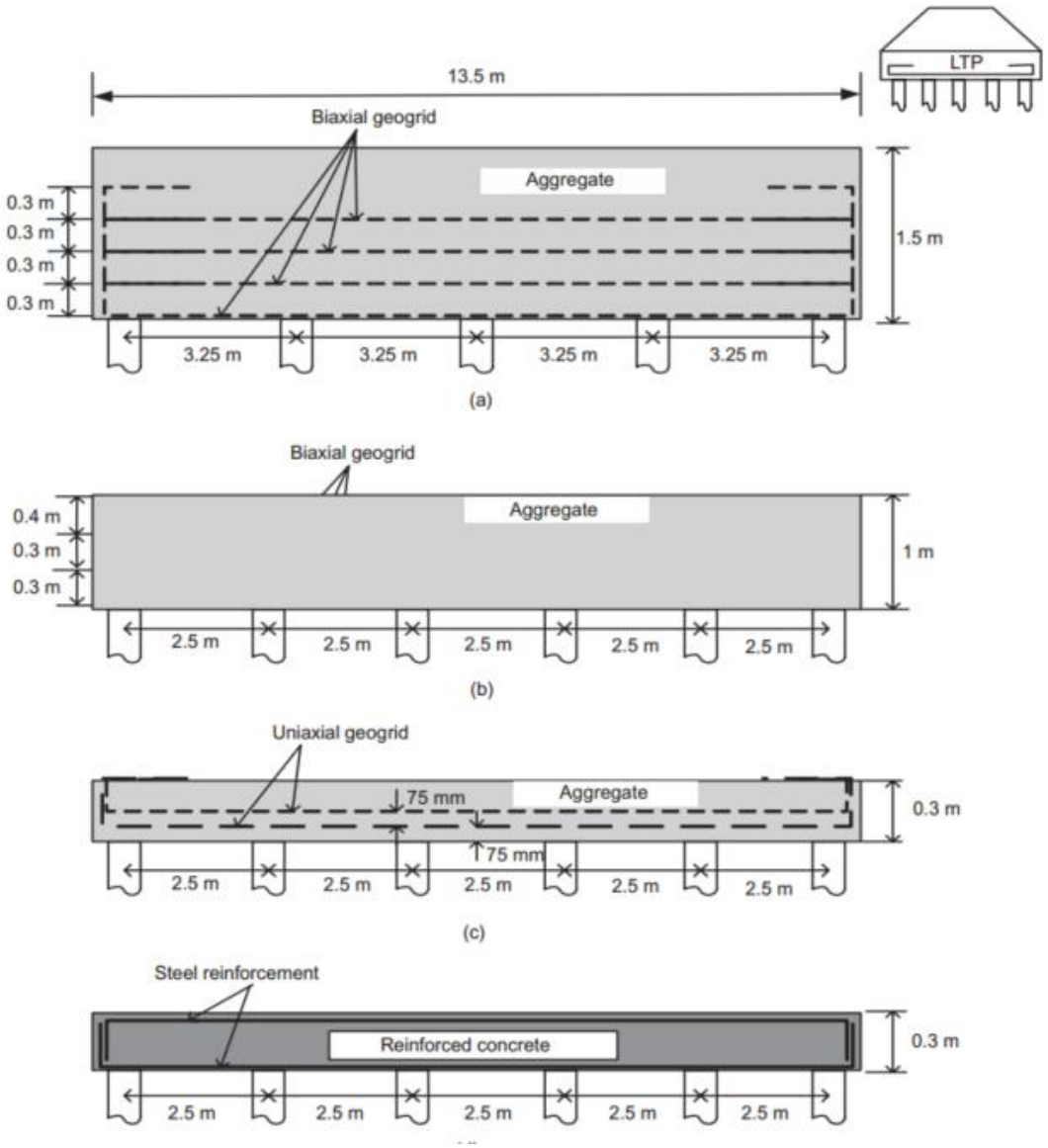

Figure 2.21: Schematic layout of the different LTPs in: (a) Beam LTP; (b) Beam LTP; (c) Catenary LTP; (d) Concrete LTP (Abdullah & Edil, 2007)

After the construction, excessive settlement was observed at several points especially in the culvert joints. The construction of discontinuous transfer platforms for culverts or utility conduits can exacerbate the amount of settlement caused by a load transfer. While insufficient column length may have facilitated the transfer of load to the soft layers, there is no indication that this was a

significant problem. Lastly, the presence of large voids (culverts) in the embankment fill might have some adverse effects on the distribution of displacements within the fill during settlement of soft layers beneath.

A remedial action that was considered was replacing the embankment fill with lightweight material (EPS blocks geofoam). There were some locations where drilled shafts were constructed to transmit load directly to deeper materials from an embankment.

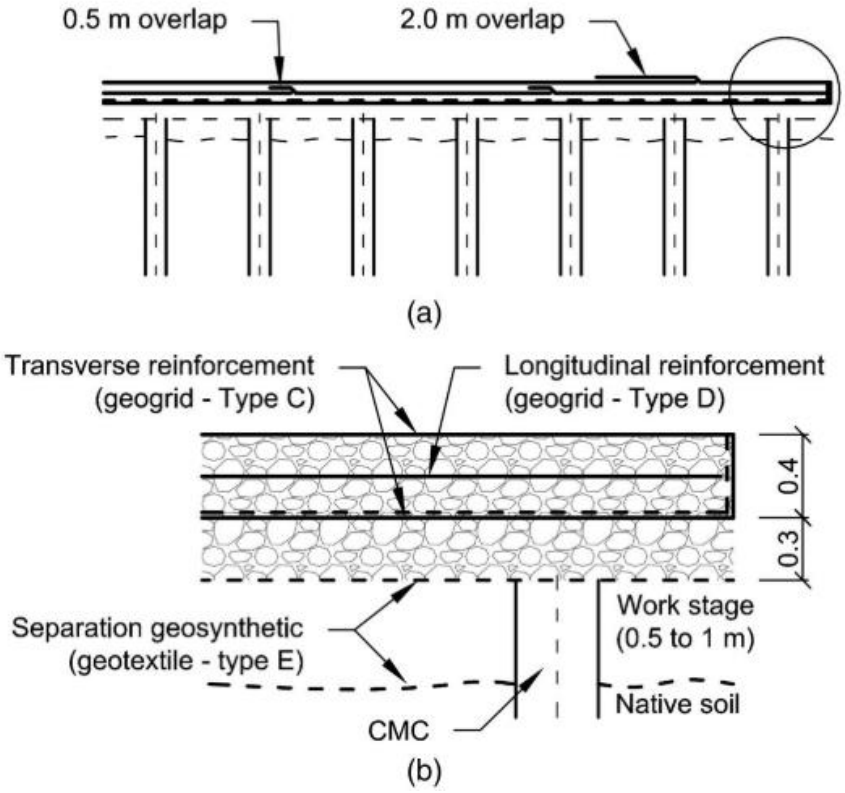

Figure 2.22: Load transfer platform for transferring loads from the embankment to the columns: (a) transverse cross section; (b) detail at the edge of the reinforced load transfer platform (Michalowski et al., 2018)

Table 2.1: Geometry and material properties of different field study of LTP in GRPS embankment

Author (s)	Nature of Study and location	Embankm-ent support	Subgrade Soil condition	Geogrid Specification				Fill Material between Geogrid	Total thickness of load transfer platform	Embankment Details
				Type of Geogrid	Property of Geogrid	No of geogrid Layers	Vertical Spacing			
Han and Akins (2002) and Alzamora et al. (2000)	Geogrid-reinforced segmental retaining walls	Jet-grout columns; Dia=1.2m, Spacing=3.0m	Organic Silt and Clay (SPT N=0 to 1); thickness 9.0 m	HDPE Uniaxial Geogrid	46.8 kN/m	4 Layers	25 cm	Compacted well graded granular fill	1.0m	Embankment height=2.0 to 8.2m, fine grained soil
	Widening of an existing roadway in South Carolina	Vibro-concrete columns; Spacing = 2.4 m	very soft clayey sand fill and organic silt marsh deposits at depths up to 10.7 m	Primary uniaxial wrapped-around secondary biaxial geogrids	l l.8kN/m (Primary uniaxial) 6.1kN/m (secondary biaxial)	2 layers	-	Lightweight fill	-	Embankment height=3.0m, lightweight backfill material
Sloan et al. (2011)	Field scale test column supported embankment test	Concrete columns; Dia= 0.61m, Spacing=3.0m	Geofoam blocks with dissolver above a concrete mat	biaxial polypropylene geogrid	86 kN/m	3-5 layers	variable	well-graded gravel with crushed rock	1.2m to 2.3m	Embankment height=1.4m-2.3m, crushed rock as backfill
Collin et al., (2005)	New residential section in Williamsburg, Virginia	Augur cast in place pile; Dia=0.45m, spacing= 2.4m trinagular	Organic Clay (OH) up to 4m; from 3 to 7m peat (PT)	biaxial geogrid	UTM[1]=29 kN/m	3 Layers	20 cm	-	0.9m	Embankment height=3.5m with 70 batter retaining wall

[1] UTM = Ultimate Tensile Strength

Table 2.1: Geometry and material properties of different Field Study of LTP in GRPS embankment (contd.)

Author (s)	Nature of Study and location	Embankment support	Subgrade Soil condition	Geogrid Specification				Fill Material between Geogrid	Total thickness of load transfer platform	Embankment Details
				Type of geogrid	Property of Geogrid	No of Geogrid Layers	Vertical Spacing			
Michalowski et al. (2018)	European route E372 in the eastern region of Poland	Controlled modulus columns (CMC); Dia=0.4m, Spacing= 1.4m to 2.0m	organic clay of a thickness of up to approximately 9.5 m	Uniaxial Geogrid	UTM= 500 kN/m (long term)	3 Layers	20 cm	Aggregate	0.7m	Embankment height=4.0-11.0m, side slope=1V:1.5H , clayey sands and silts (backfill soil)
Abdullah and Edil (2007)	Full scale test embankment at Gebeng, Pahang, Malaysia	Geopier (rammed aggregate), Dia=0.6-0.8m, Spacing=2.5-3.25m	soft silty clay/clayey silt layer up to 15m deep	Biaxial and high strength uniaxial geogrid	UTM=20 kN/m (biaxial) 370.3 kN/m (uniaxial)	4, 3 and 2 layers	0.3m and 0.75m	Aggregate	1.5m, 1.0m and 0.3m	Embankment height=3.5m, side slope=1V:1.5H
Oh and Shin (2007)	Pilot scaled field test at Incheon, Rep. of Korea	Pile dia=0.1m, pacing=0.6-0.95m	Soft marine clay	Biaxial polypropylene geogrid	UTM[2] = 12.4 kN/m	1 layer	N/A	N/A	N/A	Embankment height=2.7m
Zaman (2019)	Full scale test at Irving, Texas	RPP (4″×4″, 6″×6″), Spacing=0.9m)	High plastic clay	Biaxial geogrid	Stiffness (EA)=21.9 kN/m	1 layer	N/A	N/A	N/A	Embankmet height=1.5m, sand as backfill, 1V:1H side wall (fence)

[2] UTM = Ultimate Tensile Strength

Table 2.2: Geometry and material properties of different Numerical Study of LTP in GRPS embankment

Author(s)	Nature of the Numerical study	Embankment support	Subgrade Soil condition	Geogrid Specification				Fill Material between Geogrid	Total thickness of load transfer platform	Numeric-al Program	Embankment Details
				Type of Geosynthetic Material	Properties of Geogrid	No of Geogrid Layers	Vertical Spacing of each Geogrid Layer				
Han and Akins (2002)	A retail grocery store on uncontrolled fill site at Ohio	Augured concrete piles; Dia=0.4m, Spacing=2.6-3.0m, triangular pattern	uncontrolled fill, silty to lean clay 2.1 to 12.2m thickness	Geogrid	Tensile strength =87 kN/m	3 Layers	-	Structural fill (c'=24.0 kPa, φ'=24, γ=20kN/m3)	0.8m	hyperbolic model (Duncan and Chang, 1970)	3.7 m Structural fill with floor surcharge= 7.2 kPa
Han and Gabr (2002)	geosynthetic-reinforced pile-supported embankments	Pile dia=0.7m, spacing=3.0 m	6m of soft soil to be underlain by a very stiff layer	Geosynthetic	Stiffness =860 kN/m	1 layer	N/A	N/A	N/A	FLAC (Fast Lagrangian Analysis of Continua)	Sandy soil with height 3.0 m; 10 kPa as surcharge traffic load
Zuang and Wang(2016)	reinforced piled embankment	concrete square pile, size=0.3m, spacing=2,2.5,3.5m, square grid pattern	Soft clay	Geogrid	Stiffness = 0,3,6,12 MN/m	3 Layers	0.3m	Natural Soil	0.6 m	Abaqus 6.12	Embankment height=6m,
Oh and Shin (2007)	Geogrid reinforced pile embankment	Concrete pile, dia=0.1m, spacing=0.6-0.95m	Soft marine clay	Biaxial polypropylene geogrid	Tensile strength =12.4 kN/m	1 layer	N/A	N/A	N/A	FLAC 2D v4.0	Embankment height=2.7 m

2.7.2 Working platform

Working platforms are an essential element of many construction projects, especially where heavy plant must be operated over soft subsoils. Such pavements are generally considered to be temporary works, of-ten with little or no investigation and design to ensure safe operating conditions for the heavy plant involved. Inadequate design of such working platforms can result in very poor working conditions, such that frequent re-filling or re-grading may be required with associated down-time and delays. In severe cases heavy plant, especially tracked cranes, may become unstable resulting in collapse or overturning, and many pictures of such accidents may be found. In severe cases these accidents result in injuries or fatalities, such that they become health and safety issues, and inevitably lengthy investigations result, which are likely to include detailed scrutiny of soil data, loading and the design method used to dimension the working platform.

2.7.2.1 Construction mat

Construction mat is a lightweight and strong material which create access across soft ground with speed, agility, and safety. It is usually made of polyethylene which made it weather resistant. Construction mat can build access roads, work platforms and tracking pads even over poor soils, wet ground and difficult-to-access sites. Ground protection mats combine high crushing and flexural strength with low weight, making them an economical alternative to heavy HDPE or timber mats. Construction mat can be used for construction of access road, oil drilling roadways and platforms, wind farm staging areas, cemetery and utility access, field turf and lawn protection.

Road mat is an advanced, high-strength composite with a specific gravity less than 0.5. Since the system can be assembled and disassembled quickly, it can be reused many times during its long-

term durability, which makes it a very cost-effective option. Different types of construction mat and their uses are demonstrated in Figure 2.23.

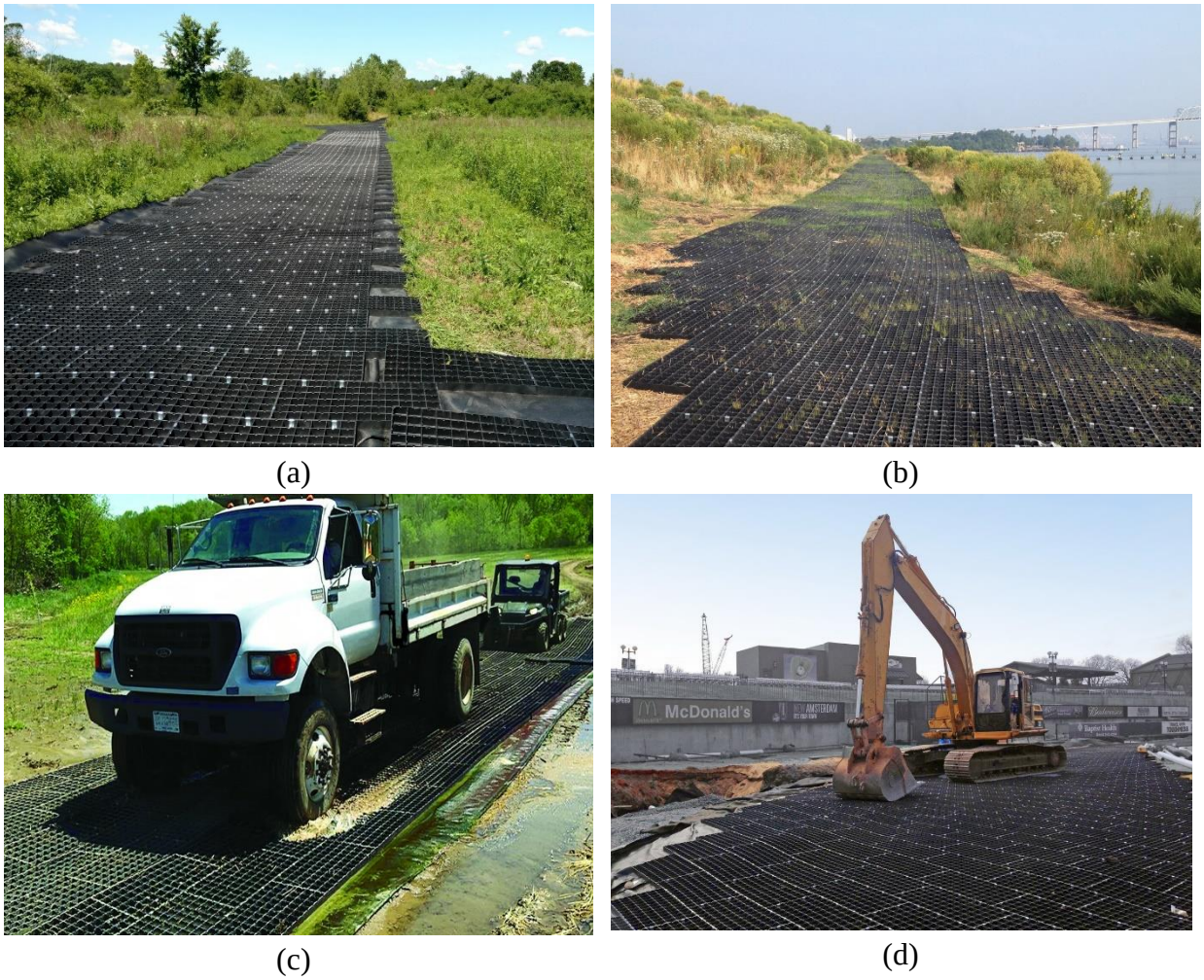

Figure 2.23: Different type's uses of construction mats. (a) site access over soft ground; (b) Minimal disturbance in environmental areas beside river; (c) heavy equipment access over wet ground (d) temporary site access and turf protection (Source: Presto Geosystems; https://www.prestogeo.com)

2.7.2.2 Geogrid stabilized working platform

Inclusion of a number of layers of stiff geogrids within a layer of sand, the load carrying capacity of that layer in a footing situation could be increased by a factor of 2.5 over the same section

without geogrid (Guido, Kneuppel, & Sweeney, 1987). A large-scale laboratory test by Watts & Jenner (2008) to assess the performance of a geogrid stabilized granular working platform concluded that the use of 2 layers of geogrids significantly increase the bearing capacity of working platforms. The research showed that the triangular pattern geogrid (TriAx®) with near-uniform radial tensile stiffness outperformed the biaxial geogrid and doubled the bearing capacity of the granular blanket without geogrid. A composite material is created by adding one or more layers of geogrid to granular layers, and this composite material is sometimes referred to as a "mechanically stabilized layer". The interlocking mechanism, as shown in Figure 2.24, which restrains the movement of aggregate particles within the geogrid apertures is identified as the lateral confinement effect that can be mobilized from a stiff geogrid. Through the interlocking mechanism and lateral confinement, the aggregate layer can be stabilized without excessive deformation of the surface.

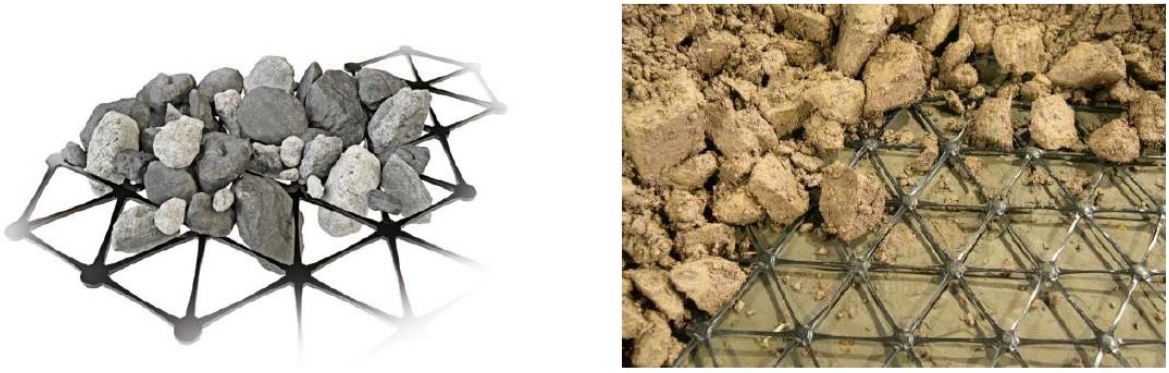

Figure 2.24: Interlocking mechanism of stiff geogrid providing lateral confinement and stabilization (Dobie et al. 2018)

2.7.2.3 Cellular foundation mattresses

Apart from using an MSL, the cellular foundation mattresses can also be used in working platform construction. A cellular foundation mattress is normally 1 m thick, consisting of a series of

interlocking cells formed using stiff polymer geogrids to contain and confine granular material providing a stiff and rough foundation to an embankment see Figure 2.25. It allows for mobilization of the maximum bearing capacity from the soft foundation soil and forms a stiff and stable working platform which supports the movement of construction plant (Ong & Dobie, 2013). It should be noted that a cellular foundation mattress is self-contained and normally does not need external anchorage beyond the embankment base whereby the conventional construction with high strength reinforcement geotextiles would require provision of anchorage length.

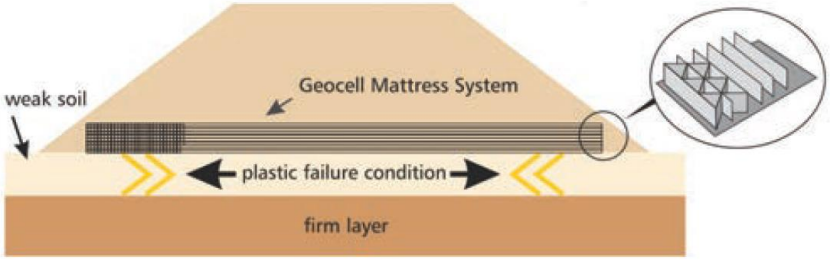

(a)

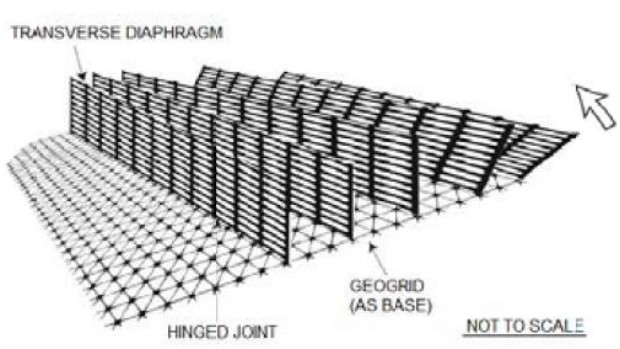

(b) (c)

Figure 2.25: Cellular mattress over soft ground: (a) Cross-section of cellular mattress; (b) SSchematic diagraam of cellular maattress fabrication; (c) Cellular mattress fabricated at project site (Ong & Dobie, 2013)

2.8 Review of analytical solution of pipe supported embankment

The construction of embankments on soft ground requires consideration of stability and settlement. Researchers have conducted several methods for prediction settlement and bearing capacity of embankment base. All of the methods can be categorized into three different approaches; analytical, empirical, and numerical (finite element) methods. Empirical methods are based on mathematically or statistically obtained values from previous projects. Regression is used as a common tool in this method to find out relationship among different parameters. Analytical methods use classic soil mechanics theory for evaluating stability using soil and pile parameters. However, its applicability is dependent on the mathematical assumptions based on boundary conditions. Several researchers all over the world have developed numerous methods for the optimization of embankment design (Terzaghi 1943; Low et al. 1994; Cao et al. 2006; Chen et al. 2008; Dev 2010; Zhang et al. 2012; Almeide et al. 2019).

Theoretical analysis along with model tests were conducted by Low et al. (1994) in order to investigate the arching in embankments on soft ground supported by pile. An alternative piled embankment system using cap beams and geotextile was investigated. Arching is said to occur whenever the vertical stress on the soft ground is less than γH.

$$\text{Efficiency, } E = \frac{P_c}{A\gamma H} \tag{2.3}$$

$$\text{Competency, } C = \frac{P_L}{a\gamma H} \tag{2.4}$$

$$\text{Stress reduction ratio, } SRR = \frac{P_S}{(A-a)\gamma H} \tag{2.5}$$

P_c = Load on one pile cap

P_s = Load on the soft ground area A-a

A = Tributary area of one pile cap

a = Area of one pile cap

The efficiency is then determined by the amount of sand placed on top of the top cap beams. Competency is the ratio of the load on the cap beam to the weight of a column of soil having the same width as the cap beam. The stress-reduction ratio is the ratio of the actual average vertical stress on the soft ground to the total embankment load. If there is no arching, efficacy is equal to (a/A) x 100%, and competency and the stress-reduction ratio both equal 1.0.

From the model test results, Low et al. (1994) concluded that efficacy increases with increasing area ratio and competency increase with increasing cap-beam spacing but is likely to approach a limiting value at large spacing. As H/s' increases, arching occurs and stress reduction ratio decreases. A constant value is reached at large H/s' ratios. Furthermore, the geotextile increases efficacy by 1.15-1.3 times that without efficacy.

Theoretical analysis of piled embankment with geotextile was conducted by Low et al. (1994) considering plane strain soil arching above cap beams. The deformed shape of geotextile is idealized to be a circular arc of radius R with a subtended angle 2θ and a maximum displacement t. The geotextile is assumed fixed at the edges of the caps. The circular arc assumption was used by Fluet et al. (1986) and Van Impe (1989). The theoretical solutions can be summarized in Figure 2.26. The dimensionless parameter η (equal to DK_G/s'^2M) may be regarded as a scaled stiffness ratio: The value of η increases with the ratio of the geotextile (axial) stiffness to the soft-ground stiffness.

The stress reduction ratios without geotextile (SRR) and with geotextile (SRR_G) was derived as following:

$$SRR = \frac{\sigma_s'}{\gamma H} \tag{2.6}$$

$$\text{SRR}_G = \frac{\sigma_s' s' - 2K_G(\theta - sin\theta)}{s'\gamma H} \tag{2.7}$$

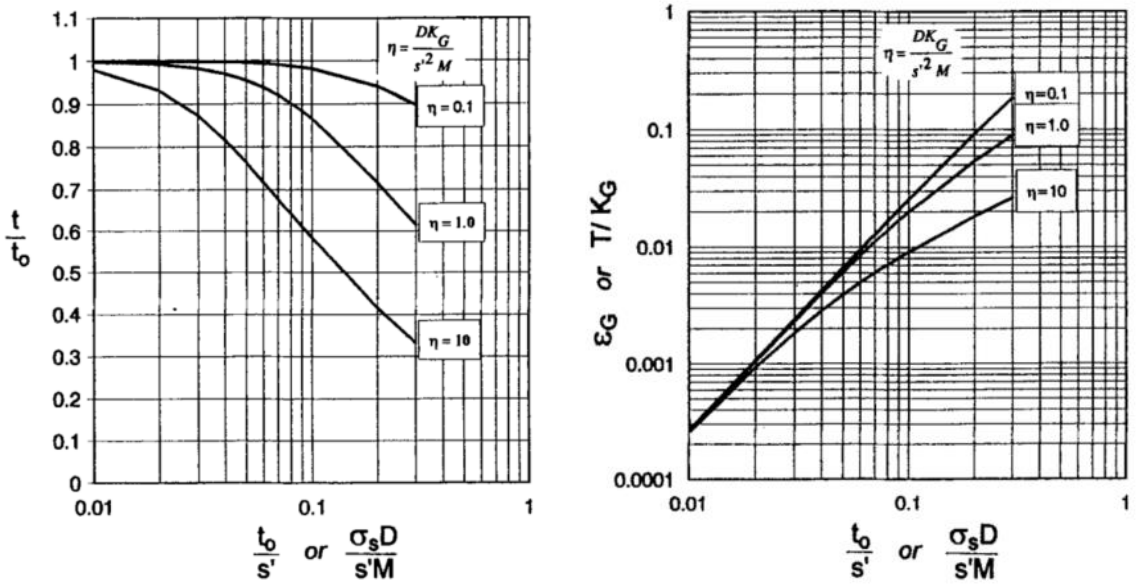

(a) (b)

Figure 2.26: (a) Theoretical settlement reduction ratio t/t_0 (b) Theoretical geotextile strain, ε_g (Low et al. 1994)

An analytical model of piled reinforced embankments based on the principle of minimum potential energy was investigated by Cao et al. (2006). The assumptions of the model are axisymmetric model, single pile with equivalent area. Effect of pile spacing, embankment height, cap size, shear modulus of embankment fill and geotextile stiffness are investigated. The pile efficacy was derived as:

$$E = \frac{P_p}{Ah\gamma} = \frac{k_p A_2}{r_e^2 \pi h \gamma} \tag{2.8}$$

$$k_p = pile\ spring\ constant = \frac{G\ r_o}{f_1} \tag{2.9}$$

Where, G is the shear modulus of soil, r_0 is the radius of the pile and f_1 is given by Shen et al. (2000).

From parametric study of analytical solution, Cao et al. (2006) found that pile spacing to embankment height ratio, cap size to pile spacing ratio and pile-subsoil stiffness ratio have pronounced influence on pile efficacy. However, shear modulus of embankment fill has lesser effect and geotextile stiffness has little effect.

A theoretical and numerical analysis was conducted by Chen et al. (2008) to investigate how geosynthetics interact with pile walls and soft soil. The soil arching efficiency, the pile wall efficiency, the differential settlement of the embankment, and the distribution of tension force in the geosynthetics have been investigated with the consideration of four key influencing factors: the elastic modulus of the pile wall, the tensile stiffness of the geosynthetics, the height of the embankment fill, and the area ratio of the pile wall.

According to Chen et al. (2008a), two terms were used to describe the amount of arching in embankments: efficiency of soil arching (ESA) and efficiency of pile wall (EPW) respectively.

$$ESA = \frac{P_{em} b}{\gamma H s} \times 100\% \tag{2.10}$$

$$EPW = \frac{P_{pw} b}{\gamma H s} \times 100\% \tag{2.11}$$

$$P_{sem} = \frac{\gamma H - m P_{em}}{1 - m} \tag{2.12}$$

$$P_{em} = \gamma H + \gamma k_a \tan\varphi \frac{(2H - h_e)h_e}{b} + \frac{2c\left(1 - 2\tan\varphi \sqrt{k_a}\right)h_e}{b} \tag{2.13}$$

$$\Delta s = \frac{\gamma k_0 \tan\varphi \left[\frac{H^3}{3} - H(H - H_e)^2 + \frac{2(H - h_e)^2}{3}\right]}{(1-m)b\,E_m} \tag{2.14}$$

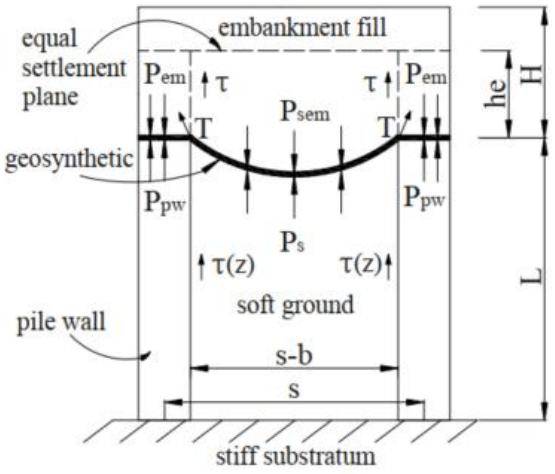

Figure 2.27: Load transfer mechanism (Chen et al. 2008a)

Where, P_{sem} = mean pressure of yield fill mass on geosynthetic; *m* is the area ratio, $m = b/s$; E_{em} is the Young's modulus of the embankment fill; *P* is the mean earth pressure in the stationary fill mass; k_a is the coefficient of Rankine's active earth pressure; φ is the friction angle of embankment fill.

Chen et al. (2008a) found that ESA and EPW increased with the elastic modulus of the pile wall, the height of the embankment fill, and the area ratio, but that tensile stiffness did not seem to affect ESA or EPW. Geosynthetics experience greater tension force with height of embankment fill, and the tensile stiffnesses and elastic moduli of pile walls decrease with increasing area ratios.

Using a closed-form solution with considerations of soil arching in the embankment fill, negative skin friction in the pile shaft, and foundation settlement, Chen et al. (2008b) derived a closed-form solution for one-dimensional loading. Their study involved determining the stress concentration at the top of the pile, axial loads and skin friction distributions, as well as the settlement of the

embankment. An axisymmetric unit cell model is illustrated in Figure 2.28. It consists of a pile and rigid cap, surrounded by foundation soil and embankment fill. Due to the soil arching effect, the differential settlement at the same elevation in the embankment decreases from the base of the embankment towards the top surface of the embankment and reaches zero differential settlement at an elevation of z = -h_e if the embankment is thick enough (Figure 2.28). This plane is known as the plane of equal settlement where the settlement and the vertical stress are equally distributed. The method suggested by Chen et al. (2008b) can determine the plane of equal settlement, the proportion of load carried by the pile and the settlement of the embankment.

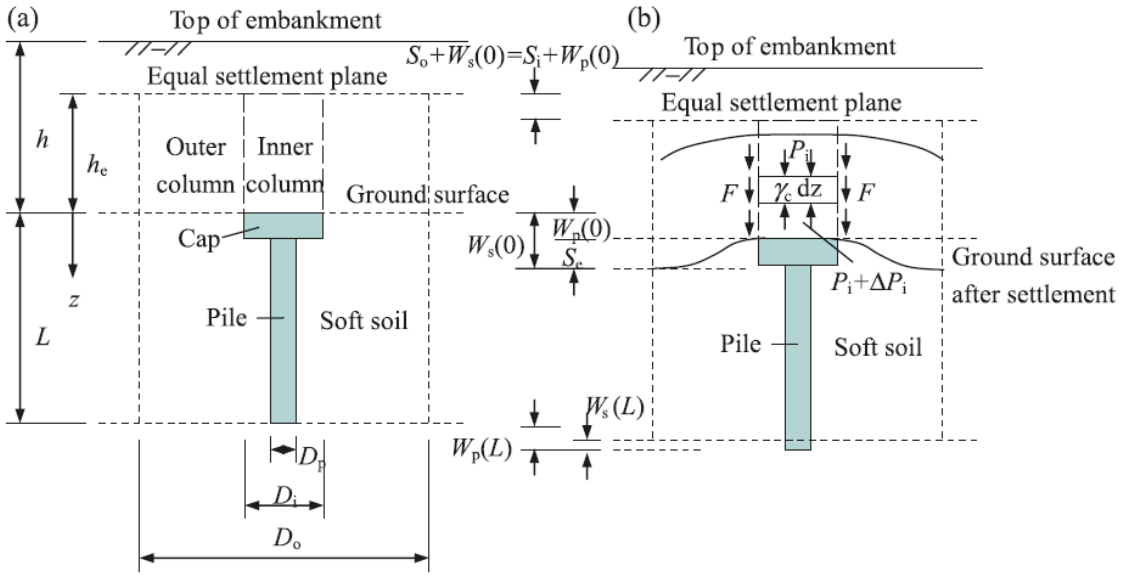

Figure 2.28: Analytical model for pile supported embankment. (a) Embankment before settlement; (b) Embankment ager settlement (Chen et al. 2008b)

Pasternak model concept was used by Deb (2010) to model the stone-column supported embankment. Where the soft soil was idealized by spring-dashpot system to include the time-dependent behavior. The stone columns and geosynthetic reinforcement are idealized by stiffer nonlinear springs and rough elastic membrane, respectively.

An embankment of granular fill that has been reinforced or piled with piles with granular fill on soft ground is analyzed by Zhuang et al. (2014) using a simplified model. The model is based on Hewlett & Randolph's (1988) arching effect in granular material. The improvements of the model are that the failure mechanisms of the arch both at the crown and at the pile cap were taken into account, three-dimensional situation was considered for reinforced piled embankment, calculation of the vertical stress carried by the subsoil due to arching effect and reinforcement for multilayered soil was proposed. On the basis of this simplified model, the influence of embankment height, one-dimensional compressive modulus of the subsoil, and stiffness of the reinforcement is investigated on stress reduction ratio (SRR) and tensile strength.

Using Hewlett & Randolph's method (1988), the regions where the arch fails to operate were either considered at the crown of the arch or at the pile cap. It was proposed by Hewlett and Randolph (1988) that the performance of pile supports at low embankment heights is determined by the condition at the crown of the arch relative to the spacing of the pile caps. The critical region moves on to the pile caps as the height of the embankment increases (Figure 2.29).

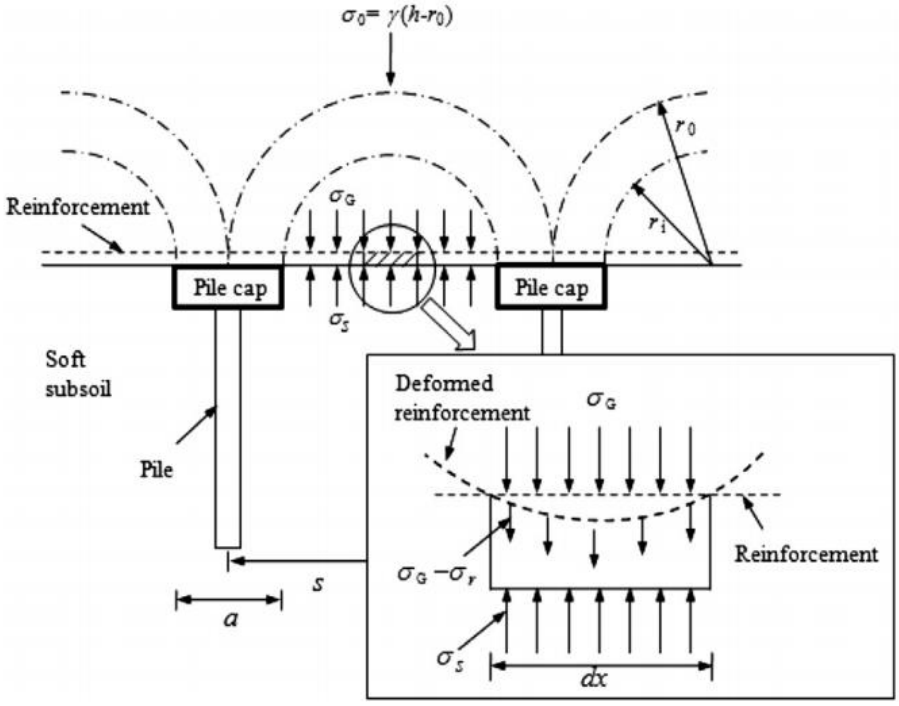

Figure 2.29: Stress analysis of the element at the centerline between piles

According to Zhuang et al. (2014), when the condition at the crown of arch is normative; the vertical stress at the base of the embankment:

$$\sigma_G = \frac{\gamma(s-a)}{\sqrt{2}}\left(\frac{2K_p-2}{2K_p-3}\right) + \gamma\left[h - \frac{s}{\sqrt{2}}\left(\frac{2K_p-2}{2K_p-3}\right)\right]\left(a-\frac{a}{s}\right)^{2K_p-2} \qquad (2.15)$$

When the condition at the pile cap is normative, the vertical stress at the base of the embankment:

$$\sigma_G = \frac{\gamma h}{\left\{\left(1-\frac{a^2}{s^2}\right) + \left(\frac{2kK_P}{K_p+1}\right)\left[\left(1-\frac{a}{s}\right)^{(1-K_p)} - \left(1-\frac{a}{s}\right)\left(1+\frac{K_p a}{s}\right)\right]\right\}} \qquad (2.16)$$

2.8.1 Stress reduction ratio (SRR)

Russell and Pierpoint (1997) suggested a method for calculating the vertical effective stress in a three-dimensional column-supported embankment application. Their expression is based upon the stress reduction ratio (SRR), which is defined as:

$$SRR = \frac{\sigma_{soil}}{\gamma H + q} \tag{2.17}$$

where σ_{soil} = stress in the embankment fill in an area not underlain by columns at the elevation of the column tops (in some design methodologies, σ_{soil} is used to design the geosynthetic reinforcement), γ = unit weight of embankment fill, H = height of embankment, and q = embankment surcharge.

The Adapted Terzaghi expression for SRR as it seems in Russell and Pierpoint (1997) is:

$$SRR = \frac{(s^2 - a^2)}{4aHk\tan\varphi}\left(1 - e^{\frac{-4aHk\tan\varphi}{(s^2 - a^2)}}\right) \tag{2.18}$$

where there is zero surcharge (q = 0), and s = center-to-center column spacing for a square arrangement of columns, a = width of square column, H = height of the embankment, K = lateral earth pressure coefficient with recommended value of 1.0, and φ = friction angle of the embankment fill.

Russell et al. (2003) suggested a value of K = 0.5 and considered the effect of a surcharge (q) on SRR which, for the ultimate limit state, is expressed as:

$$SRR = \frac{(s^2 - a^2)}{4aHk\tan\varphi}\left(1 - e^{\frac{-4aHk\tan\varphi}{(s^2 - a^2)}}\right) + \frac{q}{\gamma H + q}e^{\frac{-4aHk\tan\varphi}{(s^2 - a^2)}} \tag{2.19}$$

This method of determining the SRR for column-supported embankments is commonly called the Adapted Terzaghi Method. Both expressions apply to a square arrangement of square columns. In these expressions, the plan area of the yielding fill material (As) is equal to s^2-a^2 and the linear distance of column perimeter upon which this area acts is equal to one column perimeter or p = 4a.

Sloan et al. (2011) introduced the generalized formulation which allows for two layers of fill soil with properties of each layer defined as: $H_{1,2}$ = layer thickness, $\gamma_{1,2}$ = layer unit weight, $K_{1,2}$ = layer lateral earth pressure coefficient, $\varphi_{1,2}$ = layer friction angle. The embankment may have a surcharge, q. To simplify the expression for SRR, the following parameter can be defined as in Filz and Smith (2006):

$$\alpha_{1,2} = \frac{p\, k_{1,2} \tan \varphi_{1,2}}{A_s} \tag{2.20}$$

In the formulation of the generalized Adapted Terzaghi Method by Sloan et al. (2011), for $\alpha_{1,2} \neq 0$, the stress reduction ratio is given by:

$$SRR = \frac{\frac{\gamma_1}{\alpha_1}(1 - e^{-\alpha_1 H_1}) + \frac{\gamma_2}{\alpha_2} e^{-\alpha_1 H_1}(1 - e^{-\alpha_2 H_2}) + q e^{-\alpha_1 H_1} e^{-\alpha_2 H_2}}{\gamma_1 H_1 + \gamma_2 H_2 + q} \tag{2.21}$$

This formula for SRR allows up to two layers of embankment fill to be varied independently of unit weight, friction angle, height, and lateral earth pressure coefficient. It can be applied to any combination of column and unit cell geometries.

2.8.2 Analysis of load transfer platform

The load transfer platform (LTP) on column-improved soft soil was idealized using a mechanical model developed by Gosh et al. (2016). This model presents a simultaneous nonlinear and time-

dependent stress-strain model for soft soils, which incorporates LTP's negligible tensile strength and limited granular properties. The Winkler foundation accounts for nonlinearity through the use of a bilinear response of soil, and the cracked cross sections of granular layers represent the weak tensile strength of the materials, when compared to their compressive strength. Flexural analysis was conducted assuming the LTP as concrete beam with tension and compression occurs at the opposite site. The principle of superposition was applied to the development of the analytical solution to fourth-order complex nonhomogeneous differential equations.

2.9 Recycled plastic pin

The use of plastic has increased significantly over past few decades due to its relatively low production cost, high durability, and light weight. Plastics are usually synthetic or semi-synthetic organic polymers which have a high molecular mass and are produced from the chemical reaction of petrochemicals formed from fossil fuel. The governing differential equations were solved using a finite difference method. Results have been presented in a non-dimensional form. It was found that the height of embankment, degree of consolidation of soft soil, stiffness of the stone column material, spacing between the stone columns, use of geosynthetic reinforcement and properties of soft and embankment soils significantly influence the degree of soil arching. Specifically, soft soils with lower bearing capacities tend to arch more.

Recycled plastic pin (RPP) is manly made from recycled plastic materials. Some other materials like polymers, fly ash, saw dust (etc.) can also be used for RPP(Chen, Salim, Bowders, Loehr, & Owen, 2007). They are a made of a lightweight material and are less susceptible to chemical and biological degradation than other structural materials. RPP are installed in the failed areas to provide resistance along the slipping plane and increase the factor of safety. RPP have significant financial and environmental benefits for stabilizing shallow slope failures. Use of RPP for

engineering purposes is environment friendly especially for marine and water front application. In terms of life cycle cost analysis (LCCA), RPP is extraordinary since RPP behaves as inert material and does not degrade or react.

The RPP is an environmentally friendly material that requires minimal maintenance, resists moisture, corrosion, rot, and insects. Over half of the raw materials used for plastic lumber consists of polyolefins including high density polyethylene (HDPE), low density polyethylene (LDPE), or polypropylene (PP) (Hossain, Khan, & Kibria, 2017). As the polyolefin in the combination acts as an adhesive, it helps combine high melt plastics and additives such as fiberglass, wood fibers into a rigid structure. Moreover, additives, including foaming agents, ultra-violate (UV) stabilizers, and pigments, are added during the manufacturing process of recycled plastic lumber.

2.9.1 Manufacturing process of RPP

At the beginning of the production process, raw materials are collected, cleaned, and pulverized prior to being used for plastic lumber production. Roughly 600 mineral water/soda bottles are recycled for a single 4 in. x 4 in. RPP as shown in Figure 2.30 (Hossain et al., 2017). An extrusion machine at a production facility melts the resulting product. There are two processes by which recycled plastic lumber can be manufactured, such as the injection molding process and the continuous extrusion process (Malcolm, 1995).

Figure 2.30: Approximately 600 plastic soda bottles are used for one 4"×4" RPP

In the injection process, molds are used to define the shape and length of products, then molten plastic is injected into the molds and cooled uniformly. The product is removed after cooling. This is a relatively simple and inexpensive process; however, the production volume is limited (Malcolm, 1995). In contrast, continuous extrusion process can produce RPPs of varying lengths. During this process, a series of dies constantly extrude the molten plastic through a series of devices, shape the materials, and cool the resulting products. Nevertheless, it becomes difficult to maintain uniform and controlled cooling over the sample to avoid warping and caving of the lumber. Furthermore, a significant investment is required compared to injection molding. In contrast, the continuous extrusion process is less labor-intensive and well suited for mass production.

One of the widely used processes for manufacturing recycled plastic pins is compression molding (Lampo & Nosker, 1997). In this process, thermoplastics are mixed in batches of 50%-70% with other materials. To remove the melted material from the plasticator, a scraper is automatically adjusted before it is pressed through a heated extruder die into premeasured rolls. After processing

the loaves, the loaves are placed into the press-charging device, which alternately fills compression molds. After cooling to 40°C inside the mold, the finished products are ejected and placed on a conveyor for storage.

2.9.2 Properties of Recycled Plastic Pin (RPP)

In many cases, reinforcing members will fail due to the loads imposed by built structures and the stresses applied during field installation. These factors make engineering properties of reinforcing members of paramount importance. The engineering properties of commercially available recycled plastic members can vary greatly due to the variety of manufacturing processes and constituent mixes used in the manufacturing of recycled plastic products.

2.9.2.1 Compressive strength and flexural strength

Bowders et al. (2003) examined the different properties of RPP by evaluating a variety of production standards. The study included uniaxial compression testing and four point flexure testing. The results are shown in Table 2.3 and Table 2.4.

Compressive strengths of recycled plastic members varied from 11 MPa to 21 MPa with no cross-sectional area correction and examined at a nominal strain rate of 0.006 mm/mm/min. Compression moduli determined at 1% strain ranged from 552 MPa to 1310 MPa.

Flexural strengths for specimens loaded to failure or two percent center strain ranged from 9 MPa to 25 MPa under a nominal deformation rate 5.1 mm/min. Flexural moduli ranged from 621 MPa to 1724 MPa at 1% strain, similar to the values observed in the uniaxial compression tests with the exception of the fiberglass-reinforced material.

Table 2.3: Uniaxial compression test results of different RPP samples (Bowders et al., 2003)

Specimen Batch	No. of Specimen tested	Nom. Strain Rate (%/min)	Uniaxial Compressive Strength (MPa)		Young's Modulus, $E_{1\%}$ (MPa)		Young's Modulus, $E_{5\%}$ (MPa)	
			Avg.	Std. Dev.	Avg.	Std. Dev.	Avg.	Std. Dev.
A1	10	-	19	0.9	922	53	390	27
A2	7	0.005	20	0.8	1285	69	378	15
A3	6	0.006	20	0.9	1220	108	363	27
A4	3	0.004	20	0.9	1377	165	363	25
A5	4	0.006	12	1	645	159	225	17
A6	4	0.006	13	0.9	786	106	238	34
B7	2	0.007	14	0.5	541	36	268	3
B8	2	0.006	16	0.4	643	1	308	0.5
C9	3	0.0085	17	1.1	533	84	387	40

Table 2.4: Four point bending test results of various RPP samples (Bowders et al., 2003).

Specimen Batch	No of Specimens Tested	Nom. Def. Rate (mm/min)	Flexural Strength (MPa)	Secant Flexural Modulus $E_{1\%}$ (MPa)	Secant Flexural Modulus $E_{5\%}$ (MPa)
A1	13	-	11	779	662
A4	3	4.27	18	1388	-
A5	3	5.74	11	711	504
A6	4	3.62	10	634	443
B7	1	4.05	9	544	425
B8	1	5.67	-	816	-
C9	2	3.21	12	691	553

A comparative experimental study was conducted by Lampo and Nosker (1997) following ASTM 695-85. Compressive strength tests of Recycled Plastic Lumber were done on a total of 10 plastic samples, obtained from eight manufacturers having great variation in composition. The study calculated the material's mechanical properties based on the effective cross-sectional area based on the specific gravity measurement. The authors stated that the compressive strength test was performed at 0.1 in/min rate. From the experimental outcomes, the modulus, ultimate strength at 10% strain and yield strength at 2% offset were determined from the load-displacement data.

Table 2.5: Engineering properties of RPP obtained from different literature

Reference	**Uniaxial Compressive strength (MPa)**	**Young's Modulus, $E_{1\%}$ (MPa)**	**Flexural Strength (MPa)**	**Secant Flexural Modulus, $E_{1\%}$ (MPa)**
Chen et al. (2007)	11-20	580-1280	9-25	620-1675
Loehr & Bowders (2007)	11-21	552-1310	9-25	621-1724
Ahmed (2012)	17-21.7	344-386	16.5-32.4	1310-1379

2.9.2.2 Creep behavior of RPP

The softening of RPPs can be related to creep under sustained loads, just as it is with all polymeric materials. There are two types of creep behavior, compression creep and flexural creep. Figure 2.31 illustrates the typical deflection versus time plot for compression creep testing. After all specimens were loaded, primary creep had been completed within one day. Primary creep was followed by secondary creep, which lasted about a year. Results indicate that the specimens progressed steadily through the secondary creep stage. The creep stresses ranged from 690 to 827

kPa for the RPP specimens, and the ratio of creep stress to compressive strength varied from 4 to 6 percent, a low creep stress.

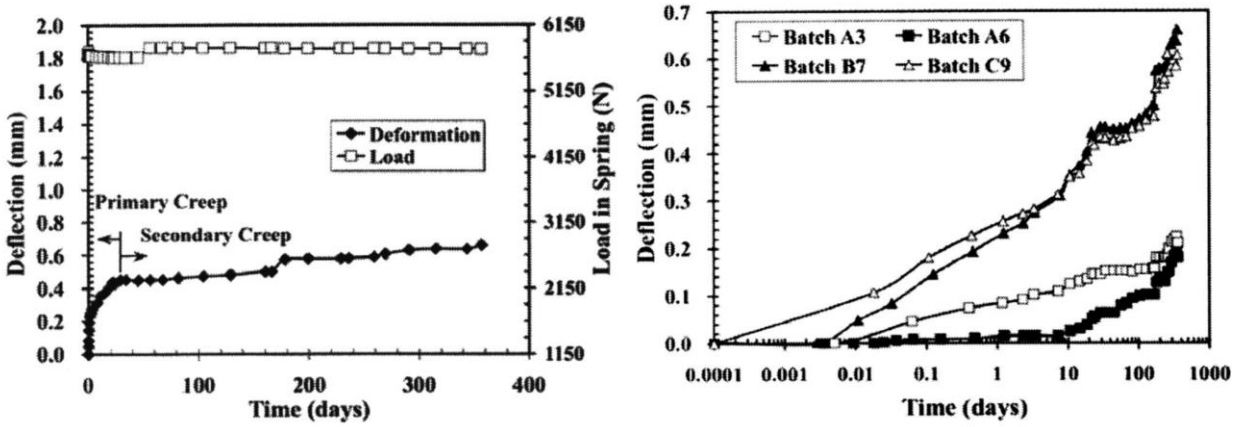

Figure 2.31: (a) Typical deflections under constant axial stress versus time of RPP (b) Deflections versus time of compressive creep tests (Chen et al., 2007)

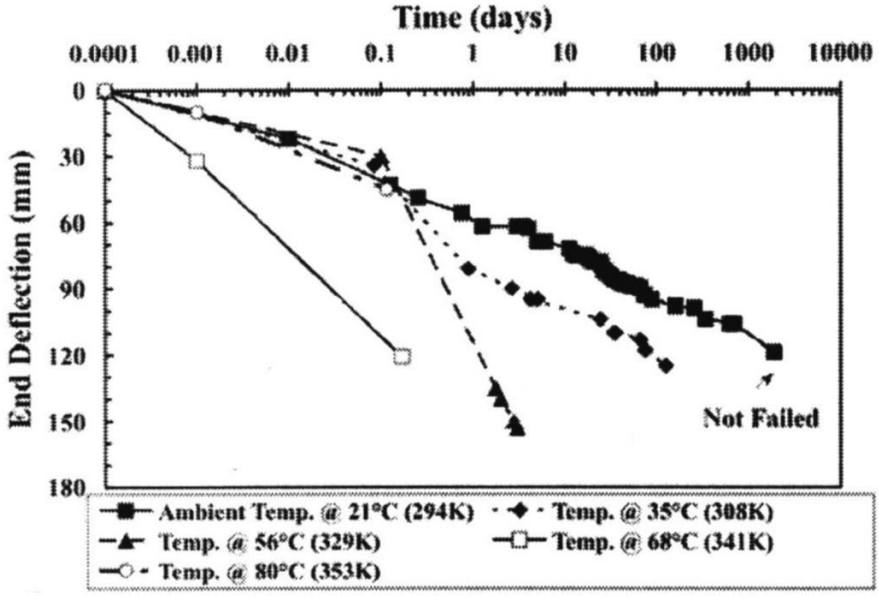

Figure 2.32: Deflection versus time response for RPP loaded with 222-N at free end of simple cantilever (Chen et al., 2007)

Accelerated creep bending tests have been conducted by Bowders et al. (2003). Based on the results of these tests, the time until creep failure occurs at the I-70–Emma site is approximately several hundred years. Therefore, on the basis of the available data, creep does not constitute a significant problem.

2.10 Limitations of the previous studies

Different ground improvement techniques are available to improve soft foundation soil such as removal, re-compaction, and replacement of existing ground soil, cement or lime stabilization, use of stone columns, sand piers, and so on. The most common method used by TxDOT is to remove and replace the existing soil with competent soil. However, this is extremely expensive and time-consuming solution. Steel and concrete piles have also been used which have similar disadvantages. A current advancement of the pile supported foundation system is to integrate geosynthetic sheet as basal reinforcement. The use of geosynthetic reinforcement increases the stability of the system by facilitating the soil arching effect. These solutions are also expensive and often use virgin material. So, instead of using piles of virgin materials, use of Recycled Plastic Pins can be viable alternative. As use of recycled plastic pin is a sustainable and cost-effective solution, further investigations are required to use it for improving the bearing capacity of embankment foundation soil. However, the design technique is limited, and no comprehensive study was conducted over the important parameters that should be considered during the design. Therefore, detailed investigation for evaluating the effectiveness of RPPs having different size and spacing is required to develop a sustainable and effective design protocols.

CHAPTER 3

PERFORMANCE EVALUATION OF RECYCLED PLASTIC PIN SUPPORTED EMBANKMENT OVER SOFT SOIL

This chapter has been published as:

Islam, M. A., Hossain, M. S., Badhon, F. F., & Bhandari, P. (2021). Performance Evaluation of Recycled-Plastic-Pin-Supported Embankment over Soft Soil. *Journal of Geotechnical and Geoenvironmental Engineering (ASCE)*, 147(6), 04021032.

ABSTRACT

This paper investigates the efficacy of Recycled Plastic Pins (RPP) for controlling ground settlement of soft foundation soil. Two field test sections (6 m × 7.5 m) were constructed over soft soil; one was left unreinforced to use it as a control section, and the other section was reinforced with RPPs. A Load Transfer Platform (LTP), composed of Recycled Crushed Concrete Aggregate (RCCA), sandwiched between two geogrid layers, was placed above the RPPs for transferring load from embankment onto the RPPs. Vertical pressures, settlements, and pore water pressures were monitored. After 260 days, a maximum settlement of 52 mm was observed for the control section, whereas, for the reinforced section, it was 23 mm. Excess pore pressure dissipated faster in the control section. The measured data indicated that the RPP supported a significant percentage of the embankment load. The in-situ measurements have proven the effectiveness of RPPs in combination with LTP in reducing settlement. The present method can be applied for any embankment construction over soft soil, bridge approaches, and widening of a highway where the foundation soil is unsuitable for regular construction.

Keywords: Recycled Plastic Pins, Embankment, Load Transfer Platform, Settlement, Soft soil, Consolidation.

3.1 Introduction

The use of embankments has been increasing nowadays for highway and railway construction. Due to rapid urbanization, embankments need to be constructed on both suitable and unsuitable locations. Designing embankments over soft foundation soils is a great challenge, especially for excessive settlements and bearing capacity failures (Xu et al. 2016). Specific techniques need to be applied for improving the serviceability of the embankments that are built over soft soil. Due to some strict requirements regarding total and differential settlement, piles are often used to support embankments.

The use of piles in conjunction with geosynthetics is a useful improvement technique for soft soil conditions. The advantages of using pile-supported earth platforms are rapid construction without preloading and easily controlled vertical and lateral deformation (Han and Gabr 2002). Different types of piles can be used, such as concrete piles, drilled shafts, vibro-concrete columns, controlled modulus columns, rammed aggregate pier, sand compaction pile, etc. Chen et al. (2010) described a field study where Y-shaped piles were used to support the embankment in China. The field measurements of pressure coming on top of piles and top of soils, differential settlement, and pore water pressure indicated the effectiveness of the pile-supported embankment technology. Hong et al. (2014) performed full-scale experiments on embankments with beam foundations supported by piles. The authors concluded that piles accompanied by beams at closer spacing could significantly reduce the settlements of piled embankments.

The use of recycled plastic has gained popularity as a sustainable method for soil stabilization in different geotechnical applications (Ujankar et al. 2020). Among the other ground improvement methods, the use of Recycled Plastic Pins (RPP) is a new technology. RPPs were initially used in Iowa and Missouri as a low-cost sustainable alternative for stabilizing highway slope(Hossain et

al. 2017). Nowadays, RPPs are being utilized in many other states of the USA as a cost-effective technology for slope stabilization (Khan et al. 2016; Hossain et al. 2017). The material used for RPP fabrication is mainly recycled plastics; some other materials like polymers, sawdust, and fly ash can also be added (Chen et al. 2007). RPPs are made of lightweight material. They offer excellent resistance against corrosion and biological degradation than concrete and steel piles. Compressive strengths and compression moduli of RPPs could vary from 11 MPa to 21 MPa and 552 MPa to 1310 MPa, respectively (Bowders et al. 2003).

For transferring the embankment load to stiffer soil strata, a load transfer platform (LTP) can be placed above the piles. This platform, composed of aggregate, gravel, or ballast, routinely consists of one or more layers of geosynthetics, which helps to transmit the surcharge load to the piles and to decrease the settlement (Abdullah and Edil 2007; Han and Gabr 2002). Analytical and numerical studies of load transfer platform have been conducted by numerous researchers (Han and Gabr 2002; Michalowski et al. 2018; Zhang et al. 2020). Demir et al. (2013) conducted field investigations to study the effectiveness of geogrid reinforced soil footings. It was found that the compacted granular fills sandwiched between two geogrid layers enhanced the bearing capacity of the foundation up to 130%. Briancon and Simon (2012) conducted several field tests of pile-supported embankments over weak foundation soil. The authors observed that the LTP with two geosynthetic layers provided more uniform stress distribution compared to a single geotextile layer.

Even though RPPs have been used for many years for slope stabilization, the lack of extensive field studies remains one of the major obstacles limiting its wider use, such as for improving the bearing capacity of weak foundation soil. Furthermore, the mechanism of load transfer depends on several factors, for example, the elastic modulus of piles, height of embankment, stiffness of

geosynthetics, and configuration of LTP. The influence of these factors is intertwined and complex, especially for RPP supported embankments. There is limited literature regarding the behavior and performance of RPP supported embankments in field-scale studies (Zaman 2019). Therefore, the understanding of RPP supported embankment for safe and economical design and construction must be investigated. The objective of this article is to evaluate the effectiveness of RPPs to improve the bearing capacity of soft soil beneath embankments. Field test sections were constructed and instrumented to monitor the performance of RPP supported embankment.

3.2 Methodology and instrumentation

3.2.1 Project Background and Site Soil Conditions

The project site is located at Irving, Texas (32°46'57.4"N, 96°56'19.0"W). For the site investigation, three boreholes were drilled, and soil samples were collected. The soil profile at the test section consisted of three main soil layers. The first layer of 0.6 m thickness was observed as a very soft layer with loose-fill materials and classified as lean clay according to the Unified Soil Classification System. The liquid limit and plasticity index were found as 22% and 10%, respectively. The following layer between the depth of 0.6 m and 2.4 m, was observed as sandy lean clay strata with low plasticity. The liquid limit and plasticity index varied between 30% to 32% and 16% to 24%. Starting from 2.4 m depth, the third layer was the Eagle Ford shale layer. The shale layer was high-plastic clay with low to medium compressibility. The water table was found 0.6 m below the existing ground level during boring. The index properties and SPT values of soil layers at various depths are shown in Figure 3.1. The particle-size distribution curves of the collected soil samples from different layers are presented in Figure 3.2. Direct shear tests, unconfined compressive strength tests, and 1D consolidation tests were performed on undisturbed

soil samples for determining the engineering properties of the soil layers. The soil layers were found as normally consolidated clay. The obtained results of soil parameters are shown in Table 3.1 Soil properties of subsoil and embankment fill. Based on the SPT values and laboratory test results, the most suitable soft location was selected for the test sections.

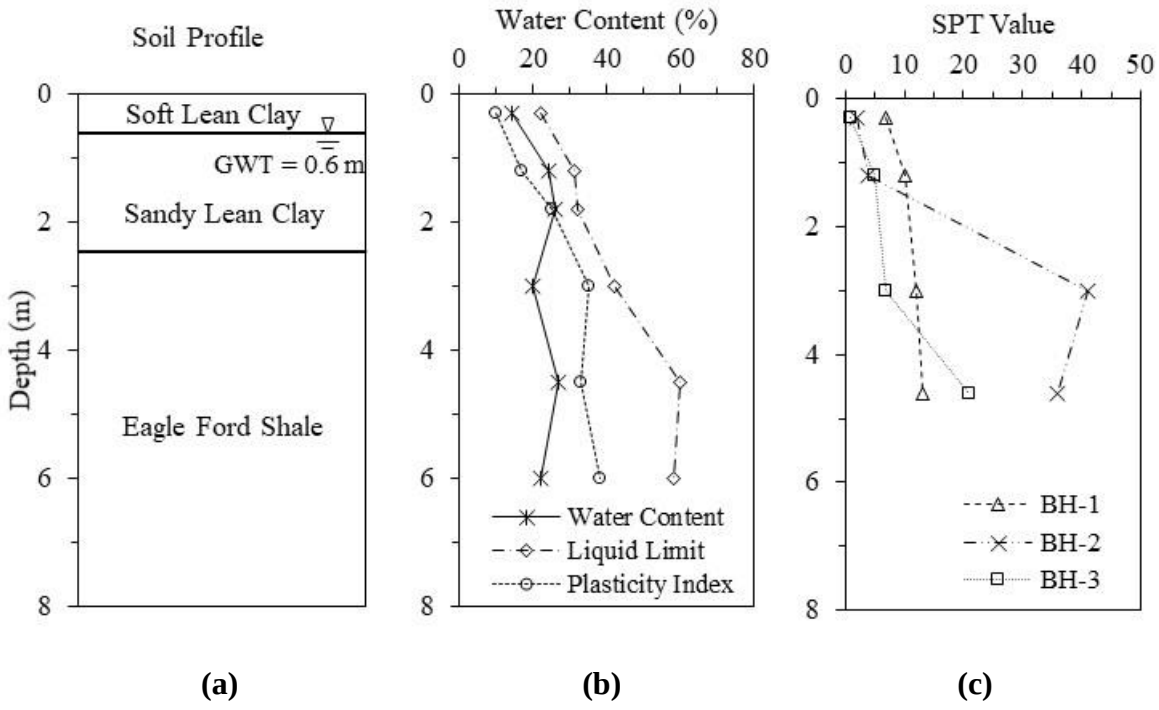

Figure 3.1 Physical properties of site soil

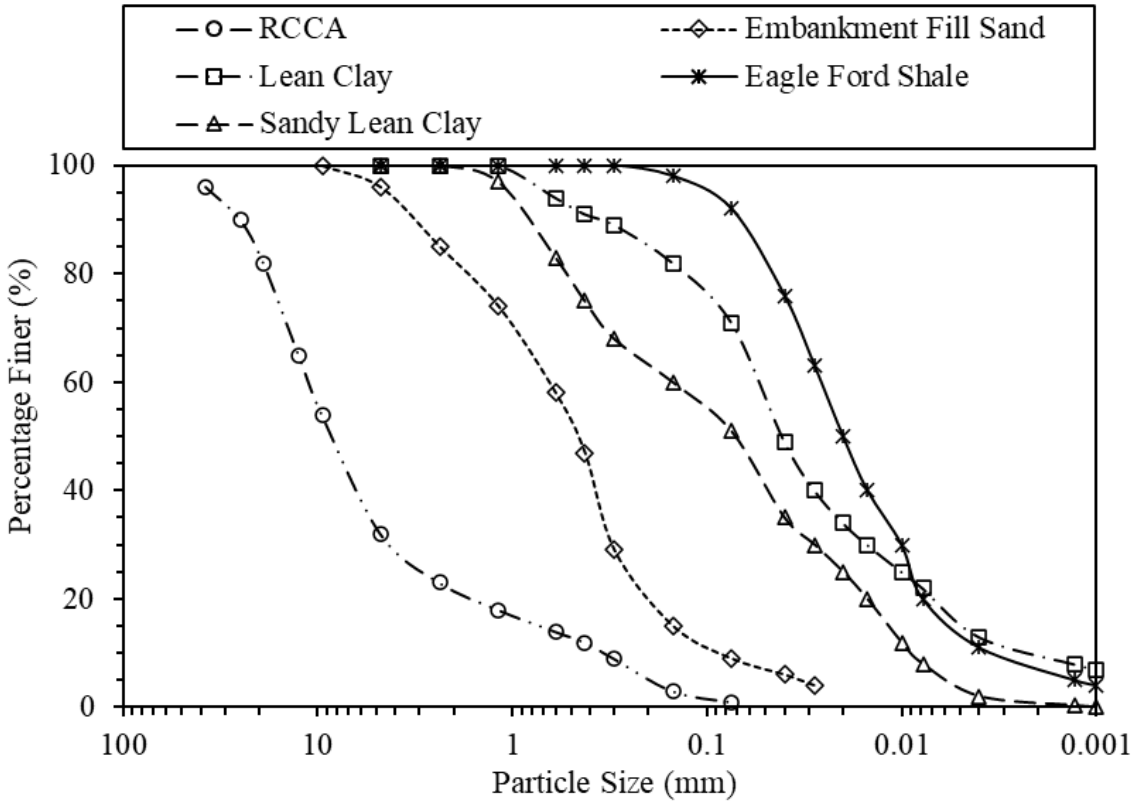

Figure 3.2 Grain size distribution curves

Table 3.1 Soil properties of subsoil and embankment fill

Material	T (m)	γ_d (kN/m^3)	q_u (kPa)	c_u (kPa)	φ' (°)	E (MPa)	k (cm/s)	C_c	c_v (m^2/day)
Embankment Fill	1.8	17.8	-	-	32	25	3.2×10^{-4}	-	-
Lean Clay	0.6	16.0	24	12	17	1.4	2.5×10^{-6}	0.28	0.015
Sandy Lean Clay	2.2	16.7	54	27	20	4.8	9.7×10^{-6}	0.20	0.02
Eagle Ford Shale	4.2	18.9	624	312	-	90	1.0×10^{-9}	-	-
RCCA	0.1	17.3	140	-	-	40.5	-	-	-

Note: T = thickness of soil layer; γ_d = dry unit weight; q_u = unconfined compressive strength; c_u = undrained cohesion; φ' = effective friction angle; E = modulus of elasticity; k = coefficient of permeability; C_c = coefficient of compressibility; c_v = coefficient of consolidation; RCCA = recycled crushed concrete aggregate

3.2.2 Ground Improvement Design and Construction Details

Two field test embankment sections were constructed to monitor the settlement, and the load transfer mechanism of RPP supported embankments. The length, width, and height of the test embankments were 7.6 m, 6 m, and 1.8 m, respectively, with a side slope of 1V:1.5H. One test section was reinforced with 3 m long (15 cm × 15 cm) RPPs. The properties of RPPs are presented in Table 3.2 Engineering properties of Recycled Plastic Pin. The detailed design of the test sections is shown in Figure 3.3 Layout and design of reinforced section and control section.

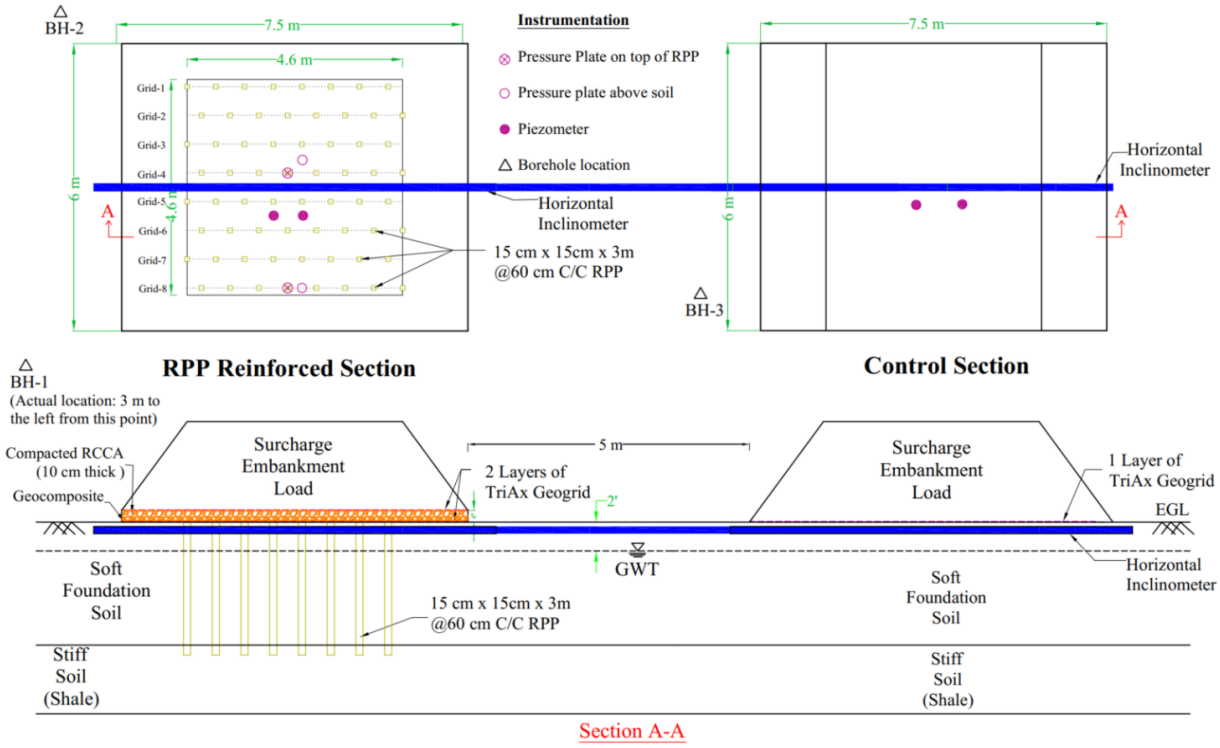

Figure 3.3 Layout and design of reinforced section and control section

3.2.2.1 *RPP Installation*

The installation of RPPs was conducted during May 2019. A total of 64 RPPs (15 cm square size) were installed in a staggered configuration with an on-center spacing of 60 cm. The RPPs were driven into the ground using a conventional track excavator equipped with a hydraulic breaker hammer, as shown in Figure 3.4 (b).

Table 3.2 Engineering properties of Recycled Plastic Pin

Parameter	Value[a]
Cross-section	15 cm × 15 cm
Length	3 m
Modulus of Elasticity (MPa)	1170
Compressive Strength (MPa)	31
Tensile Strength (MPa)	24.9
Specific Gravity (g/cc)	0.93
Coefficient of Friction-Static	0.253
Coefficient of Friction-Kinetic	0.175

[a] RPP properties (estimated from the manufacturer and Bowders et al. 2003).

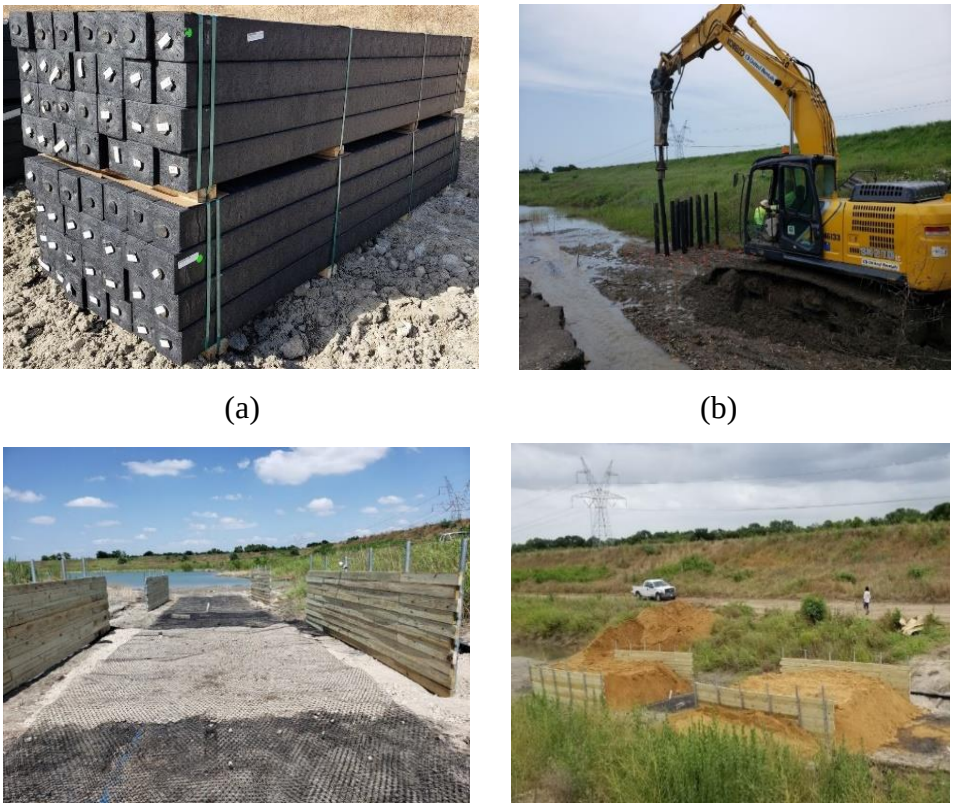

(a) (b)

(c) (d)

Figure 3.4 Construction of field sections: (a) 3 m long (15 cm×15 cm) RPPs; (b) Installation of RPPs; (c) Construction of LTP; (d) Application of surcharge load (Images by Md Azijul Islam)

The average driving time, penetration rate, and installation time of RPPs were recorded and presented in Table 3.3. The maximum penetration rate was found as 1.19 m/min, while the minimum was found as 0.12 m/min. Since there was a shale layer with high shear strength at a depth of 2.4 m, the resistance to drive the bottom 0.9 m of RPPs was higher. Therefore, it required more time and driving energy for driving the bottom 0.9 m of RPPs. The average machine maneuvering and mobilization time was found 4.5 min for each RPP installation. This time is high compared to the other study sites (Khan et al. 2016 and Zaman et al. 2019) since the current site location was quite soft compared to the other sites, due to which it was difficult to maneuver the machine. The average penetration rate was 0.69 m/min, which implied that one RPP (3 m long) could be installed within 4.5 minutes. With the consideration of machine maneuvering and mobilization, the average installation rate was found 0.32 m/min. Thus, 60-70 RPPs can be installed in one day for a similar type of site condition.

3.2.2.2 *Construction of Load Transfer Platform (LTP)*

The design of the LTP was influenced by the results obtained by Briancon and Simon (2012) and Abdullah and Edil (2007). Based on the study of piled embankments reinforced with geosynthetics, Briancon and Simon (2012) concluded that the use of two layers of geogrid would provide the maximum efficiency of a piled embankment system because of its higher stiffness. Therefore, in this study, the geosynthetic reinforced LTP consisted of an aggregate layer sandwiched between two geogrid layers (Figure 3.3). In the context of sustainable engineering, Recycled Crushed Concrete Aggregate (RCCA) was selected as the aggregate layer in the LTP (Imtiaz 2020). The properties and grain size distribution curves of RCCA are given in Table 3.1 and Figure 3.2, respectively.

Table 3.3 Driving and penetration time of RPP installation

Average machine maneuvering and mobilization time (min)	Soil profile	Location of RPP	Average driving time* (min)	Total driving with maneuvering time (min)	Penetration rate* (m/min)	Average installation rate including maneuvering time (m/min)
4.5	Top 2.1 m (soft layer)	Grid-1	2.6	5.8	0.82	0.37
		Grid-2	2.3	5.5	0.93	0.39
		Grid-3	2.5	5.7	0.85	0.38
		Grid-4	1.9	5.1	1.12	0.42
		Grid-5	2.6	5.8	0.82	0.37
		Grid-6	2.3	5.5	0.93	0.39
		Grid-7	2.1	5.3	1.02	0.41
		Grid-8	1.8	5.0	1.19	0.43
	Bottom 0.9 m (shale)	Grid-1	1.4	2.8	0.65	0.33
		Grid-2	1.5	2.9	0.61	0.32
		Grid-3	1.8	3.2	0.51	0.29
		Grid-4	2.5	3.9	0.37	0.24
		Grid-5	2.1	3.5	0.44	0.27
		Grid-6	3.3	4.7	0.28	0.20
		Grid-7	2.7	4.1	0.34	0.23
		Grid-8	7.5	8.9	0.12	0.10

*Machine maneuvering time is excluded from driving rate

Tensar® TriAx® Geogrid was used for the construction of LTP. TriAx geogrid has isotropic stiffness characteristics and triangular aperture geometry. Therefore, it can dissipate the radial stress effectively, which results in an improved reduction of subgrade stresses. The properties of the geogrid are outlined in Table 3.4.

To facilitate drainage during the consolidation process, one layer of geocomposite was placed just above the RPPs. Above the geocomposite, a layer of geogrid was placed. One meter of lap length was maintained for the connection between two parts for both the geocomposite and geogrid. After

that, a 100 mm thick RCCA layer was placed and compacted with a tamping rammer. The top layer of geogrid was set, and thus the construction process of LTP was completed (Figure 3.4c).

Table 3.4 Engineering properties of geogrid

Parameter	Longitudinal/Transverse[a]	Diagonal[a]	General[a]
Structure			Triaxial
Aperture shape			Triangular
Rib shape			Rectangular
Rib pitch (mm)	40	40	
Mid-rib depth (mm)	1.2	1.2	
Mid-rib width (mm)	1.1	1.1	
Tensile stiffness @0.5% strain (kN/m)			225
Isotropic stiffness ratio			0.6
Junction efficiency (%)			93
Chemical degradation resistance (%)			100
UV-resistance (%)			70

[a]Properties were obtained from the manufacturer

3.2.2.3 *Application of Surcharge Load*

Two wooden walls were constructed facing each other for both the reinforced and control sections. The objective of the wall on two sides is to ensure uniform embankment loading over the soft foundation soil. The other two sides were kept open to put the surcharge load in 1V:1.5H slopes. The surcharge load was applied using silty sand material. At every 30 cm lift thickness of the surcharge load, the soil was compacted and leveled with a tamping rammer. After placement of a total 1.2 m surcharge load, the top surface was leveled, and a slope of 1V:1.5H was prepared for embankment shape (phase-1). After three months, another 0.61 m of sand was loaded above the two sections; thus, the total height of the surcharge load was 1.8 m (phase-2). The completed test sections after applying the surcharge load are shown in Figure 3.4(d).

3.2.2.4 *Instrumentation Plan*

To monitor the settlement and load distribution efficiency, the test sections were instrumented with horizontal inclinometers, piezometers, and pressure plates. A 25-m long continuous horizontal inclinometer casing was installed for both control and reinforced sections (Figure 3.3). One end of the inclinometer casing was fixed using 1-m deep concrete grouting. Field monitoring was conducted regularly for observing the settlement behavior of the foundation soil.

Four pressure plates were installed, two on RPPs, and two on adjacent soil between RPPs. Two pressure plates were placed in the middle of the section, while the other two were placed at the edge of the section, as shown in Fig. 3, to observe the pressure variation at two different locations. Piezometers were used for measuring excess pore water pressure and the depth of the groundwater table. A total of four driven point piezometers was installed in the site: two were installed at the RPP reinforced section, and the other two were installed at the control section (Figure 3.3). The piezometers were pushed through the soft ground to 0.9 m, 1.2 m, and 1.8 m depths. Since the groundwater table was found between 0.6 m to 2.4 m depth, the piezometers were driven into that zone. After installing the pressure plates and piezometers, the sensors were attached to a data logger for continuous data collection.

3.3 Results and Discussion

3.3.1 Settlement Profile of Test Sections

The settlement results from the inclinometer are presented in Figure 3.5. At the end of phase-1 loading, the maximum settlement of reinforced and control sections was 17 mm and 36 mm, respectively. The settlement in the control section was 53% more than the reinforced section. After phase-2 loading and 260 days of monitoring (5th March 2020), the maximum ground settlement in

the control section was found as 52 mm. In contrast, in the reinforced section, the maximum settlement was 23 mm. Comparing to the control section, the decrease in the settlement was 56% in the reinforced section.

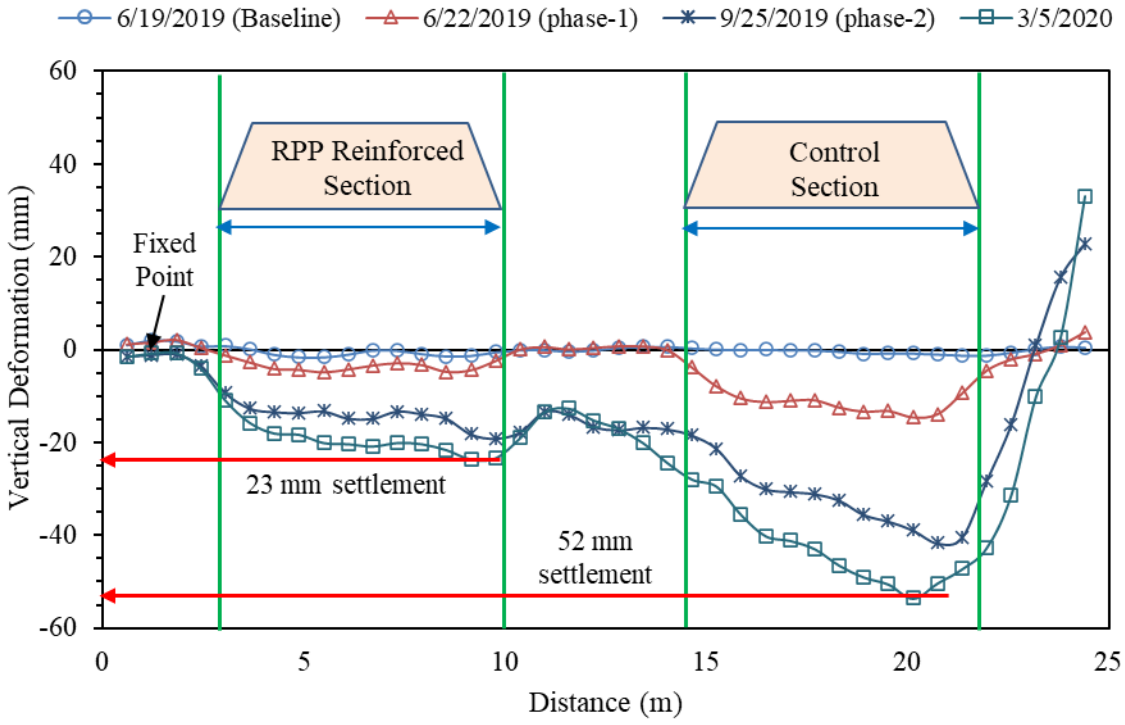

Figure 3.5 Settlement profile of control and reinforced section

Since the left end of the inclinometer casing was fixed, the maximum settlement was observed at the right side of both the sections rather than in the middle of the sections. At the end of the control section, a sharp rise of the curves was observed because of the free movement of that end. The settlement in the reinforced section was found almost uniform throughout the section, whereas more settlement was found towards the right edge of the control section. Although the distance between the two sections was 5 m, the reinforcing action of the RPP supported section might have some effect on the continuous inclinometer casing; thus, the settlement profile of the control section was not uniform.

The comparison of the settlement reduction with other literature was studied with respect to a common term 'settlement improvement factor (n)'. This term can be defined as the ratio of the settlement between the control section and the reinforced section (Elsawy and El-Garhy 2017) as follows:

$$n = \frac{S_{\max\,(control)}}{S_{\max\,(reinforced)}} \tag{3.1}$$

The effect of spacing to diameter ratio (s/d), and embankment height to clear spacing ratio (H/s'), on the behavior of geosynthetics, reinforced piled embankment was studied. Figure 3.6 (a) shows the comparison of n with s/d ratio for different field and numerical studies. From the present study, the n values were found to be 2.06 (H = 1.2 m) and 2.23 (H = 1.83 m) for s/d ratio of 3.75. Elsawy and El-Garhy (2017) conducted a numerical study of soft ground improved by granular pile supported raft foundation. The authors showed the variation of n with s/d, which is in close proximity to the current study. The results from other field studies (Abdullah and Edil 2007; Oh and Shin 2007; Bergado et al. 2009) provided a low value of n compared to this study. A numerical study was conducted by Han and Gabr (2002) using only one layer of geosynthetic, in which the settlement improvement factor was found only 1.12. The authors did not consider any LTP, which resulted in an exceptionally low n value. Oh and Shin (2007) conducted a field study on geogrid reinforced pile-supported embankments focusing on the effect of s/d ratio. Results from the present study differ only 24% compared to the results from Oh and Shin (2007). The variation of n with H/s' was also studied comparing with other literature (Fig. 6b). The n values of this study are consistent with the results obtained from Oh and Shin (2007) and Elsawy and El-Garhy (2017) with a maximum difference of 13%. The present study differs only 20% compared to the results

of Abdullah and Edil (2007). Compared to all other studies, the present study shows a high value of n, signifying the effectiveness of LTP and RPP system.

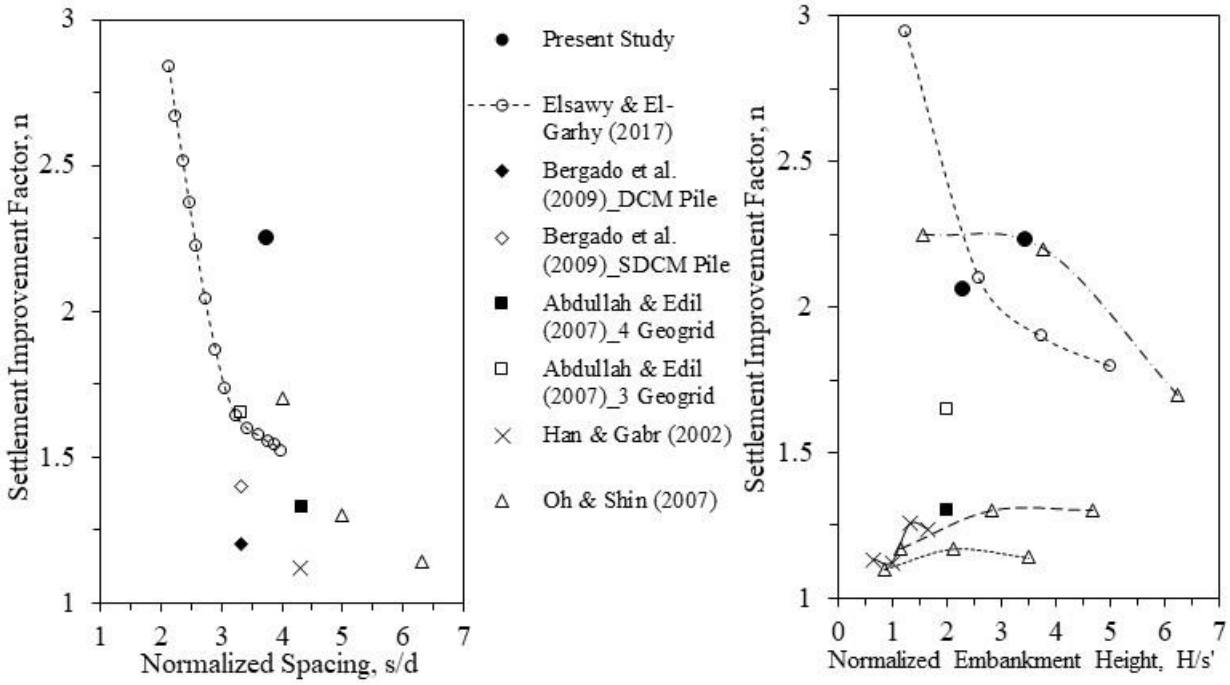

(a) (b)

Figure 3.6 Comparison of settlement improvement factor with other studies

3.3.2 Dissipation of Excess Pore Water Pressure

Piezometer data from different depths indicate the current pore pressure conditions of the test sections under surcharge loading. From the initial piezometer readings, it was found that the groundwater table was 0.56 m below the existing ground level, which was similar to the result obtained during the drilling. After applying the surcharge load, the pore water pressure increased suddenly due to the stress increase. In Figure 3.7, there is a sudden peak for each piezometer reading due to additional stress. With time, the pore water pressure dissipated slowly, and the increased stress converted from pore water pressure to effective stress. The excess pore water pressure at the control section at 1.2 m depth increased from 7 kPa to 17.8 kPa. The excess pore water pressure was found similar to the stress increase calculated from the Boussinesq charts. A

similar result was also found for the control section piezometer at 0.9 m depth. In contrast, the excess pore water pressure in the RPP reinforced section was less compared to the values obtained using the Boussinesq charts. This is because the surcharge load was transferred into the bottom layer of the soil through RPPs. Thus, the increased stress was distributed through the RPPs to deep stiffer strata, which would eventually decrease the ultimate settlement. Furthermore, the excess pore water pressure dissipated faster in the control section compared to the reinforced section, resulting in earlier primary consolidation settlement.

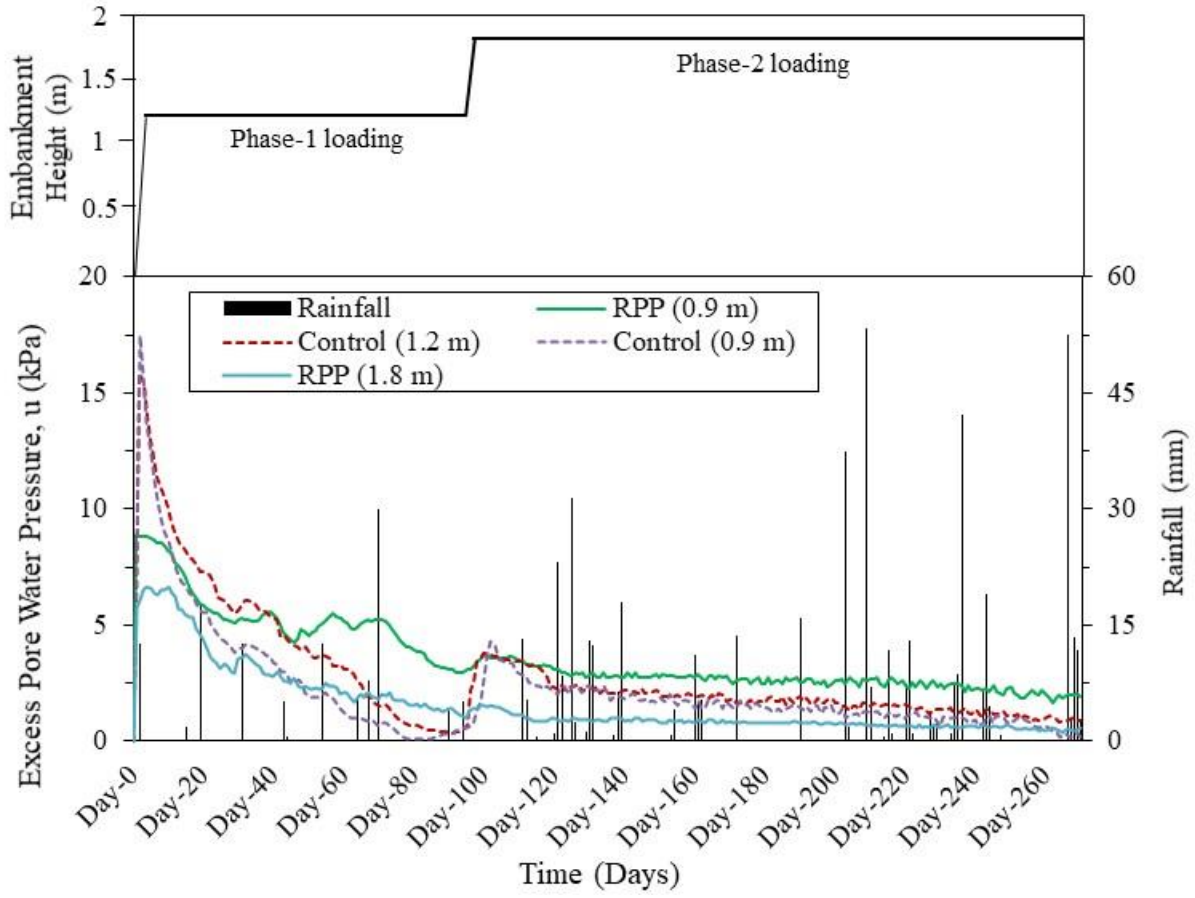

Figure 3.7 Dissipation of excess pore pressure with time

3.3.3 Comparison of Ground Settlement

The observed settlement results from inclinometer readings were compared with calculated settlements from analytical methods. For the control section, the primary consolidation settlement was calculated using the laboratory consolidation tests results. Subsequently, the time-dependent consolidation was also computed using Terzaghi's 1D consolidation theory (Terzaghi 1925). The computed settlements are shown in Figure 3.8. It is observed that, despite being slightly underestimated for the phase-1 loading and slightly overestimated for the phase-2 loading, the measured settlements were in good agreement with the calculated results, with the maximum differences within 20%. The ground surface settlement increases with the consolidation of the soft soil and then moves towards the ultimate primary consolidation settlement.

Zhuang and Wang (2017) developed a theoretical method to estimate the settlement of pile and soil for the reinforced piled embankment over weak foundation soil. The authors considered the load transfer mechanism accounting for soil arching and geosynthetics reinforcement along with the soil-pile interaction. Based on the nonlinear 1D consolidation theory (Davis and Raymound 1965), Zhunag and Wang (2017) derived the settlement of soil for a piled embankment over soft soil (w_s) as follows:

$$w_s(z) = 2.3\, m_v \sigma_0' \log\left(\frac{\sigma_0'}{\sigma_0' + q}\right) H_c \left[1 - \frac{z}{H_c} - \sum_0^{\infty} \frac{2}{M^2} \cos\frac{Mz}{H_c} e^{-M^2 T_v}\right] \quad (3.2)$$

where M = (π/2) (2m+1); m = an integer; T_v = time factor; m_v = volume compressibility, which can be computed as 1/ E_0 (Constraint modulus of soil); σ_0' = initial effective stress; q = surcharge pressure, and H_c = thickness of the soft layer.

The settlement of foundation soil for reinforced embankment was calculated using equation (2) and presented in Figure 3.8. It is observed that the theoretical solution of the reinforced section

overestimates the settlement by a maximum of 51% compared to the measured settlement results. The settlement obtained from a theoretical solution developed by Zhuang and Wang (2017) and Terzaghi (1925) for reinforced and control sections, respectively, in comparison with the measured settlements, are presented in Figure 3.9. The settlement prediction using Terzaghi (1925) method is in close agreement with the obtained field values of the control section. However, the predicted values of the reinforced section are higher compared to the measured values. Zhuang and Wang (2017) considered only one layer of geosynthetic reinforcement; however, in this study, LTP with higher stiffness was used, which can increase the efficiency of the load transfer mechanism. Therefore, RPP reinforced section, in addition to LTP, produced less settlement compared to the results obtained from the analytical solution of Zhuang and Wang (2017).

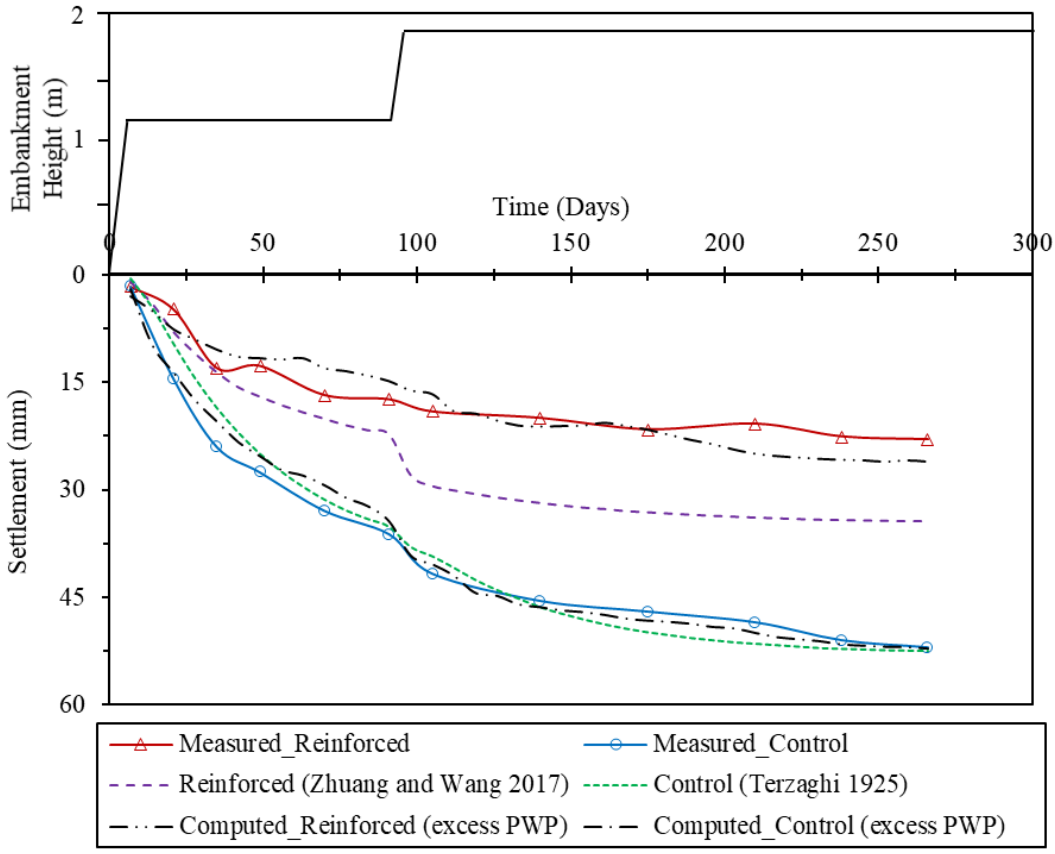

Figure 3.8 Comparison of calculated ground settlement with measured results

The settlements of the soft soil were also calculated from the excess pore water pressure dissipation using equation (2) and presented in Fig. 8. The measured data shows the trend of the settlement profile, which is similar to the results obtained from the piezometer data. The slight difference between the two settlement results might be caused by some heavy rainfall events shown in Figure 3.7. There was a slight rise in the excess pore water pressure curve due to the significant rainfall events. However, the maximum differences between field measured data and computed data from excess pore water pressure are found to be 15% and 23% for the control and reinforced sections, respectively.

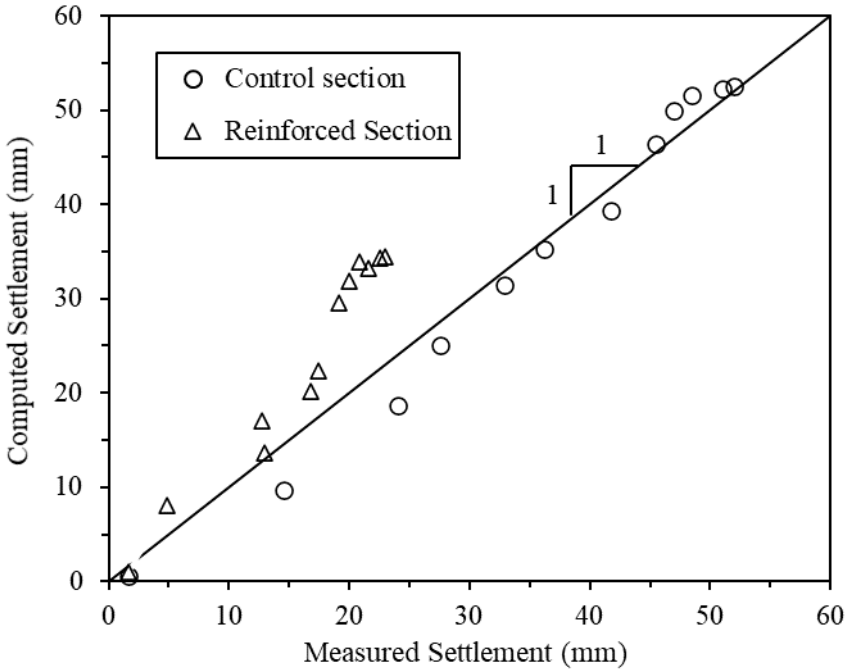

Figure 3.9 Comparison between measured settlements and computed values by Terzaghi (1925) and Zhuang and Wang (2017)

3.3.4 Load Transfer

The pressure variations on RPPs and soil are presented in Figure 3.10. During phase-1 loading, the pressure on RPPs was found to be about 32 kPa, whereas the pressure was found about 13.4 kPa on the soil. The average of the two positions was 23.8 kPa, which was close to the applied pressure.

The increase of average pressure on RPPs compared to adjacent soil was found to be 103% and 737% for phase-1 and phase-2 loadings, respectively. Since the edge pressure plates were at the edge of the loading where the 1V:1.5H slope starts, the applied pressure on this location was found less than the total surcharge pressure. The difference in pressure between RPPs and adjacent soil indicates the effective transfer of load onto RPPs. The pressure difference between RPPs and adjacent soil was found higher during phase-2 loading compared to phase-1. With the increase of embankment height, the arching mechanism became more active, which results in higher load distribution on RPPs. After the application of the phase-2 loading, the pressure on RPP jumped to 153.6 kPa, whereas pressure on soil increased slightly. Furthermore, the pressure on the middle RPP was found higher than the pressure at the edge of the section. The pressure difference in both middle and edge locations indicated that the load transfer on RPPs was effective for both locations, even though the LTP was discontinued beyond edge location.

The pressure on RPPs changes significantly with heavy rainfall events. At 203 and 209 days, there were two heavy rainfall events with an intensity of 37 mm and 53 mm, respectively. The pressure on the RPPs increased between 4% to 7% for both middle and edge location. Since highly permeable sandy soil was used as a surcharge load, the effect of saturation due to rainfall was temporary.

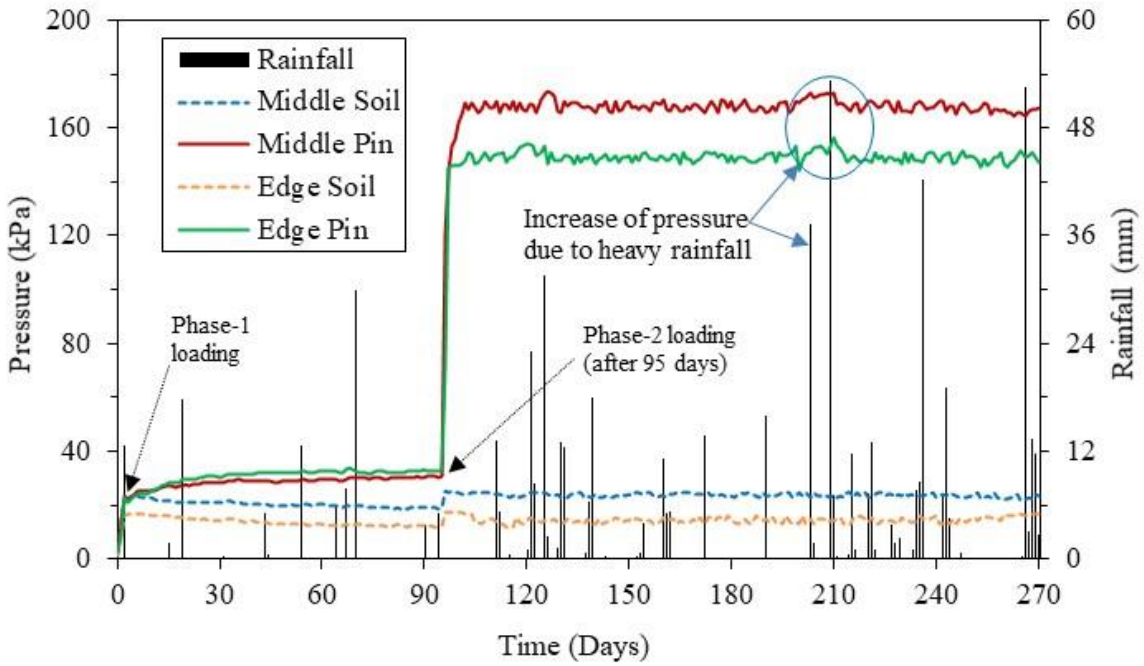

Figure 3.10 Pressure variation on RPP and adjacent soil in between RPPs

Zhao et al. (2019) reported a case study about a highway embankment project, where Prestressed Tubular Piles (PTC) and geosynthetics were utilized. The resulting embankment load was 91.2 kPa, and the average earth pressure on the soil was 42.2 kPa, which is about 46.3% of the embankment load. For the present study, the embankment load was 33 kPa, and the average earth pressure acting on the soil was 20 kPa, which is 54% of the embankment load. Zhao et al. (2019) also observed the average earth pressure on top of the pile as 279.7 kPa, which is 207% higher than the embankment load. The measured values from this study indicated that the RPPs experienced a 334% higher load than the embankment load. The higher value of load sharing indicates that RPPs, in combination with LTP, is more effective in distributing the embankment load to stiffer strata.

3.3.5 Comparison of Stress Reduction Ratio and Stress Concentration Ratio with Other Field Studies

Stress Reduction Ratio (SRR) and Stress Concentration Ratio (SCR) were calculated to analyze load distribution on RPPs. The SRR can be defined as the ratio of the average vertical stress applied on the ground surface between RPPs to the overburden stress due to embankment load and surcharge on the embankment (according to Low et al. 1994), expressed as

$$SRR = \frac{\sigma_s}{\gamma H + q_0} \tag{3.3}$$

where σ_s = average vertical stress applied on the ground surface between piles, γ = unit weight of embankment load, H = embankment height, and q_0 = surcharge load.

The Stress Concentration Ratio (SCR) can be defined as the ratio of measured vertical stress acting on the top of RPPs (σ_p) to that acting at the ground surface between the RPPs (Liu et al. 2012) and is given by

$$SCR = \frac{\sigma_p}{\sigma_s} \tag{3.4}$$

Using the terms, SRR and SCR, the load transfer mechanism can be quantified. A low value of SRR and a high value of SCR indicates the most effective load transfer from the embankment to the RPPs. The comparisons of SRR and SCR with different field studies are shown in Figure 3.11. Although the data are scattered, the SRR increases, and SCR decreases with an increase of s/d ratio. This trend follows the results obtained from Oh and Shin (2007). It is observed that the measured SRR value for the edge location is lower than the middle location and vice versa for the measured SCR values. The average SCR was found almost 8.3, which indicates the efficacy of the load transfer platform. Zhao et al. (2019) conducted a similar study of the PTC pile-supported embankment and found the value of SCR and SRR as 6.6 and 0.46, respectively. The measured

values of SRR and SCR for the middle location are in very close agreement with values obtained by Zhao et al. (2019) with a difference of only 12% and 10%, respectively. The results of SCR from Liu et al. (2007) is almost similar to the current study (11% difference), the results of SRR is much lower than Liu et al. (2007) with a difference of 46%. The maximum value of SCR and the minimum value of SRR were found for Chen et al. (2010) in which the authors used square pile caps along with tube piles, resulting in lower clear spacing. This comparison proves the efficiency of RPP with LTP compared to other similar methods for load transfer.

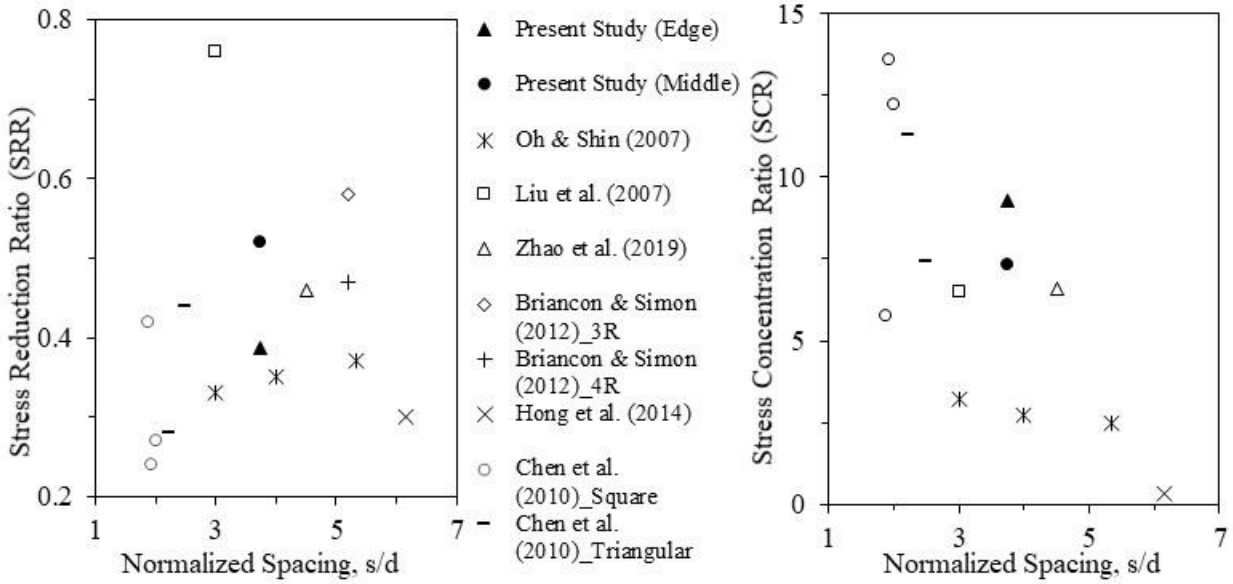

Figure 3.11 Comparison of Stress Reduction Ratio and Stress Concentration Ratio with other studies

3.3.6 Comparison of SRR with Analytical Methods

Analytical models for calculating SRR were evaluated for the comparative study. The adapted Terzaghi method, modified BS8006 method (BSI 2010), and EBGEO (2011) method were compared to evaluate the SRR.

3.3.6.1 *Adapted Terzaghi Method*

Terzaghi (1943) developed an analytical method of the arching effect due to the transfer of pressure from a soil mass onto piles. Later, the Terzaghi's method was modified by Russell and Pierpoint (1997), considering the three-dimensional effect of the piled embankment. Russell and Pierpoint (1997) proposed an analytical method for calculating the SRR as follows:

$$SRR = \frac{(s^2 - a^2)}{4HaK\ tan\varphi'}\left(1 - e^{\frac{-4HaK\ tan\varphi'}{(s^2 - a^2)}}\right) \tag{3.5}$$

where s = pile spacing; a = width of the pile cap (in this study, a = RPP size); φ' = effective friction angle of the embankment fill; H = embankment height, and K = empirical constant, which is taken as 0.7 for this study according to Yun-Min et al. (2008) and Terzaghi (1943).

3.3.6.2 *Modified BS8006 Method*

Russell and Pierpoint (1997) also modified the BS8006 for the 3D nature of piled embankment, and SRR for H > 1.4 (s-a) can be expressed as follows

$$SRR = \frac{2.8\ s}{(s + a)^2 H}\left[s^2 - a^2\left(\frac{\sigma_p}{\gamma H}\right)\right] \tag{3.6}$$

where σ_p = stress on RPP, which can be calculated as follows:

$$\left(\frac{\sigma_p}{\gamma H}\right) = \left(\frac{c_a a}{H}\right)^2 \tag{3.7}$$

where H = embankment height, s = pile spacing; a = width of pile cap; γ = unit weight of the embankment fill; and c_a = arching coefficient, which can be considered as H/a – 0.07 according to Zuang and Cui (2016).

3.3.6.3 *EBGEO (2011)*

EBGEO (2011) developed a theoretical method to study a pile reinforced embankment. The SRR can be expressed as follows:

$$SRR = \frac{\lambda_1^{\chi}}{H}\left\{H\,(\lambda_1 + H_c^2\lambda_2)^{-\chi} + H_c\left[(\lambda_1 + \frac{H_c^2\lambda_2}{4})^{-\chi} - (\lambda_1 + H_c^2\lambda_2)^{-\chi}\right]\right\} \qquad (3.8)$$

where

$$\chi = \frac{D(K_p - 1)}{\lambda_2 s};\ \lambda_1 = \frac{(s-a)^2}{8};\ \lambda_2 = \frac{s^2 + 2as - a^2}{2s^2}$$

where, H = embankment height; a = width of pile cap; s = maximum pile spacing; K_p = coefficient of passive earth pressure and H_c = s/2 for H > s/2.

Figure 3.12 shows the variation of SRR with normalized embankment height H/s', where s' is the maximum clear spacing between RPPs. The SRR decreases with increasing H/s' indicating that more vertical stress is transferred onto the pile. However, the graphs tend to approach a limiting value, signifying that the increase of soil arching effect will be negligible at higher embankment heights. The SRR at 1.2 m embankment height for edge RPPs was overestimated by EBGEO (2011), adapted Terzaghi method, and modified BS8006 method, with errors of 8.1%, 30.0%, and 46.5%, respectively. The SRR computed from the adapted Terzaghi method shows the best agreement with the measured SRR of the middle RPPs. However, for the edge RPPs, adapted Terzaghi methods overestimate the SRR value by 93% for the 1.83 m embankment height. The analytical model described here did not consider the effect of the composite action of LTP; therefore, most of the analytical models overestimate the SRR. Thus, the inclusion of LTP can decrease the SRR, which indicates more load will be transferred to RPPs, resulting in a more effective system.

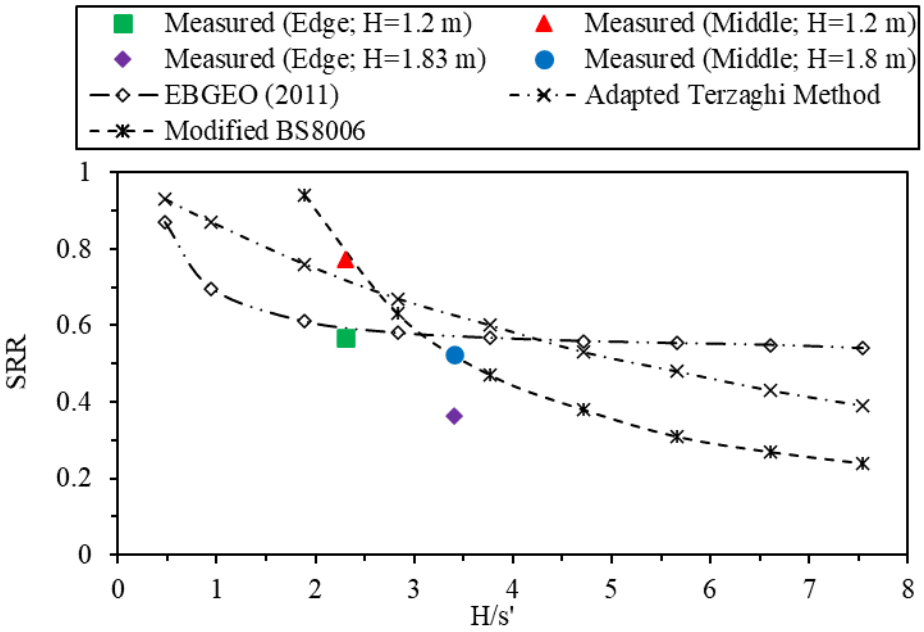

Figure 3.12 Comparison of measured and computed SRR

3.4 CONCLUSIONS

This paper describes a field study of embankments constructed on soft foundation soil. Two test sections (control and RPP reinforced) were constructed and monitored through extensive instrumentation. Based on the field instrumentation, the main results and conclusions are summarized as follows:

1. The maximum settlement in the control section was 52 mm, whereas, in the reinforced section, the maximum settlement was 23 mm. The decrease in settlement of the reinforced section was 56% compared to the control section.
2. The excess pore water pressure in the control section was higher than in the reinforced section. Thus, the magnitude of consolidation settlement would be higher in the control section than the reinforced section. For both phase-1 and phase-2 loadings, the dissipation of excess pore water pressure was faster in the control section compared to the reinforced section resulting in

more consolidation settlement in the control section.

3. The measured consolidation settlement of the test sections was compared with analytical methods and excess pore water pressure data. The settlement profile for the control shows the best agreement with the computed values. However, the computed settlement from the analytical study of Zhuang and Wang (2017) overestimates the settlement prediction with a maximum difference of 51%.
4. The pressure on RPPs was found higher compared to the pressure on the soil, which indicates an effective load transfer mechanism to RPPs. The increase of the average pressure on the RPPs compared to adjacent soil was found to be 103% and 737% for phase-1 and phase-2 loading, respectively.
5. The average value of SRR and SCR was 0.45 and 8.3, respectively, which indicated a higher efficiency of load transfer compared to other field studies.
6. Three analytical methods for soil arching - EBGEO (2011), adapted Terzaghi method, and modified BS8006 method, were compared to evaluate the SRR. Among them, the adapted Terzaghi method was in good agreement with the obtained SRR values.

The present study can be useful for any embankment construction over soft soil, including bridge approaches and widening of any highway where the foundation soil is unsuitable for regular construction.

CHAPTER 4

AN ANALYTICAL METHOD FOR EVALUATING LOAD TRANSFER IN RECYCLED-PLASTIC-PIN-SUPPORTED EMBANKMENT

This chapter has been submitted as:

Islam, M. A., Hossain, M. S., Badhon, F. F., & Bhandari, P. (2021). An Analytical Method for Evaluating Load Transfer in Recycled-Plastic-Pin-Supported Embankment. *International Journal of Geomechanics* (Under Review; Manuscript ID: GMENG-6910).

ABSTRACT

The load transfer efficiency of a geosynthetic-reinforced and Recycled Plastic Pin (RPP) supported embankment is influenced by interactions among embankment fill, geosynthetics, and foundation soil. In this paper, an integrated method based on force equilibrium, soil arching, and stress distribution is developed to calculate differential settlement and stresses on RPPs and adjacent soil in between RPPs. The load transfer mechanism accounted for soil arching and tensioned membrane effects were comprehensively studied. The proposed analytical method was validated with measured results from a field study. Furthermore, the method was also compared with other field study and design methods. A parametric study is also conducted to observe the effects of influential factors such as RPP size, spacing, tensile stiffness of geosynthetics, and friction angle of aggregates used in LTP. The results indicate that more efficiency of load transfer can be achieved with larger size and closer spacing of RPPs. The tensile stiffness of geosynthetic also has a greater influence on the load transfer mechanism.

Keywords: Recycled Plastic Pins, Load Transfer Platform, Embankment, Arching effect, Analytical solution

Nomenclature

a_r	Area ratio
b	Width of RPP
H	Embankment height
h_c	Critical height of the embankment
h_L	Thickness of Load Transfer Platform
K_g	Tensile stiffness of geosynthetic
L	RPP length
s	Spacing between RPPs
T	Tensile force in geosynthetic
T_u	Mobilized tensile strength of upper geosynthetic
T_l	Mobilized tensile strength of lower geosynthetic
ε	Tensile strain in geosynthetic
σ_p	Stress acting on RPP
σ_{pem}	Mean pressure of surcharge load on RPP
σ_s	Stress acting on adjacent soil in between RPPs
σ_{sem}	Mean pressure of surcharge load on geosynthetic
θ	Deflection angle of geosynthetic at the edge of RPP
φ_L	Friction angle of aggregates in LTP
Δw_{max}	Settlement of foundation soil between the piles
$\Delta\sigma_3$	Additional confining stress in LTP

Abbreviations

BS	British Standard
EBGEO	Empfehlungen für den Entwurf und die Berechnung von Erdkörpern mit Bewehrungen aus Geokunststoffen
GRPS	Geosynthetic-Reinforced Pile-Supported
LTP	Load Transfer Platform
RPP	Recycled Plastic Pin
SCR	Stress Concentration Ratio
SRR	Stress Reduction Ratio

4.1 Introduction

Geosynthetic reinforced pile supported (GRPS) embankments have been extensively throughout the world because of their low cost and small settlements compared to conventional ground improvement methods (Zhuang and Wang 2017). The use of piles and high strength geosynthetics has made the embankment construction on soft soil much easier and quicker. GRPS embankments are used to enhance the bearing capacity, durability, and control total and differential settlements of weak foundation soil.

Instead of using concrete piles, Recycled Plastic Pins (RPP) can be a good alternative considering the economy and sustainability. Application of RPP in slope stabilization is a popular method in many states of the USA because of its low cost, easy installation, and long-term performance (Hossain et al. 2017). Very recently, RPP has been used as a measure of increasing bearing capacity of foundation soil for different geotechnical structures like an embankment, mechanically stabilized earth, etc. RPP is manufactured from recycled waste plastics, along with some other

materials such as polymers, additives, and fly ash. Thus, it is a lightweight material and can resist chemical and biological degradation when it is underground. RPP has a good compressive strength (11 MPa to 21 MPa) which made it effective as load-bearing piles (Bowders et al. 2003).

The load distribution mechanism of the GRPS embankment depends on the soil arching developed on the embankment fill. The load transfer mechanism can be improved with the help of the Load Transfer Platform (LTP), which consists of a single layer geosynthetic or multiple layers geosynthetics placed in between aggregate or sand layers. The load transfer mechanism involves stress redistribution of both embankment fill and foundation soil which depends on the interactions among embankment fill, LTP, piles, and foundation soil.

The soil arching mechanism has been studied by many researchers and various analytical solutions have been developed for evaluating the stresses on piles and adjacent soil (Terzaghi 1943; Chen et al. 2008a; Chen et al. 2008b; Deb 2010; Ghosh et al 2017; Zhuang and Wang 2017 and Pham 2020a). There are very few simple and exhaustive analytical models for quantifying the load transfer between soil and piles. There are also different design guidelines available for estimating the vertical stresses on the piles and soil, as well as the tensile force in the geosynthetics (Terzaghi 1943; Hewlett and Randolph 1988; BS8006 1995; Filz and Smith 2007; EBGEO 2011; Pham 2020b).

Chen et al. (2008b) investigated the interactions between piles based on a simplified unit cell theory; however, no geosynthetics or LTP were considered. The BS8006 (1995) method investigated the potential role of foundation soil support, however, they suggested that it should not be considered for design purposes. Filz and Smith (2007) developed an analytical method based on the stiffness of geosynthetic, piles, subgrade soil, and embankment fill for calculating the

load distribution on piles. The EBGEO (2011) method investigated the reactions of the foundation soil and incorporated the soil arching and tension membrane effects considering the compressive modulus of soft soil. However, neither method considered the effect of the differential settlement on soil arching. Numerical methods are sometimes quite effective to investigate the load transfer mechanism of GRPS embankment, however, without an accurate calibration, this method can produce erroneous results. Furthermore, numerical methods are usually time-consuming and difficult to apply for practical designs (Liu et al. 2017).

Most of the analytical methods are based on conventional circular concrete piles, which may not be applicable for RPPs. Only few field studies were conducted to investigate the effectiveness of RPP for ground improvement (Zaman 2019; Islam et al. 2021a; Badhon et al. 2021). Some numerical studies investigated the settlement behavior for different RPP and LTP combinations (Islam et al. 2021b). Many studies considered LTP as a single layer of geosynthetics (Zhunag and Wang 2017; Chen et al. 2008a; Liu et al. 2017). However, the efficiency of LTP can be greatly enhanced if dense aggregate layers can be used in between multiple layers of geosynthetics (Abdullah and Edil 2007; Briancon and Simon 2012). There is very limited study to comprehensively investigate the combined influence of RPP and LTP on settlement reduction and load transfer efficiency. Often pile caps are used with concrete piles for increasing the load transfer efficiency. The use of LTP instead of pile caps provides a continuous base that minimizes the differential settlement as well as increases the load transfer efficiency.

This study aims to investigate the load transfer mechanism of a geosynthetic reinforced and RPP supported embankment. An analytical method considering vertical force equilibrium of a unit-body of RPP is developed for evaluating the settlements and stresses on RPPs and adjacent soil. This method is validated with measured results obtained from the field test sections. Furthermore,

the proposed analytical method is compared with other similar studies and available design methods. A parametric study is conducted to observe the effects RPP size, spacing, tensile stiffness of geosynthetics, and friction angle of aggregates used in LTP.

4.2 DEVELOPMENT OF THEORETICAL SOLUTION

4.2.1 Analytical Model

Usually, in geosynthetic reinforced pile-supported embankments, the piles are installed in a square or triangular arrangement. Also, the center-to-center spacing between piles is much smaller than the overall width of the embankment (Liu et al. 2017). Hence, to analyze the soil arching and load transfer mechanism in a simplified way, a unit cell concept is adopted in this study. Figure 1 shows a unit cell that includes one RPP and the surrounding foundation soil, embankment fill, and load transfer platform from its tributary area.

With the construction of the embankment, consolidation settlement occurs in the soft subsoil which causes differential settlement between RPP and the foundation soil. This differential settlement induces the movement of the embankment fill downward, which is resisted by the shearing stresses developed in the embankment. Thus, the stress on the subsoil decreases while the stress on the RPPs increases. This phenomenon is known as soil arching which can be enhanced by using geosynthetic reinforced LTP. The differential settlement at the same elevation is reduced from the base of the embankment toward the top edge of it due to the soil arching effect. If the embankment height is enough, then the differential settlement reaches zero at a specific plane, which is referred as the plane of equal settlement (Terzaghi 1943). This height is also called the critical height of embankment (h_c) as shown in Figure 4.1.

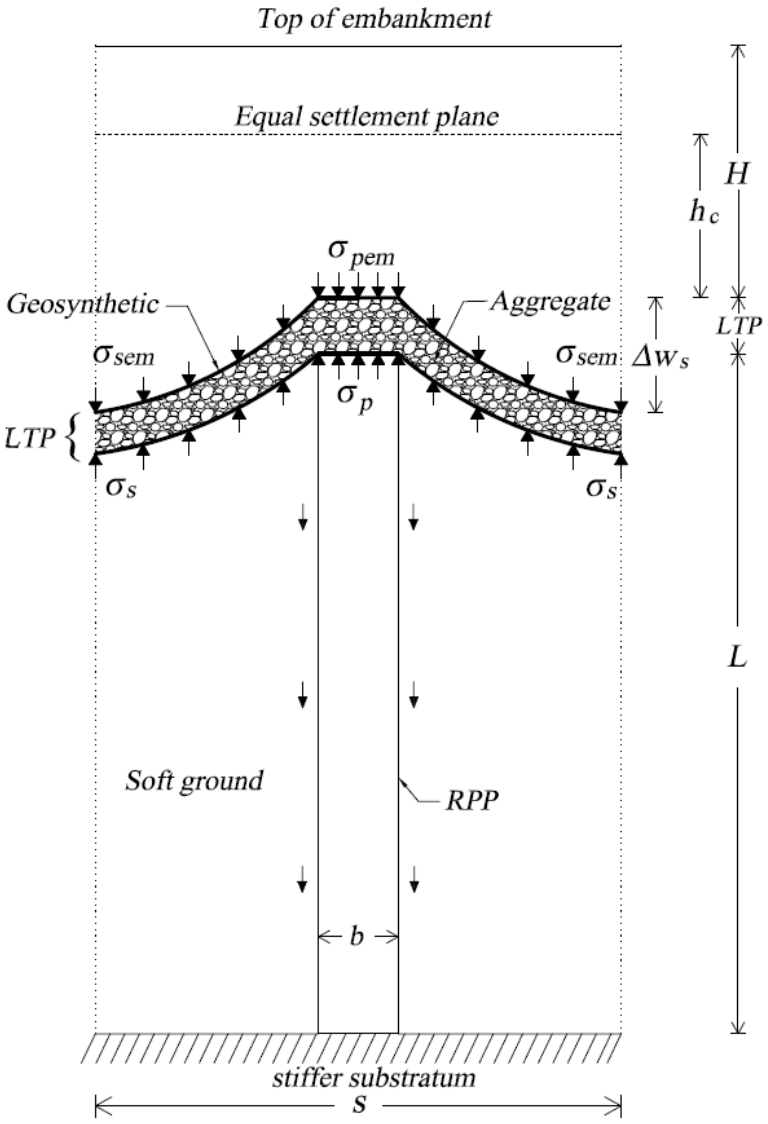

Figure 4.1 Analytical model for geosynthetic reinforced RPP supported embankment.

To evaluate the efficiency of the soil arching, two terms can be used: Stress Concentration Ratio (SCR) and Stress Reduction Ratio (SRR). The SCR is defined as the ratio of measured vertical stress acting on the top of the pile (σ_p) to the overburden vertical stress due to embankment weight (γH) and is given by

$$SCR = \frac{\sigma_p}{\gamma H} \tag{4.1}$$

The SRR is defined as the ratio between the average vertical stress applied on the surface of subsoil between piles (σ_s) and the overburden vertical stress due to embankment weight (according to Low et al. 1994), expressed as

$$SRR = \frac{\sigma_s}{\gamma H} \tag{4.2}$$

4.2.2 Analysis of Soil Arching

Following assumptions are used to develop the analytical framework for the geosynthetic reinforced and RPP supported embankment:

a) The embankment fill and the load transfer platform are homogenous, isotropic, and elastic-perfectly plastic compressible materials.
b) The embankment fill and subsoil are assumed to have the plane-strain condition.
c) The compression of embankment fill and foundation soil is one-dimensional. The stresses and strains of the subsoil are evenly distributed at certain heights.
d) The active earth pressure theory of Rankine is applicable.
e) The unit weight of the LTP and embankment fill are assumed the same. Also, the weight of the geosynthetics is assumed negligible.

Due to the soil arching, drag load becomes active in the embankment fill. Thus, the active earth pressure is induced by the yield fill mass. Taking a unit element with a thickness of dz above the RPP, the force equilibrium in the vertical direction can be expressed as:

$$(\sigma + d\sigma)b = \sigma b + \gamma b dz + 2\left[\left(\gamma z k_a - 2c\sqrt{k_a}\right)\tan\varphi + c\right]dz \tag{4.3}$$

Where σ is the average stress in the stationary fill mass; c and φ are the cohesion and friction angle of the embankment load, respectively; k_a is the Rankine's active earth pressure coefficient, $k_a = \tan^2(45 - \varphi/2)$.

When $H < h_c$, the solution of equation (3) becomes

$$\sigma(z) = \gamma z + \gamma k_a \tan\varphi \cdot \frac{z^2}{b} + 2c\frac{\left(1 - 2\tan\varphi\sqrt{k_a}\right)z}{b} \tag{4.4}$$

Assuming, z = H, equation (4) yields

$$\sigma_{pem} = \gamma H + \gamma k_a \tan\varphi \cdot \frac{H^2}{b} + 2c\frac{\left(1 - 2\tan\varphi\sqrt{k_a}\right)H}{b} \tag{4.5}$$

Again, when $H > h_c$, the solution of equation (3) becomes:

$$\sigma(z) = \gamma z + z k_a \tan\varphi \frac{\left[z^2 - (H - h_c)^2\right]}{b} + \frac{2c\left(1 - 2\tan\varphi\sqrt{k_a}\right)(z - H + h_c)}{b} \tag{4.6}$$

Assuming, z = H, equation (6) yields

$$\sigma_{pem} = \gamma H + \frac{\gamma k_a \tan\varphi\,(2H - h_c)h_c}{b} + 2c\frac{\left(1 - 2\tan\varphi\sqrt{k_a}\right)h_c}{b} \tag{4.7}$$

The equilibrium equation of the vertical forces in the embankment fill requires that:

$$\sigma_0(z) = \frac{\gamma z - a_r \cdot \sigma(z)}{1 - a_r} \tag{4.8}$$

Assuming z = H, equation 8 becomes:

$$\sigma_{sem} = \frac{\gamma z - a_r \cdot \sigma_{pem}}{1 - a_r} \tag{4.9}$$

Where $\sigma_0(z)$ is the average stress in yield fill mass over soft foundation soil, σ_{sem} is the average stress of yield fill mass on geosynthetic, a_r is the area ratio, $a_r = \frac{b}{s}$.

The settlement of the embankment fill will be equal to the settlement of the stationary fill mass at the equal settlement plane, namely:

$$w_p(0) + w_{pem} = w_s(0) + w_{sem} \tag{4.10}$$

Where $w_p(0)$ and $w_s(0)$ are the average settlements of RPP and foundation soil at the top elevation of RPP, respectively; w_{pem} and w_{sem} are the average deformations of embankment fill over RPP and foundation soil, respectively.

The maximum differential settlement Δw_{max} at the RPP top elevation can be expressed as:

$$\Delta w_{max} = w_{pem} - w_{sem} = \int_{H-h_c}^{H} \frac{\sigma(z) - \sigma_0(z)}{E_f} dz \tag{4.11}$$

where E_f is the modulus of elasticity of the embankment fill. The modulus of elasticity of the embankment fill soil is assumed the same throughout the section.

While designing road embankments, engineers often keep the final height of the embankment fill greater than the critical height (h_c) of the embankment [6]. Thus, the differential settlement of the pavement will be minimum. Furthermore, if the embankment fill consists of sandy soil, then the cohesion, c will be zero. For H > h_c and c = 0; the equations (4.6) and (4.8) can be substituted in equation (4.11) which yields:

$$\Delta w_{max} = \frac{\gamma k_a \tan\varphi \left[\frac{H^3}{3} - H\,(H - h_c)^2 + 2\frac{(H - h_c)^2}{3}\right]}{(1 - a_r)\, b\, E_f} \tag{4.12}$$

From equation (4.12), the maximum differential settlement can be obtained if the embankment material property and the critical height of the embankment are known. Numerous methods are available for determining the critical height of an embankment. The critical heights for different design methods are summarized in Table 4.1. Usually, the critical height is greatly influenced by the difference between pile spacing, and pile size. Various design methods use critical heights in different ranges which can vary from 1.4 (s-a) to 2.5 (s-a).

Table 4.1 Critical height determination for different design methods

Design method	Critical height, h_c
Terzaghi (1936)	2.5 (s - a)
Carlsson (1987)	1.87 (s - a)
Hewlett & Randolph (1988)	1.4 (s - a)
BS 8006 (1995)	1.4 (s - a)
Horgan & Sarby (2000)	1.545 (s - a) to 1.92 (s - a)

If the foundation soil is saturated clay, consolidation settlement will occur. Therefore, the differential settlement will be a function of consolidation soil parameters, surcharge load, and time. Zhuang and Wang (2017) developed an analytical method for a geosynthetic reinforced piled embankment on elastoplastic consolidated soil which can be expressed as follows:

$$\Delta w_{\max(z)} = 2.3\, m_v \sigma_0' \log\left(\frac{\sigma_0'}{\sigma_0' + q}\right) H_c \left[1 - \frac{z}{H_s} - \sum_0^{\infty} \frac{2}{M^2} \cos\frac{Mz}{H_s} e^{-M^2 T_v}\right] \qquad (4.13)$$

where M = (π/2) (2N+1); N = natural number; T_v = time factor; m_v = volume compressibility, which can be derived as 1/ E_0 (Constraint modulus of soil); σ_0' = initial effective stress; q = surcharge load applied on the top surface of foundation soil, and H_s = thickness of the drainage path of the soft clay layer.

4.2.3 Tensioned Membrane Effect

By soil arching effect, a significant portion of load transfers from foundation soil to the RPPs. An LTP consisting of an aggregate layer sandwiched between two geosynthetics can transfer the surcharge load to piles more efficiently compared to a single layer of geosynthetic (Briancon and Simon 2012). The applied embankment load on the soft subsoil will be partially transmitted to the RPPs by a tension T_u and T_l of both upper and lower geosynthetics. The deformed shape of the geosynthetic develops tension through which the surcharge load is indirectly transferred to the RPP from the soft foundation soil. This phenomenon is known as the tension membrane effect (Liu et al. 2017).

For analyzing the tension membrane effect, the deformed shape of the geosynthetics is important. The deformed geosynthetics has been assumed as a circular shape in order to determine the tensile force in the geosynthetics. Although some studies used parabolic shape for the deformed geosynthetics (Liu et al. 2017), a circular shape can be assumed for a simpler approach (Chen et al. 2008a). Figure 4.2 shows the analytical model for the deformed circular shape of geosynthetics. In this analysis, the following assumptions are made:

a) Circular deflection of geosynthetic between RPPs is assumed.
b) The vertical deformation of geosynthetic at the top of RPP is negligible.
c) In LTP, the aggregate is in a fully confined state.
d) The deformation of geosynthetic is elastic.

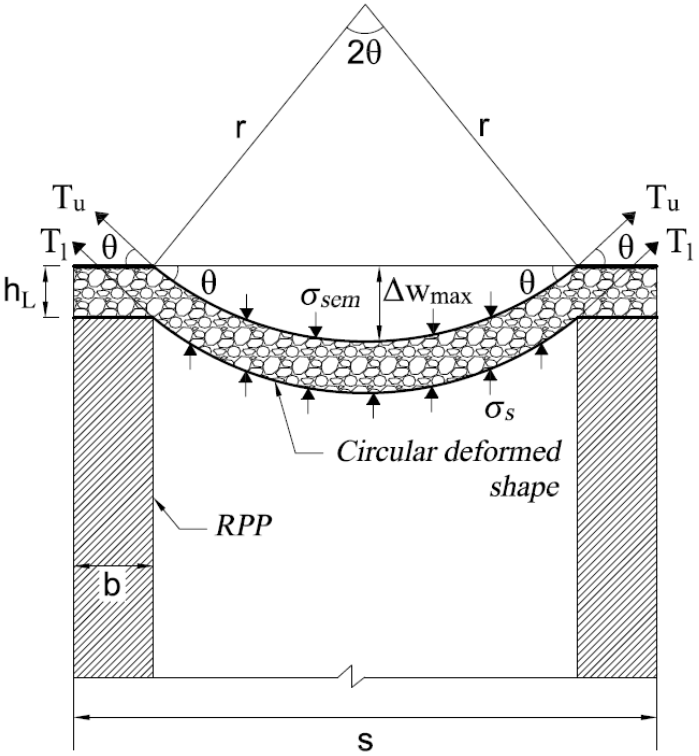

(a)

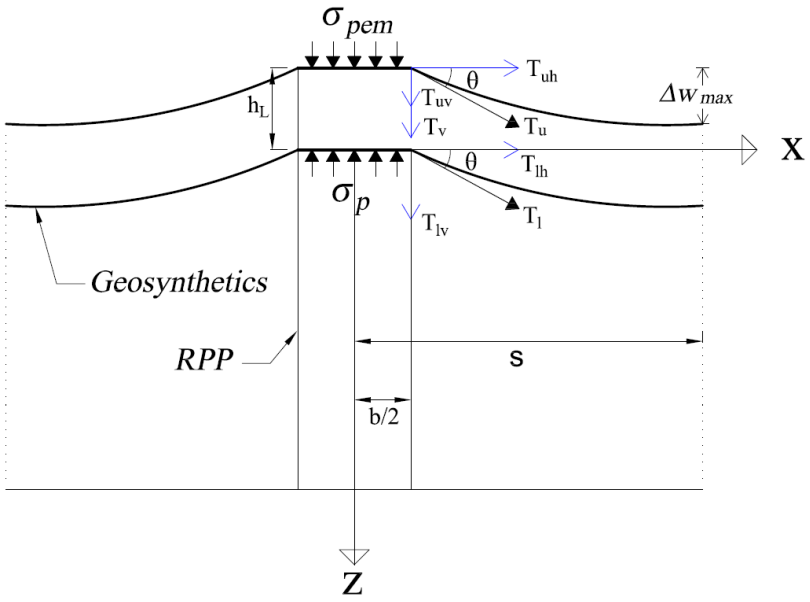

(b)

Figure 4.2 Assumed circular shape of deformed geogrid (a) geosynthetics on soft ground; (b) geosynthetics on RPP

The deformed shape of geosynthetic is idealized with a circular arc (radius, r), a subtended angle 2θ, and a maximum deformation, Δw_{max} at the midway between two RPPs (Figure 4.1).

From geometry,

$$sin\theta = \frac{4\Delta w_{max}(s-b)}{4\Delta w_{max}^2 + (s-b)^2} \tag{4.14}$$

If the subtended arc length of the circle is y, then

$$y = (s-b) * \theta * \left[\sqrt{1 + \frac{1}{(\tan\theta)^2}}\right] \tag{4.15}$$

Where θ is in radian.

The strain in geosynthetic will be:

$$\varepsilon_g = \frac{y-(s-b)}{(s-b)} \tag{4.16}$$

The strain of geosynthetic can be determined from equation (4.16) if the maximum differential settlement is known along with RPP size and spacing.

If the geosynthetic deforms elastically, the tension force of geosynthetic,

$$T_u = \varepsilon K_g \; and \; T_l = \varepsilon K_g \tag{4.17}$$

Where K_g is the elastic stiffness of geosynthetic reinforcement; T_u and T_u are the mobilized tensile strength of upper and lower geosynthetic respectively.

From Figure 4.2 (b), the vertical and horizontal component of upper and lower geosynthetic can be expressed as:

$$T_{uh} = T_u \cos\theta \quad and \quad T_{uv} = T_u \sin\theta \tag{4.18}$$

$$T_{lh} = T_l \cos\theta \quad and \quad T_{lv} = T_l \sin\theta \tag{4.19}$$

The additional confining stress benefitted from the friction between geosynthetic and aggregate can be added to the existing radial stress σ_3, as demonstrated in Figure 4.3. If the horizontal component of geosynthetics (T_{uh} & T_{lh}) completely contributes to the additional confining stress, the average additional confining stress in the LTP can be expressed as:

$$\Delta\sigma_3 = \frac{(T_u + T_l)\, cos\theta}{h_L} \tag{4.20}$$

From the confining effect, the other vertical component T_{v2} is as follows:

$$T_{v2} = \Delta\sigma_3 h_L tan\varphi_L = (T_u + T_l)\, cos\theta\, tan\varphi_L \tag{4.21}$$

Where, φ_L is the friction angle of the aggregate in LTP.

Therefore, the stress on RPP is as follows:

$$\sigma_p = \frac{\gamma Hs + 4(T_{uv} + T_{lv} + T_{v2})\, s}{b} \tag{4.22}$$

The stress on subsoil between RPPs is as follows:

$$\sigma_s = \frac{\gamma Hs - 4(T_{uv} + T_{lv} + T_{v2})\, s}{s - b} \tag{4.23}$$

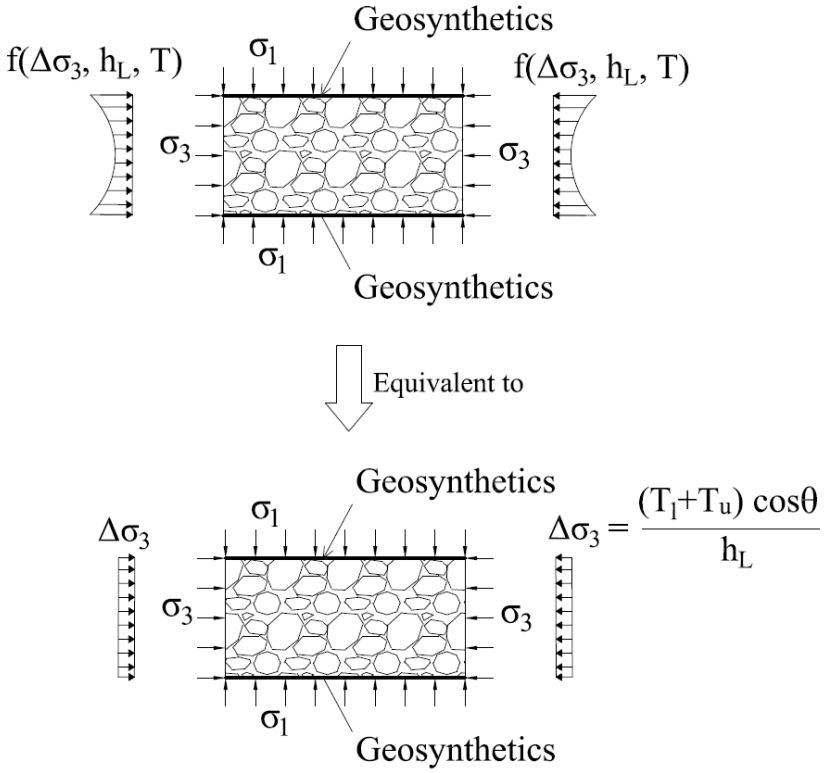

Figure 4.3 Lateral confining effect of geosynthetic

4.2.4 Analysis of bearing capacity

For a single RPP, the point load capacity will be the result of skin friction and end bearing. However, if RPPs are installed in a fully saturated soft soil with a stiffer stratum at the bottom, there will be no contribution of skin friction, rather negative skin friction will develop which tends to drag the RPP downwards. Thus, RPPs in saturated clays under undrained condition (φ = 0), the net ultimate load can be as follows:

$$Q_P = N_c^* \, c_u \, A_p - \, Q_n \tag{4.24}$$

Where c_u is the undrained cohesion of the soil below the tip of the RPP; Q_n is the negative skin friction; A_p is the cross-sectional area of an RPP; N_c^* is the bearing capacity factor that include

the shape and depth factors. According to Meyerhof's method, N_c^* can be assumed as 9 for saturated clay (Das 2015).

The negative skin friction for clay fill over granular soil or stiff strata can be expressed as:

$$Q_n = \frac{pK_0\gamma_f' H_f^2 \tan\delta'}{2} \tag{4.25}$$

Where H_f is the height of the fill, K_0 is the earth pressure coefficient, can be expressed as $1 - \sin\varphi'$; p is the perimeter of the RPP; γ_f' is the effective unit weight of the clay fill; δ' is the soil-pile friction angle ≈ 0.5 – 0.7 φ'.

Since, the surcharge load from embankment distributed both RPP and soft soil, the bearing capacity of the RPP supported embankment will be contributed by both RPP and soft foundation soil. The ultimate bearing capacity, q_u can be expressed as

$$q_u = \frac{Q_p * SCR * \eta + N_c c_u F_{cs} F_{cd} A_s * SRR}{A} \tag{4.26}$$

Where, N_c is Terzaghi's bearing capacity factor, for soft clay and undrained condition (φ=0), N_c=5.7; F_{cs} is shape factor; F_{cd} is depth factor; η is the group efficiency; A_s is the area of soft foundation soil except RPP = $A - A_p$.

By substituting equation (4.22) and (4.23) into equation (4.1) and (4.2), the SCR and SRR can be determined. The substitution of equation (4.1), (4.2) and (4.24) into (4.26) yields the bearing capacity of a geosynthetic reinforced and RPP supported embankment.

4.3 Comparison and Validation

4.3.1 Comparison with field test sections

Validation of the current analytical model is carried out suing two well-instrumented field test sections. The computed results from the model are compared with the measured results from the field test sections. A total of 64 Nos RPPs were installed in one section while the other section was used as a control section for reference. 3 m long and 15 cm square RPPs were used in this study. A load transfer platform was placed consisting of one layer of recycled concrete aggregate, sandwiched between two layers of triaxial geogrid as shown in Figure 4.1. The properties of the foundation soil, RPP, and geogrid are presented in Table 4.2, Table 4.3, and Table 4.4, respectively.

Table 4.2 Soil properties of subsoil and embankment fill

Material	T (m)	γ_d (kN/m^3)	q_u (kPa)	c_u (kPa)	φ' (°)	E (MPa)	k (cm/s)	C_c	c_v (m^2/day)
Embankment Fill	1.8	17.8	-	-	32	25	3.2×10^{-4}	-	-
Lean Clay	0.6	16.0	24	12	17	1.4	2.5×10^{-6}	0.28	0.015
Sandy Lean Clay	2.2	16.7	54	27	20	4.8	9.7×10^{-6}	0.20	0.02
Eagle Ford Shale	4.2	18.9	624	312	-	90	1.0×10^{-9}	-	-
RCCA	0.1	17.3	140	-	-	40.5	-	-	-

Note: T = thickness of soil layer; γ_d = dry unit weight; q_u = unconfined compressive strength; c_u = undrained cohesion; φ' = effective friction angle; E = modulus of elasticity; k = coefficient of

permeability; C_c = coefficient of compressibility; c_v = coefficient of consolidation; RCCA = recycled crushed concrete aggregate

Table 4.3 Engineering properties of Recycled Plastic Pin

Parameter	Value[a]
Cross-section	15 cm × 15 cm
Length	3 m
Modulus of Elasticity (MPa)	1170
Compressive Strength (MPa)	31
Tensile Strength (MPa)	24.9
Specific Gravity (g/cc)	0.93
Coefficient of Friction-Static	0.253
Coefficient of Friction-Kinetic	0.175

[a] RPP properties (estimated from the manufacturer and Bowders et al. 2003).

Table 4.4 Engineering properties of geogrid

Parameter	Longitudinal/Transverse[a]	Diagonal[a]	General[a]
Structure			Triaxial
Aperture shape			Triangular
Rib shape			Rectangular
Rib pitch (mm)	40	40	
Mid-rib depth (mm)	1.2	1.2	
Mid-rib width (mm)	1.1	1.1	
Tensile stiffness @0.5% strain (kN/m)			225
Isotropic stiffness ratio			0.6
Junction efficiency (%)			93

Chemical degradation resistance (%)	100
UV-resistance (%)	70

[a]Properties were obtained from the manufacturer

Each test section was equipped with inclinometer casing and pressure plates. There is a continuous 25 m long inclinometer casing installed in both sections. A total of four pressure plates were instrumented: two on top of RPP and two on the adjacent soil in between RPPs. Surcharge load was applied in three phases. During phase-1 loading, 1.2 m height of sand was placed on the test sections. Phase-2 and phase-3 loadings were applied with an additional 0.61 m height embankment fill for each phase. The test sections were monitored regularly for 510 days. The settlement profile and the pressure plate results are presented in Figure 4.4 and Figure 4.5, respectively.

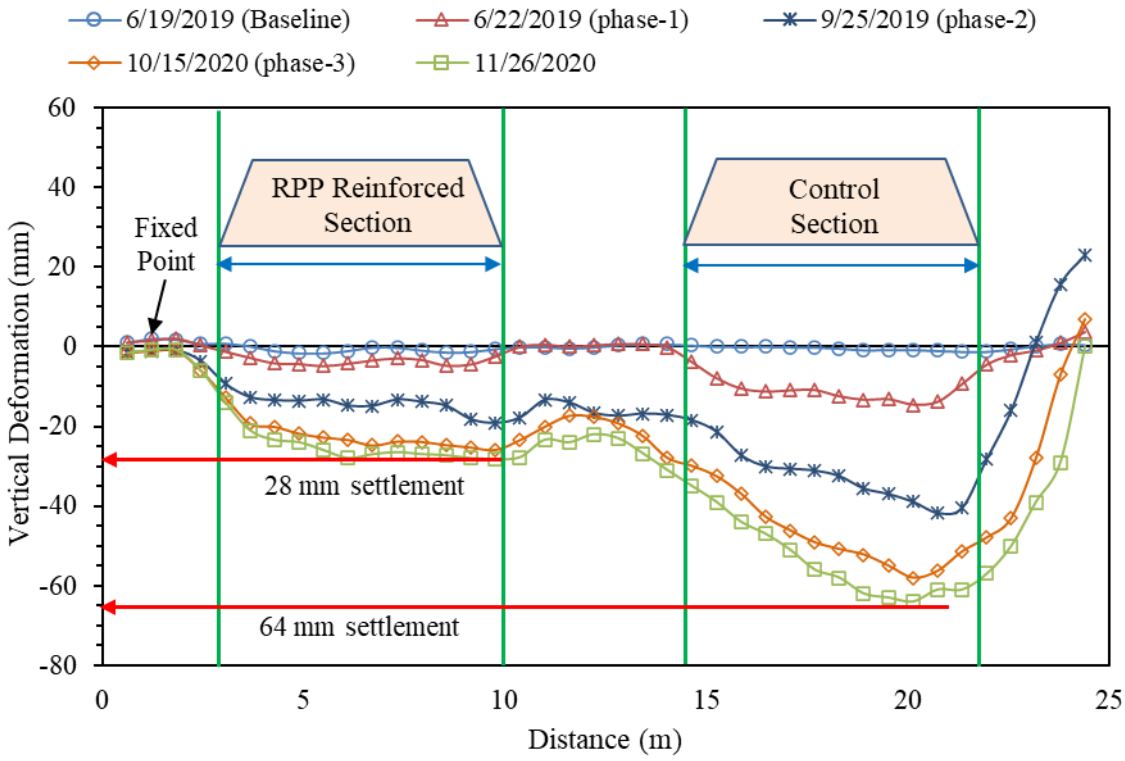

Figure 4.4 Settlement profile of reinforced and control section

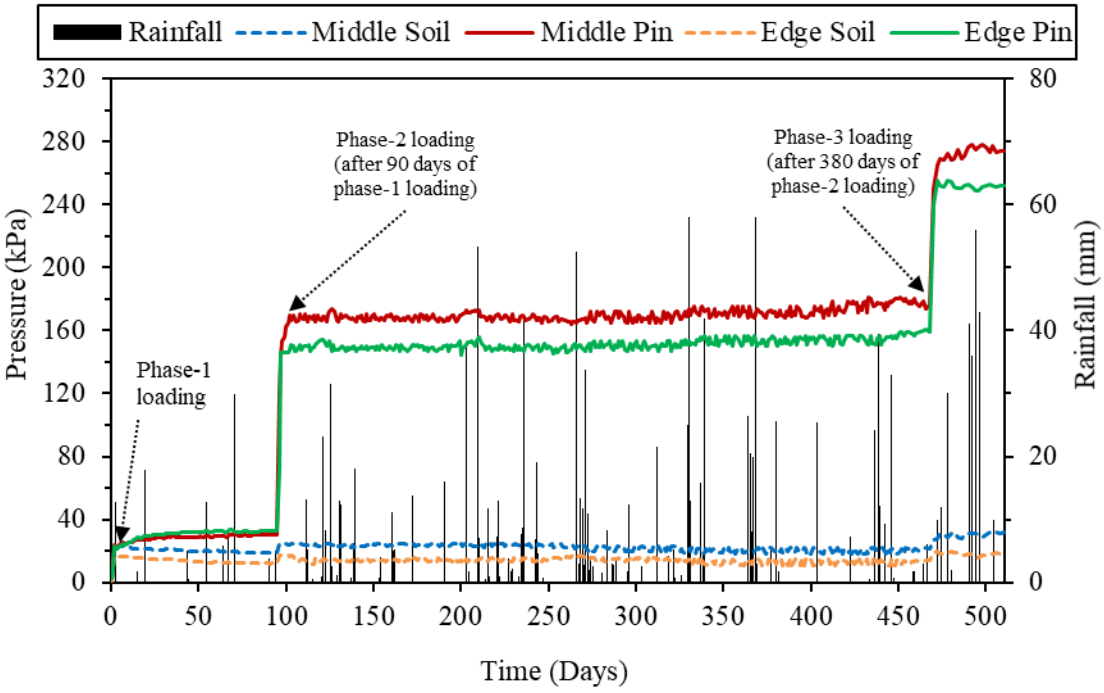

Figure 4.5 Pressure variation on RPP and adjacent soil in between RPPs

4.3.1.1 *Comparison of ground settlement*

The settlement data obtained from the measured field data is shown in Figure 4.6. Settlement for the reinforced section was also computed from the proposed method (Equation 13) and settlement for the control section was calculated from Teraghi's 1D consolidation theory (Terzaghi 1925). Figure 6 illustrates the comparison between measured settlement and computed settlement. Based on the results of the control section, the prediction of the settlement using Terzaghi (1925) method coincides closely with the field values. However, the predicted values are found higher than the measured values for the reinforced section. As compared to the measured settlement results, the theoretical solution to the reinforced section is overestimated by up to 28%.

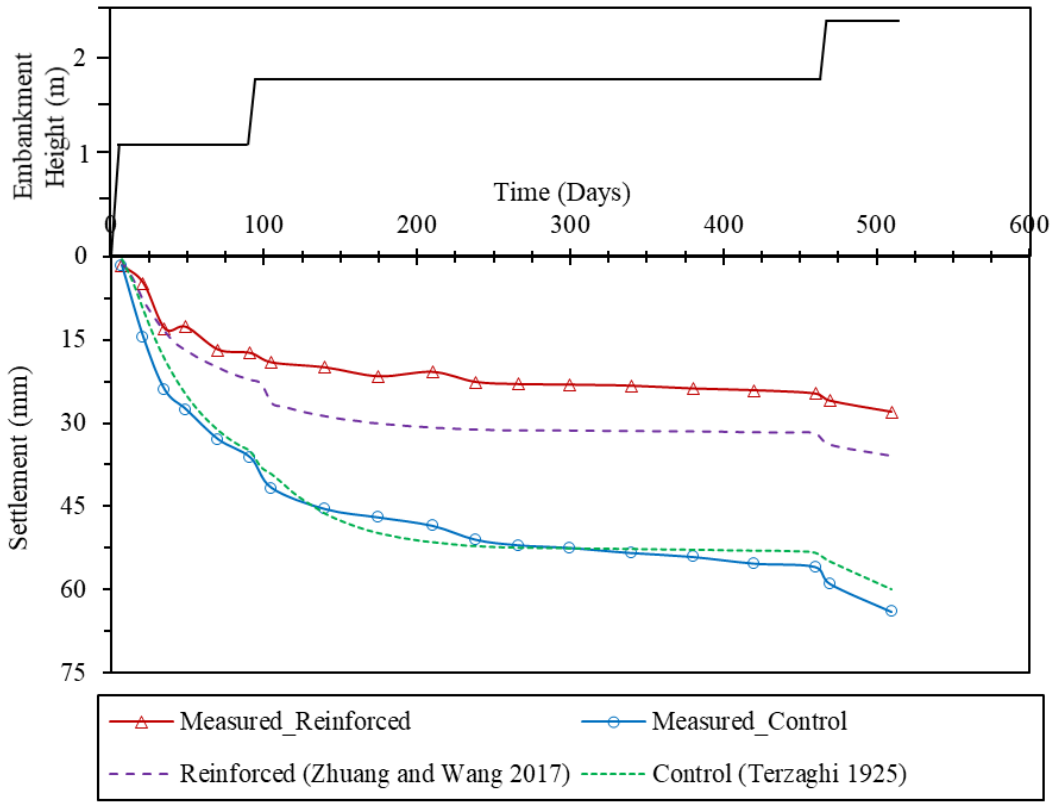

Figure 4.6 Comparison of calculated ground settlement with measured results

4.3.1.2 *Comparison of load transfer*

SCR and SRR were calculated to analyze the load distribution on RPPs. A low value of SRR and a high value of SCR indicates the most efficient load transfer from the embankment to the RPPs. A comparison of the SRR and SCR values with the field results is presented in Figure 4.7. It is observed that computed SCR and SRR from analytical study overestimates compared to the field results. During phase-1 loading, the difference between SCR and SRR is 66%.7% and 22.8%, respectively compared to the field results. There might be some construction flaws at the initial stage of loading for which the soil arching is often found less effective. Sometimes, the placement of geosynthetics could not be stretched properly in field condition which might affect the arching mechanism at the beginning. Gradually, the soil arching develops, and the construction flaws get minimized.

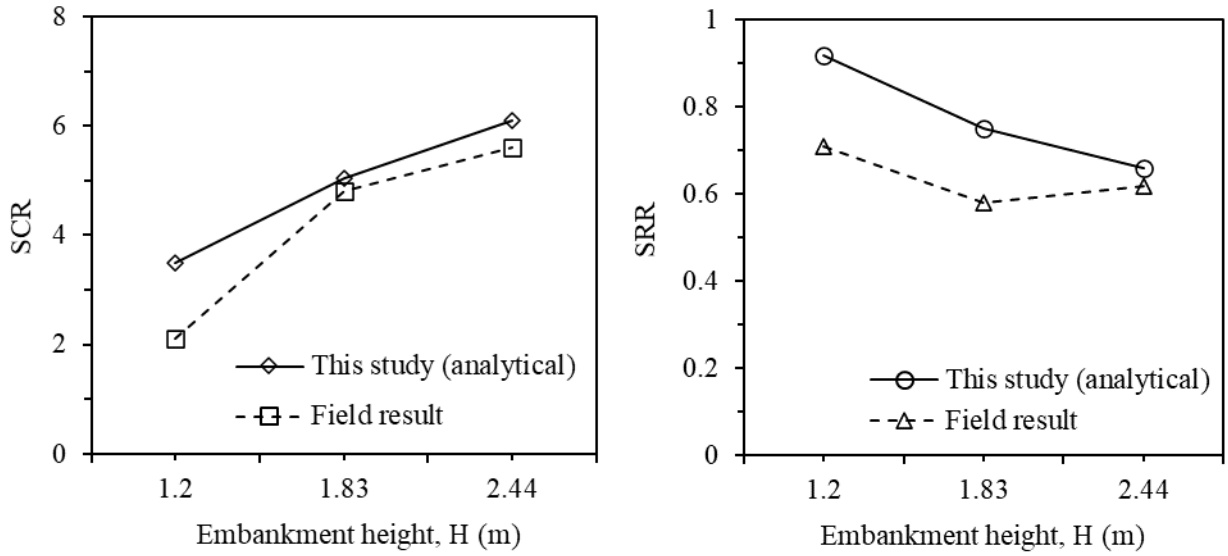

Figure 4.7 Comparison of calculated SCR and SRR with field results

With the loading advancements, the difference between the analytical model and field results decreases. The analytical model is found in good agreement with field results at higher embankment loads. After the application of phase-3 loading, the SCR and SRR differ only 8.7% and 6.5%, respectively compared to the measured field results.

4.3.2 Comparison with other studies

This analytical model is also compared with two field studies conducted on geosynthetic reinforced piled embankments. Briancon and Simon (2012) performed a full-scale experiment on the performance of pile-supported embankment over soft soil. Four test sections were constructed: three were reinforced with concrete piles and one was a control section. To compare with the proposed analytical method, one reinforced section with two geogrid layers is selected. The piles were 0.38 m in diameter, constructed with a 2 m center to center spacing. A 94.8 kPa embankment pressure was applied above the test sections. From the field results, the maximum different settlement was found 37 mm.

The parameters of the embankment were used to predict the stresses on the pile and adjacent soil using equations (22) and (23) respectively. Afterward, SCR and SRR were calculated from equations (1) and (2). On the other hand, SCR and SRR were computed from the pressure plate results reported by Briancon and Simon (2012). The comparison of SCR and SRR between the proposed analytical method and field results are shown in Figure 4.8. The present method underestimates the SCR by 62% and overestimates the SRR by 31%. Briancon and Simon (2012) used two geogrid layers within three layers of compacted granular fill. However, in the present model, only one layer of aggregate in between two layers of geosynthetics was considered. Furthermore, due to the application of a compacted granular fill in the middle of piles and geogrids, the soil arching mechanism was found more effective in the test sections of Briancon and Simon (2012). Therefore, the predicted values of SCR and SRR differs from the field results. Since the proposed method reports slightly less efficiency of soil arching, this method can be used for conservative design approaches.

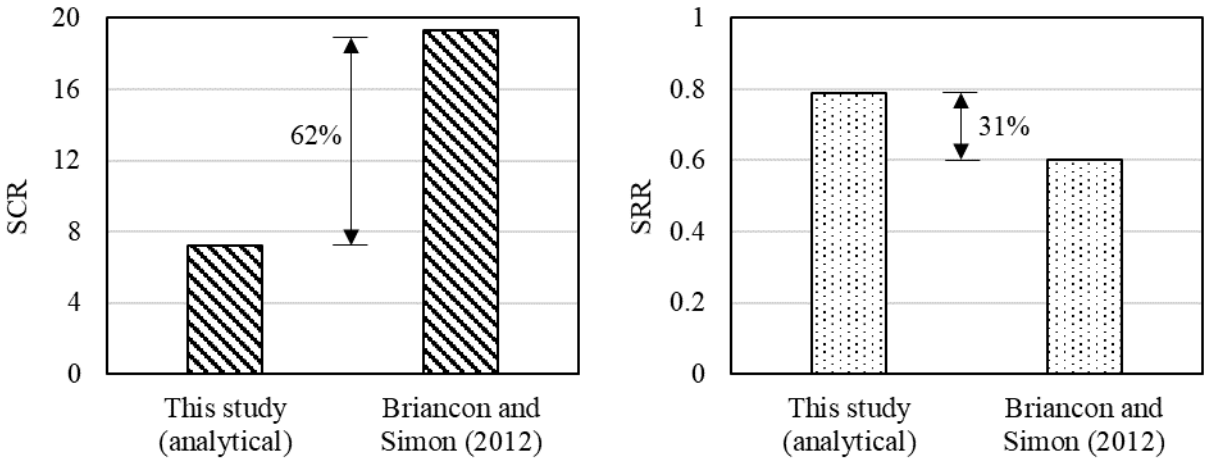

Figure 4.8 Comparison of SCR and SRR between the present analytical model and field results of Briancon and Simon (2012)

The present analytical solution is also validated with different available design methods for geosynthetic reinforced and pile-supported embankment. Three design methods are selected based on their suitability with the present study: adapted Terzaghi method (Terzaghi 1943; Russel and Pierpoint 1997), modified BS8006 method (Russel and Pierpoint 1997), and EBGEO method (EBGEO 2011). The design parameters of the test section constructed by Briancon and Simon (2012) are used to evaluate SRR with the aforementioned methods.

The SRR is computed from the field test section of Briancon and Simon (2012) using the adapted Terzaghi method, modified BS8006 method, EBGEO 2011 method, and current study method. The results are presented in Figure 4.9. It can be observed that the SRR value obtained from the present study are in close agreement with the other methods. However, the mentioned methods were developed based on a single layer of geosynthetics, no load transfer platforms were considered. Therefore, some slight differences (8 to 36%) were observed between the present study and other methods.

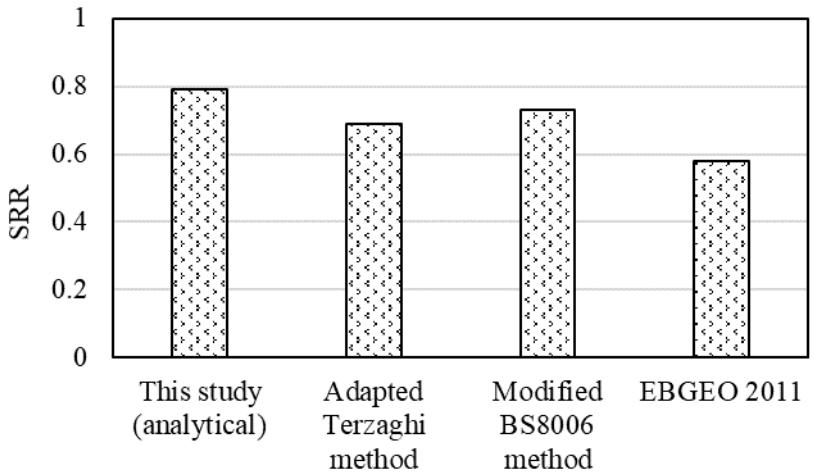

Figure 4.9 Comparison of SRR with available design methods

4.4 PARAMETRIC STUDIES

For understanding the load transfer behavior of RPP supported embankment, a parametric study is conducted based on the proposed analytical method. This parametric study investigates the effect of influential parameters such as RPP size, spacing, tensile stiffness of geosynthetics, and LTP properties on the load transfer mechanism.

For the parametric study, the analytical calculations are carried out based on the parameters of the field study discussed in section 3.1. Properties of the foundation soil, RPP, and geosynthetics are tabulated in Tables 2, 3, 4, respectively. To investigate the effect of one parameter, the remaining parameters were kept constant.

4.4.1 Influence of RPP size and spacing

Three different RPP sizes are considered for this study based on their availability in the market: 10 cm × 10 cm, 15 cm × 15 cm, and 25 cm × 25 cm. RPP spacing was varied from 0.5 m to 2.0 m, which are the typical RPP spacing used in piled embankments (Zaman 2019). RPP size and spacing were used along with other field parameters to determine σ_p and σ_s from equations (22) and (23). Afterward, SCR and SRR were calculated from equations (1) and (2). The variation of SCR and SRR for different RPP sizes and spacings are presented in Figure 10. It can be observed that both SCR and SRR increases with increasing RPP spacing. This indicates that at higher RPP spacing, the efficiency of load transfer is high. Also, SRR tends to approach a limiting value at higher spacing.

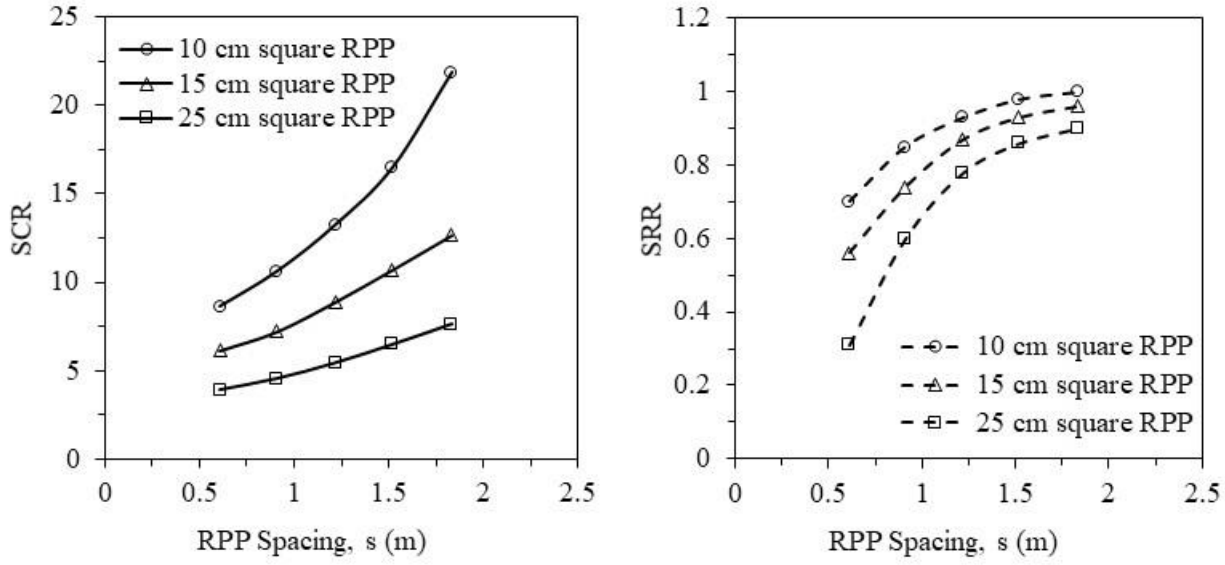

Figure 4.10 Influence of RPP size and spacing on SCR and SRR

4.4.2 Influence of tensile stiffness of geosynthetics and friction angle of LTP

The influence of geosynthetics' tensile stiffness on the behavior of the piled embankment is investigated by varying the tensile stiffness from 100 kN/m to 600 kN/m. During the analysis, a constant value was applied to the rest of the parameters. Figure 11 illustrates that, with the increase of tensile stiffness, SCR increases in a linear trend. Therefore, high strength geosynthetic offers more load transfer into RPPs.

In LTP, aggregate plays a very important role in maximizing load transfer efficiency. The confining stress in between two layers of geosynthetic will be more effective if coarser material is used instead of finer material (Abdullah and Edil 2007; Briancon and Simon 2012; Islam et al. 2021a). The friction angle of LTP was varied from 20° to 40° for investigating the influence on the load transfer mechanism. From Figure 11, it can be observed that with the increase of friction angle, the slope of the lines increases. Therefore, compacted dense aggregates will offer more efficiency compared to loose sand.

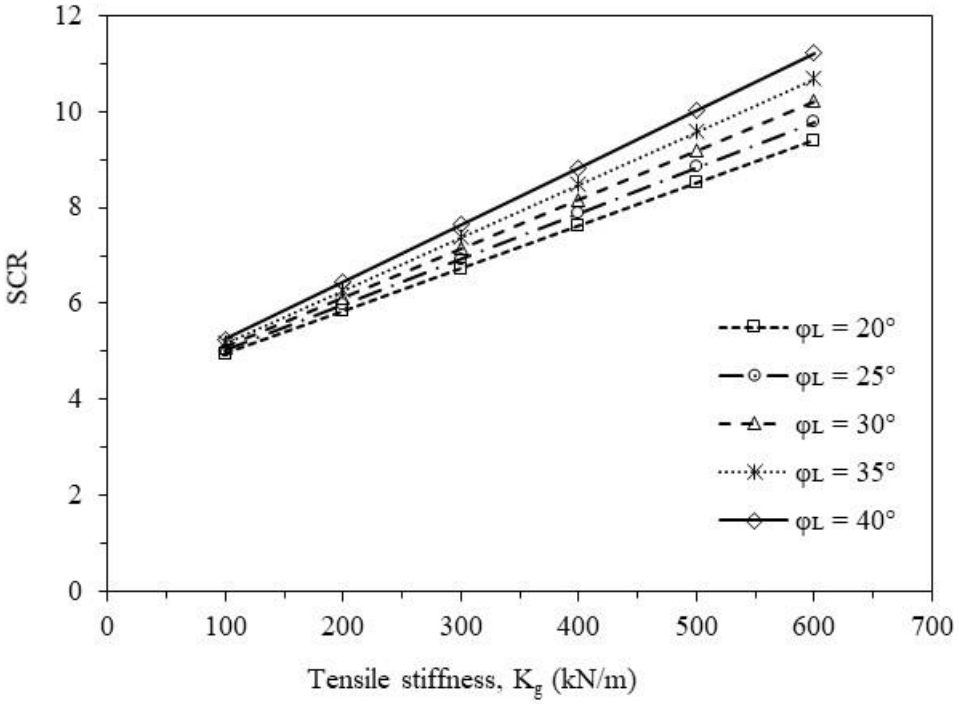

Figure 4.11 Influence of tensile stiffness of geosynthetics and friction angle of LTP on SCR

4.5 Design example for evaluating bearing capacity of RPP reinforced section

A calculation example is presented in this section to show the steps involved in determining bearing capacity of RPP supported embankment. Figure 4.12 shows an embankment along with soil profile. The height of the embankment is 1.8 m. The backfill soil is silty sand with an average unit weight of 20 kN/m^3 and drained friction angle of 35°. The foundation soil consists of two layers: the soft clay layer underlain by eagle ford shale layer. The undrained cohesions of the soft clay layer and the eagle ford shale layer are 12 kPa and 312 kPa, respectively. The thickness of the soft clay layer is 2.4 m whereas the eagle ford shale layers extend downwards. The ground water table is located 0.6 m below the existing ground level. Therefore, the soft clay layer is subjected for consolidation settlement.

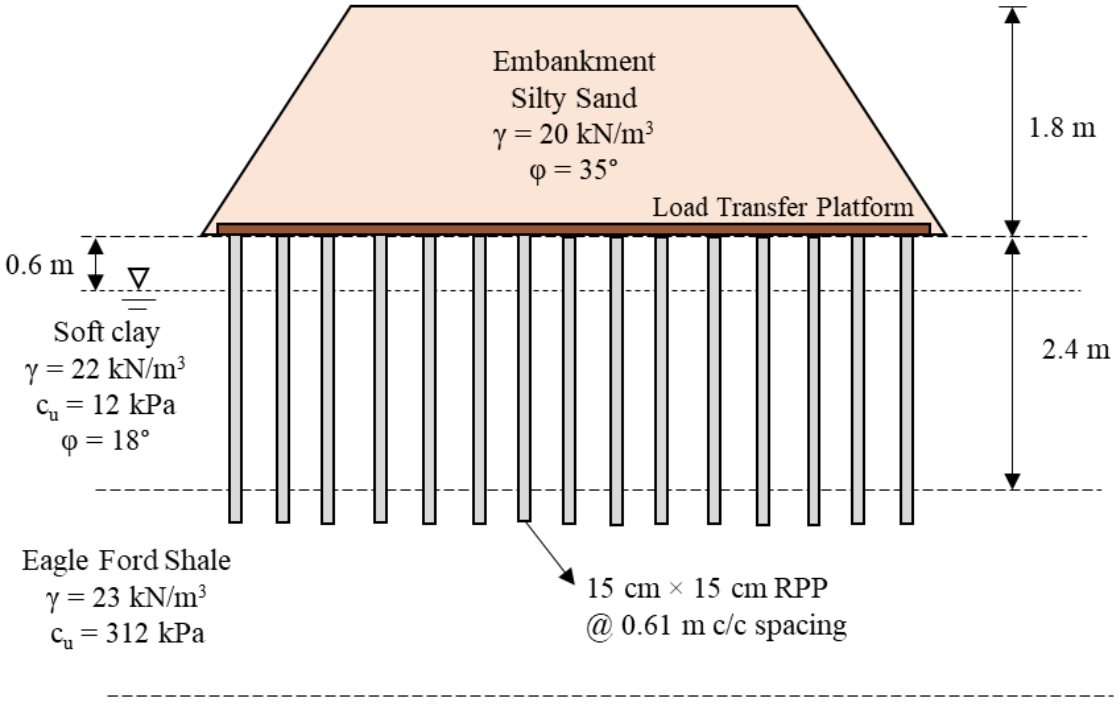

Figure 4.12 Reference embankment and soil profile for design calculation

The soft soil is improved by Recycled Plastic Pins (RPPs) of 15 cm × 15 cm. The length and spacing of the RPPs is 3 m and 0.61 m, respectively. Thus, the RPPs are supported by the stiffer layer of eagle ford shale. A load transfer platform is placed just above the RPPs to facilitate the load transfer mechanism. Triaxial geogrid have a tensile stiffness of 225 kN/m is used. The bearing capacity of RPP supported embankment will depend on different factors, such as RPP size, RPP spacing, tensile stiffness of geosynthetics, and foundation soil properties. The step-by-step calculation for determining the bearing capacity for RPP supported embankment is presented below:

Step-1: Calculation of maximum settlement

Since ground water table is present in this example, equation 4.13 can be used to determine the maximum settlement in between RPPs.

For H_s = 1.2m, σ_0' = 14.6 kPa, q = 36 kPa, H_c = 0.8 m, C_v = 0.015 m^2/day, substituting these values in equation 4.13,

$$\Delta w_{\max(z)} = 2.3\, m_v \sigma_0' \log\left(\frac{\sigma_0'}{\sigma_0' + q}\right) H_c \left[1 - \frac{z}{H_s} - \sum_0^{\infty} \frac{2}{M^2} \cos\frac{Mz}{H_s} e^{-M^2 T_v}\right]$$

The maximum settlement of foundation soil between RPPs will be, $\Delta w_{\max}$ = 36 mm.

Step-2: Calculation of deflection angle of geosynthetics

Using s = 0.61 m, b = 0.15 m, $\Delta w_{\max}$ = 36 mm, in equation 4.14,

The deflection angle of geosynthetics at edge of RPP,

$$sin\theta = \frac{4\Delta w_{max}(s-b)}{4\Delta w_{max}^2 + (s-b)^2} = \frac{4 \times 36(0.61 - 0.15)}{4 \times 36^2 + (0.61 - 0.15)^2}$$

$$\theta = 17.9°$$

Step-3: Determination of subtended arc length

From equation 4.15, the subtended arc length of deflected geosynthetics will be

$$y = (s-b) * \theta * \left[\sqrt{1 + \frac{1}{(\tan\theta)^2}}\right] = (0.61 - 0.15) * 17.9 \frac{\pi}{180} * \left[\sqrt{1 + \frac{1}{(\tan 17.9)^2}}\right]$$

$$y = 0.467\ m$$

Step-4: Determination of strain in geosynthetics

From equation 4.16, the strain of the geosynthetic will be

$$\varepsilon_g = \frac{y - (s-b)}{(s-b)} = \frac{0.467 - (0.61 - 0.15)}{(0.61 - 0.15)} = 0.01625$$

Step-5: Determination of tensile forces of geosynthetics

For K_g = 225 kN/m, from equation 4.17, the mobilized tensile strength of upper and lower geosynthetic will be

$$T_u = T_l = \varepsilon K_g = 0.01625 * 225 = 3.657 \text{ kN/m}$$

From equation 4.18, the vertical component of upper and lower geosynthetic will be:

$$T_{uv} = T_{lv} = T_u \sin\theta = 3.657 * \sin(17.9) = 1.12\ kN/m$$

From equation, 4.21, the other vertical component due to confining stress will be:

$$T_{v2} = \Delta\sigma_3 h_L tan\varphi_L = (T_u + T_l)\ cos\theta\ tan\varphi_L$$

$$T_{v2} = (3.657 + 3.657)\cos(17.9)\tan(35) = 4.87\ kN/m$$

Step-6: Determination of stress on RPP

From equation 4.22, the stress of RPP is as follows:

$$\sigma_p = \frac{\gamma Hs + 4(T_{uv} + T_{lv} + T_{v2})\ s}{b}$$

$$\sigma_p = \frac{20*1.8*0.61+4(1.12+1.12+4.87)*0.61}{0.15} = 262.1 \text{ kPa}$$

Step-7: Determination of stress on adjacent soil between RPPs

From equation 4.23, stress on subsoil between RPPs is as follows:

$$\sigma_s = \frac{\gamma Hs - 4(T_{uv} + T_{lv} + T_{v2})\ s}{s - b}$$

$$\sigma_p = \frac{20*1.8*0.61-4(1.12+1.12+4.87)*0.61}{0.61-0.15} = 10.02 \text{ kPa}$$

Step-8: Determination of SCR and SRR

From equation 4.1, the SCR can be determined as follows:

$$SCR = \frac{\sigma_p}{\gamma H} = \frac{262.1}{20 * 1.8} = 7.28$$

Similarly, from equation 4.2, the SRR can be determined as follows:

$$SRR = \frac{\sigma_s}{\gamma H} = \frac{10.02}{20 * 1.8} = 0.28$$

Step-9: Determination of net ultimate load carried by single RPP

From equation 4.24, the RPPs in saturated clays under undrained condition (φ = 0), the net ultimate load can be as follows:

$$Q_P = N_c^* \, c_u \, A_p - \, Q_n = \, N_c^* \, c_u \, A_p - \frac{pK_0\gamma_f' H_f^2 \tan\delta'}{2}$$

$$Q_P = \, 9 * 312 * 0.15 * 0.15 - \frac{4 * 0.15 * (1 - sin18) * (22 - 9.81) * 1.8^2 * \tan(0.6 * 18)}{2}$$

$$Q_P = 61 \; kN$$

Step-10: Determination of group efficiency

The group efficiency of RPPs can be determined by using Converse-Labarre equation.

The group efficiency (η) is expressed as:

$$\eta = 1 - \left[\frac{(n_1 - 1)n_2 + \, (n_2 - 1)n_1}{90 \, n_1 n_2}\right] \tan^{-1}(b/s)$$

For 15 cm × 15 cm RPPs at 0.61 m center to center spacing, the group efficiency will be

$$\eta = 0.727$$

Step-11: Determination of ultimate bearing capacity:

The ultimate bearing capacity can be determined from equation 4.26.

$$q_u = \frac{Q_p * SCR * \eta + N_c c_u F_{cs} F_{cd} A_s * SRR}{A}$$

$$q_u = \frac{61 * 7.28 * 0.727 + 5.7 * 12 * 1 * 1 * (0.61^2 - 0.15^2) * 0.28}{0.61 * 0.61}$$

$$q_u = 885.7\ kPa = 18493.4\ psf$$

Thus, the bearing capacity of the RPP supported embankment can be determined following the above steps.

Bearing capacity without RPP reinforcement and LTP

For the soft foundation soil, the bearing capacity without any ground improvement can be determined using the general bearing capacity equation proposed by Meyerhof (1963). The general bearing capacity equation can be expressed as follows:

$$q_u = c' N_c F_{cs} F_{cd} F_{ci} + q N_q F_{qs} F_{qd} F_{qi} + \frac{1}{2} \gamma B N_\gamma F_{\gamma s} F_{\gamma d} F_{\gamma i} \quad (4.27)$$

In this equation, c′ = cohesion; q = effective stress at the level of the bottom of the foundation; γ = unit weight of soil; B = width of foundation; $F_{cs}, F_{qs}, F_{\gamma s}$ = shape factors; $F_{cd}, F_{qd}, F_{\gamma d}$ = depth factors; $F_{ci}, F_{qi}, F_{\gamma i}$ = load inclination factors; N_c, N_q, N_γ = bearing capacity factors.

For the present example, the latter two term will be zero since depth of the foundation = 0 and φ = 0. Substituting the soil parameters of present example in equation 4.27:

$$q_u = c' N_c F_{cs} F_{cd} F_{ci} + q N_q F_{qs} F_{qd} F_{qi} + \frac{1}{2} \gamma B N_\gamma F_{\gamma s} F_{\gamma d} F_{\gamma i} = 12 * 5.14 * 1 * 1 * 1 + 0 + 0$$

$$q_u = 61.7\ kPa = 1288.3\ psf$$

Therefore, the soft foundation soil has a bearing capacity of 61.7 kPa before any kinds of ground improvement. On the other hand, when the foundation soil was improved with 15 cm 15 cm RPP @ 0.61 m spacing, the bearing capacity was found 885.7 kPa. Thus, the bearing capacity for RPP and LTP supported embankment is 14.3 times higher compared to the control section.

For different combinations of RPP size and spacing, the bearing capacity was evaluated for the same example embankment. Figure 4.13 shows the net bearing capacity for different RPP size and spacing. It is also evident that, with the increase of RPP size and decrease of spacing, the net bearing capacity increases.

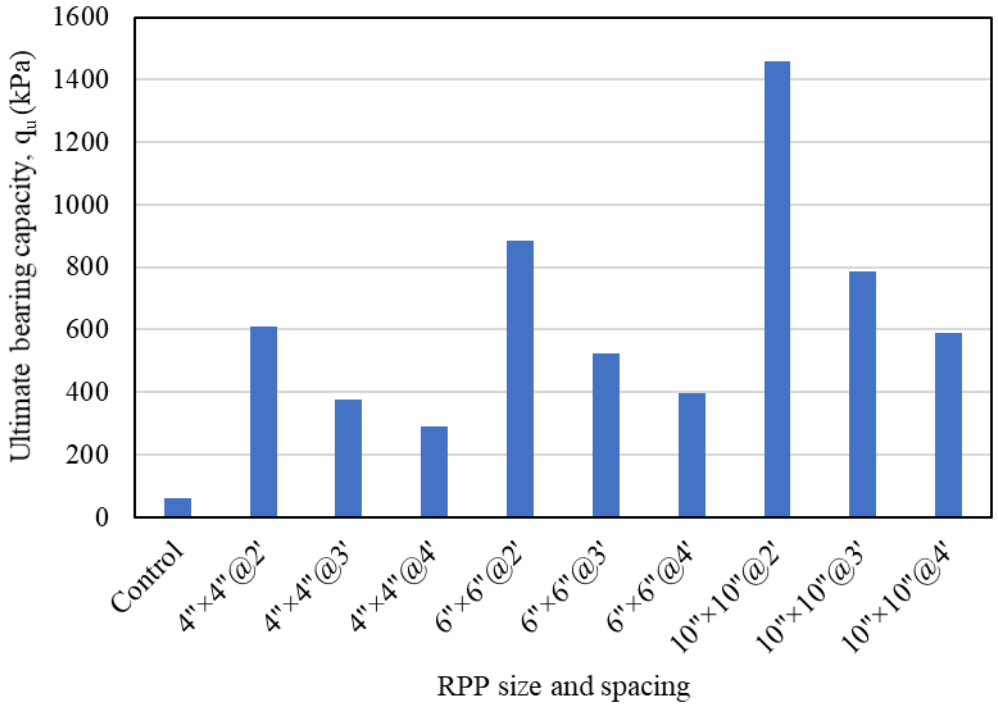

Figure 4.13: Ultimate bearing capacity for different RPP size and spacings

4.6 Conclusions

This paper presented a simple analytical solution for the geosynthetic reinforced and RPP supported embankment on soft soil. In the development of the analytical solution, only vertical

deformations were assumed for the embankment, RPPs, and foundation soil. The geosynthetics were considered to deform in a circular shape in response to a uniform embankment load. Using vertical force equilibrium of a unit cell consisting of one RPP and surrounding soil, the analytical solution was obtained.

The present method is validated by comparing the obtained values with the field results of well-instrumented test sections. The results demonstrate that the proposed analytical solution can provide dependable and consistent results for the differential settlement, SCR, and SRR. The current method was also compared with another similar field study and some standard design methods. In all the cases, the predicted results are in good agreement with other methods.

A parametric study is also performed to investigate the effect of different design parameters such as RPP size, spacing, tensile stiffness of geosynthetics, and friction angle of LTP on load transfer mechanism. The analysis data indicates that with an increase in the size of RPP installed at closer spacing, SCR will increase and SRR will decrease. Furthermore, the application of high strength geosynthetics in combination with compacted aggregate will increase the efficiency of the load transfer platform.

The proposed method is simpler compared to the existing methods for evaluating the stresses on RPPs and adjacent soil. Besides, there is no need for trial values which is often required for some of the design methods such as EBGEO 2011. However, the current analysis method can be further improved by considering more variable parameters for reliable and accurate prediction.

CHAPTER 5

NUMERICAL ANALYSIS OF RECYCLED PLASTIC PIN SUPPORTED EMBANKMENT WITH GEOSYNTHETIC PLATFORM

ABSTRACT

Construction of embankment over soft foundation soils is incredibly a challenging task due to the risk of bearing failure and excessive settlement of foundation soil. Most of the available conventional methods for addressing these problems are either expensive or time-consuming or both. Therefore, research has been striving to develop a sustainable alternative to the current conventional methods. A noble approach to improve the soft foundation soil could be the use of Recycled Plastic Pins (RPP) in combination with geosynthetics. The objective of this study is to evaluate the effectiveness of RPP in improving the bearing capacity of soft foundation soil using finite element analysis. The numerical investigation was conducted using finite element software PLAXIS 2D. The model was calibrated against the field measured data in the context of settlement and pressure variations. The performance of the RPP supported embankment was evaluated with maximum consolidation settlement, differential settlement, and soil arching effect. Furthermore, an extensive parametric study was performed to evaluate the effect of RPP size, and spacing, load transfer platform, stiffness of geosynthetics, and shear strength of embankment fill.

Keywords: Recycled Plastic Pins, Load Transfer Platform, Embankment, Numerical Modeling, Soil Arching

5.1 Introduction

The uses of Geosynthetic Reinforced Pile Supported (GRPS) embankments are increasing day by day to construct highways and railways over soft foundation soil. GRPS embankments are becoming popular due to their rapid construction, low cost, and small total and differential settlements compared to those of the traditional soft soil–improvement methods (Han and Gabr 2002). The surface and embankment loads are partially transferred to the piles by arching action that occurs in the granular embankment fill material, resulting in stress reduction on the subsoil. The inclusion of tensile reinforcement enhances the load transfer mechanism and considerably minimizes the maximum as well as differential settlements (Islam et al. 2021a).

Several studies have been reported on the arching mechanism and analysis of pile-supported embankment. The effectiveness of geogrid reinforced, and pile-supported embankment was evaluated by Oh and Shin (2007) with field tests and numerical analysis. They found that the geosynthetic reinforcement slightly interferes with soil arching and helps reduce differential settlement of structures over the soft ground. Pham (2020) investigated the influence of different factors such as soil arching in embankment fill tensioned membrane effect of geosynthetics, support of the soft subsoil. The author concluded that the efficacy of the pile-supported embankment increases with an increase in friction angle of embankment fill, geosynthetic stiffness, degree of consolidation of subsoil. On the other hand, efficacy decreases with the increase of modulus of subsoil.

Geosynthetics have been used extensively for improving the deformation and the stability of embankments and pavements (Ahmed and Islam 2020). To enhance the effectiveness of pile-supported embankment, a load transfer platform (LTP) is usually provided at the base of the

embankment to minimize the overall deformation of the embankment (Abdullah and Edil 2007). Geosynthetics can be employed within well-graded aggregate layers. The interaction between multiple layers of the geosynthetic reinforcement and granular fill results in a stiff LTP beam with less differential settlement. Briancon and Simon (2012) investigated the performance of piled embankment over soft soil through a full-scale experimental study and reported how the load transfer mechanism is different for single and multilayer reinforcement. Abdullah and Edil (2007) conducted a field-scale study over soft ground to evaluate the performance of different types of LTP. It was found that biaxial geogrid with three or more layers minimized the differential settlement compared to two-layer uniaxial geogrid or concrete LTP.

Numerical analysis nowadays is often used for evaluating the performance of piled embankment (Pham 2020, Islam et al. 2021b). Han and Gabr (2002) carried out a numerical study to investigate pile-soil-geosynthetic interaction and concluded that the GRPS system reduces settlement, while larger stiffness of piles promotes a higher soil arching effect. Finite element (FE) analysis was conducted by Rowe and Liu (2015) to investigate the effect of different LTPs. The authors found that the inclusion of piles decreases the settlement at the subsoil surface to 52% of that in the unimproved section. The addition of a single layer of geotextile reinforcement further reduced settlement to only 31% of that of the unimproved section.

Among the available methods, Recycled Plastic Pin (RPP) is a new technology for ground improvement. RPP was first used in the state of Missouri and Iowa as a sustainable option for highway slope stabilization (Hossain et al. 2017). Nowadays, RPP is being utilized in many other states of the USA as a cost-effective solution for slope stabilization (Khan et al. 2016; Hossain et al. 2017; Bhandari et al. 2020). RPP could be a viable alternative to piles for improving the bearing capacity of soil by increasing its stiffness (Badhon et al. 2021). Compressive strengths of RPP

ranged from 11 MPa (230 ksf) to 21 MPa (439 ksf) at a nominal strain rate of 0.006 %/min while compression moduli determined at one percent strain ranged from 552 MPa (11529 ksf) to 1310 MPa (27360 ksf) (Bowders et al. 2003; Chen et al. 2007). Compared to concrete or steel piles, RPPs are lightweight and less susceptible to chemical degradation. RPPs are predominantly polymeric material, fabricated from recycled plastics and other waste materials (Bowders et al. 2003; Chen et al. 2007). Approximately 600 recycled water/soda bottles are used for a 3 m × 100 cm^2 (Length × Area) RPP (Hossain et al. 2017). Therefore, the use of RPP reduces the waste volume entering the landfill and provides an additional market for recycled plastic (Loehr et al. 2000; Bhandari 2021).

Even though RPP is being used for slope stabilization projects, the lack of a well-defined design procedure remains one of the biggest barriers limiting its wider use, such as for improving the bearing capacity of soft soil. Engineers must have a comprehensive understanding of the behavior of RPP supported embankments to carry out safe and economical design and construction. Very few studies have been conducted on the behavior of geosynthetic reinforced and pile-supported embankment (Islam et al. 2021b). However, there is no extensive parametric study for investigating the influential parameters such as RPP size and spacing, geosynthetic stiffness, types of LTP, shear strength of embankment fill, etc. The objective of this study is to evaluate the effectiveness of RPP in improving the bearing capacity of soft foundation soil using finite element analysis. The numerical investigation was conducted using finite element software PLAXIS 2D. An extensive parametric study was performed to evaluate the effect of important parameters for load transfer and settlement reduction. The results from the present study will assist in deriving a more economical design and in improving the efficiency of RPP supported embankments.

5.2 METHODOLOGY

5.2.1 Model development

The RPP supported embankment with LTP was idealized by the PLAXIS 2D program (Plaxis 2D reference Manual 2020). PLAXIS 2D is a finite element package that can perform deformation and stability analyses for different geotechnical applications. The elastic-perfectly plastic Mohr-Coulomb soil model was utilized for deformation analyses using 15 node triangle elements. A plane strain model was used in the analysis. Standard fixities were applied as boundary conditions at the base and the sides of the model (Kibria et al. 2014; Ahmed et al. 2020).

A model was generated to simulate the vertical loading in both the control and reinforced section (Figure 5.1). The non-reinforced and RPP reinforced soft soils under embankment loading were idealized by PLAXIS 2D (2020) program. RPP was modeled using an elastic plate element. RPPs with a length of 10 ft (3 m) and three different cross-sections were considered: 4" × 4" (10 cm × 10 cm), 6" × 6" (15 cm × 15 cm) and 10" × 10" (25 cm × 25 cm). The modulus of elasticity (E) was considered as 448 MPa (Bowders et al. 2003). The properties of RPP for different cross-sections are presented in Table 5.1. To simulate the interaction between RPP and soil, interface material was applied. Interface strength reduction factor (R_{inter}) was considered 0.7 for all soil layers.

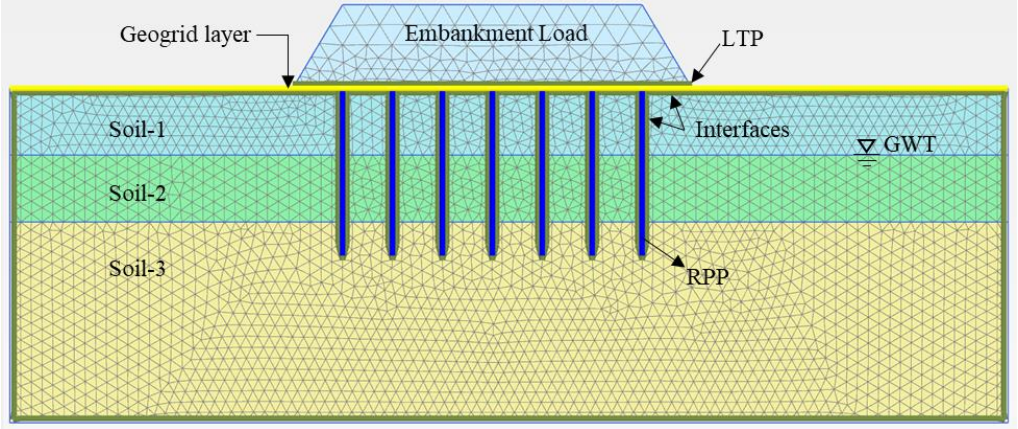

Figure 5.1 The geometry and connectivity plot of the PLAXIS model

Table 5.1 RPP properties

Section	Modulus of Elasticity, E (MPa)	EA (kN/m)	EI (kN m^2/m)	w (kN/m/m)	Poisson's ratio, υ
4"×4" (10 cm×10 cm)	448	14.6×10^3	13.1	0.09	0.25
6"×6" (15 cm×15 cm)	448	35.0×10^3	66.1	4.14	0.25
10"×10" (25 cm×25 cm)	448	94.8×10^6	8812.7	5.79	0.25

The objective of the numerical analysis is to model the RPP supported embankments over soft soil for long-term consolidation analysis. The model was adopted based on the field results of Islam et al. (2021a). The finite element model was simulated with three layers of native soil profile along with applied soil surcharge load (Table 5.2). Native soil consists of 1.8 m (2 ft) of lean clay at the top (soil layer 1), underlain by 2.2 m (7.2 ft) of sandy lean clay (soil layer 3). At 2.8 m (9 ft) depth, eagle ford shale was encountered which was continuous till 12 m (40 ft). Silty sand was used for embankment loading. Since the embankment fill had high permeability, there was no accumulation

of pore water pressure after rainfall beneath the embankment. All the soil layers were considered to exhibit drained behavior for considering consolidation effect.

In the load transfer platform (LTP), one layer of Recycled Crushed Concrete Aggregate (RCCA) was considered which was sandwiched between two layers of geogrid. Tri-axial geogrid was modeled by using a linear elastic sheet element, which acts as an isotropic element at each node and unable to work under compression. Tensile stiffness (EA) was considered as 225 kN/m according to manufacturer specification (Islam et al. 2021a). Field results from Islam et al. (2021a) were used to calibrate the model to better predict field scenarios.

5.2.2 Model calibration and validation

Islam et al. (2021a) conducted a field study with two test sections: control and reinforced section with 6"×6" RPPs installed at 0.6 m center to center spacing. The deformation results from the field study were used to calibrate the present FE model. Islam et al. (2021a) reported the settlement results for 270 days with two stages of loading condition. Therefore, the FE model was simulated to determine the consolidation settlement for 270 days of construction. The calibration was performed by back analysis of the foundation soil properties. Several iterations were performed by changing the soil parameters within a certain range as obtained from the laboratory tests (Islam et al. 2021a). Table 5.2 shows the back-calculated soil properties along with all the soil parameters used in the calibrated model. Various interface angles ranged from 0.67 to 0.7 were selected for the optimum calibration of the model.

The inclinometer results from Islam et al. (2021a) showed that the control and the reinforced section settled 34.4 mm and 17.1 mm with phase-1 loading (1.2 m embankment height) after 91 days. After the application of phase-2 loading (1.8 m embankment height), the settlements were

found 52.2 mm and 23 mm, respectively. From the calibrated models, the settlements for control and reinforced sections were found 34.0 mm and 21.3 mm (Phase-1 loading) and 53.9 and 27.9 mm (phase-2 loading), respectively (Figure 5.2). The settlement curves with time are in good agreement with the obtained field results (Figure 5.2). The result from numerical models only differs a maximum of 3.3% and 24.6% for the control and reinforced section, respectively. The model results of the reinforced section overestimate the field results. The effect of compaction due to the pile driving was not considered in the numerical model which might be one factor for the overestimation.

Table 5.2 Soil properties of subsoil and embankment fill used in the model

Parameter	**Symbol**	**Embankment Fill**	**Lean Clay**	**Sandy Lean Clay**	**Eagle Ford Shale**	**RCCA**
Thickness	T (m)	1.8	0.6	2.2	4.2	0.1
Dry unit weight	γ_d (kN/m^3)	17.8	16.0	16.7	18.9	17.3
Cohesion	c_u (kPa)	-	12	27	312	-
Friction angle	φ' (º)	32	17	20	-	40°
Modulus of Elasticity	E (MPa)	25	1.4	4.8	90	40.5
Permeability	k (cm/s)	3.2×10^{-4}	2.5×10^{-6}	9.7×10^{-6}	1.0×10^{-9}	-
Compression index	C_c	-	0.28	0.20	-	-
Coefficient of consolidation	c_v (m^2/day)	-	0.015	0.02	-	-
Material model		Mohr-Coulomb	Mohr-Coulomb	Mohr-Coulomb	Mohr-Coulomb	Mohr-Coulomb
Loading Condition		Drained	Drained	Drained	Drained	Drained
Interface		0.67	0.7	0.7	0.7	0.7

The present model was further validated with the pressure plate data from Islam et al. (2021a). The stresses on RPP and adjacent soil in between RPP were compared between the present study and Islam et al. (2021a). Also, middle and edge locations were considered for the comparison. The comparison between the field and predicted model data is shown in Figure 5.3. It can be observed that the results from the predicted model are consistent with the field results. The maximum difference of pressure on soil was found 47.0% while the maximum difference of pressure on RPP was found only 10.7%. Therefore, the present FE model could successfully simulate the behavior of foundation soil settlement.

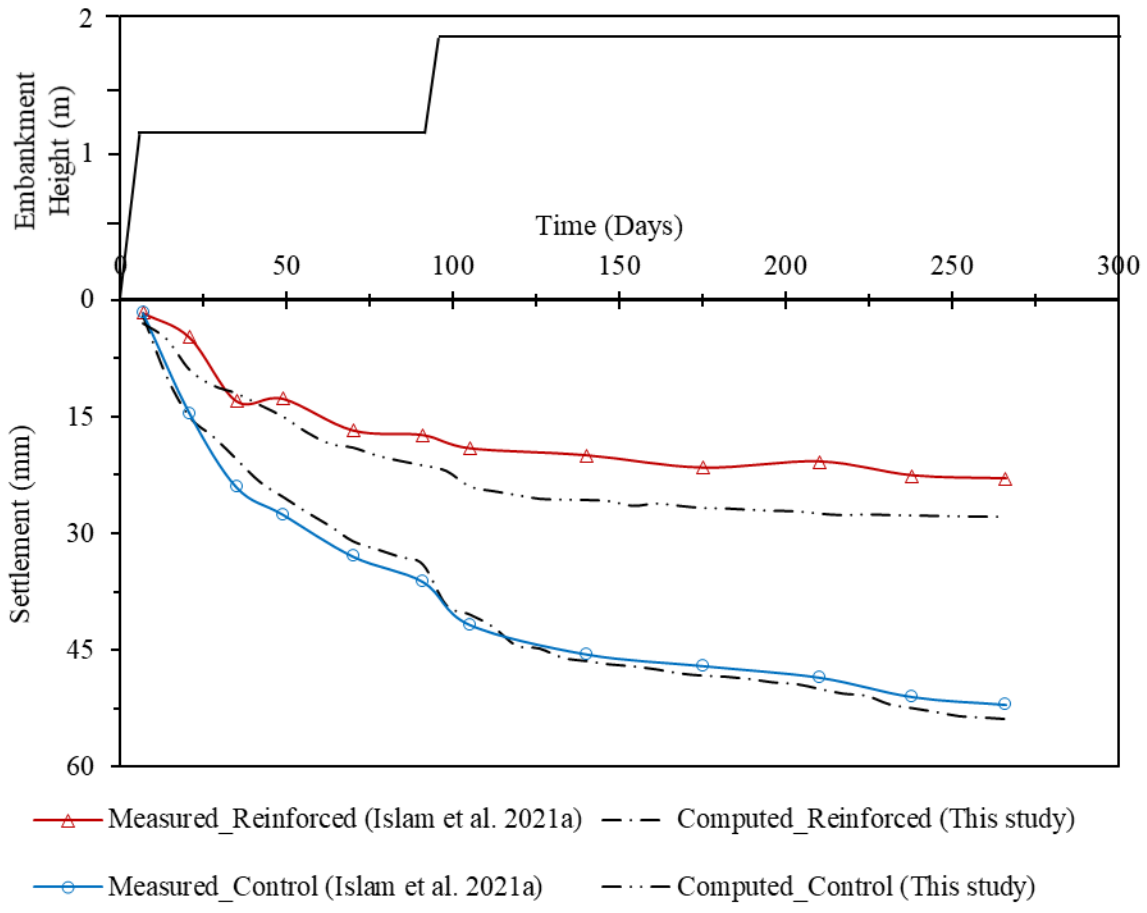

Figure 5.2 Comparison between predicted model results and measured field results from Islam et al. (2021a).

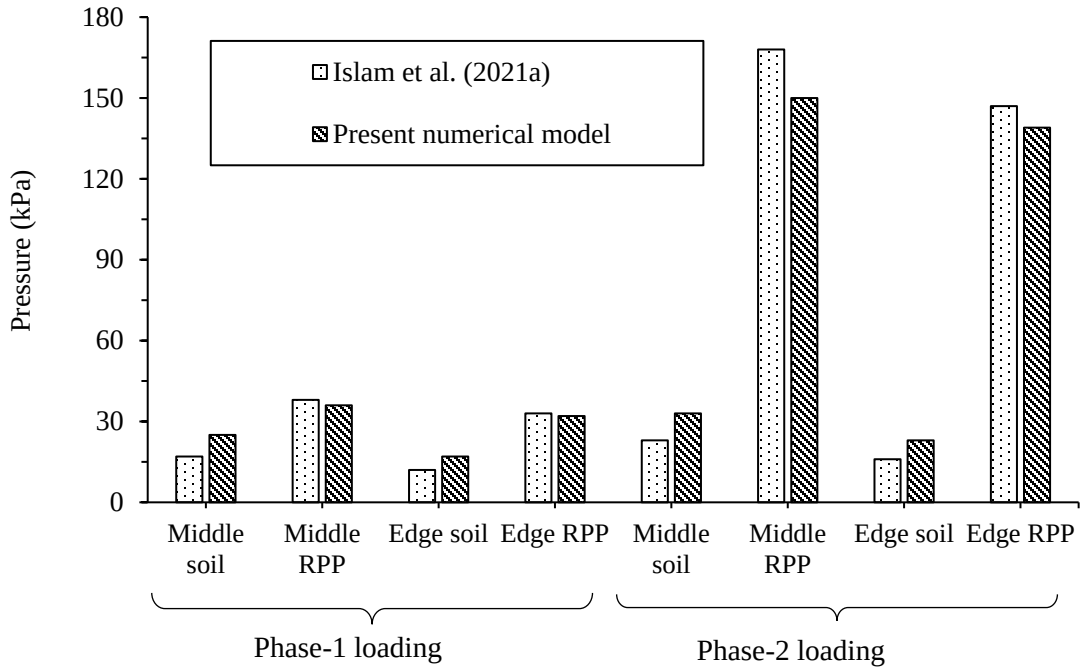

Figure 5.3 Comparison of stresses between present study and Islam et al. (2021a)

5.3 Result and Discussion

5.3.1 Performance evaluation of RPP reinforced section

The identical soil parameters used in the calibrated model were utilized to perform the deformation analysis for the reinforced test section. The model details for the reinforced section are presented in Figure 1. Vertical deformation diagrams (displacement contour) of the control and 15 cm × 15 cm (6"×6") RPP reinforced section are presented in Figure 5.4. It is evident that the RPP is supporting the loads from the embankment, and the load from the soil is being transferred to the RPP by the arching effect of geogrid. Also, underneath the foundation, the soil is trying to move laterally to accommodate the settling structure, which is also restricted by the RPP. Thus, RPP helps to provide additional support and minimizes the settlement.

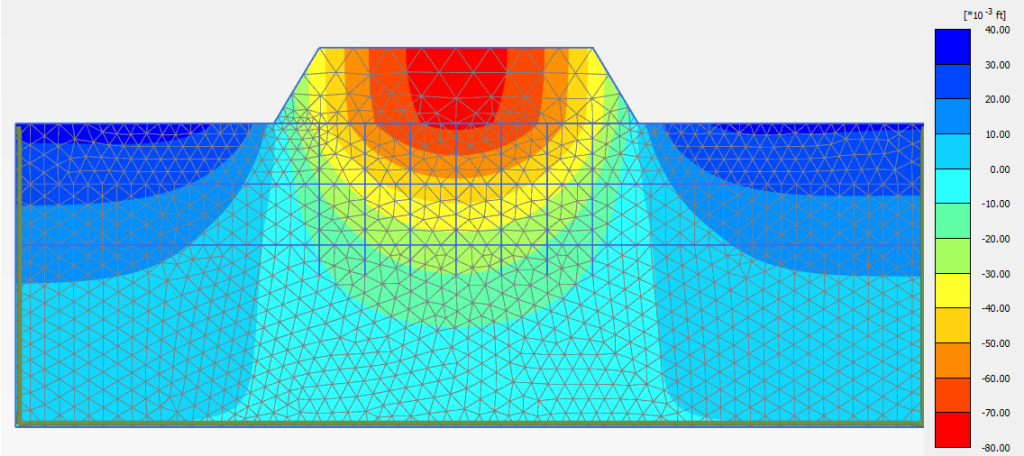

(a)

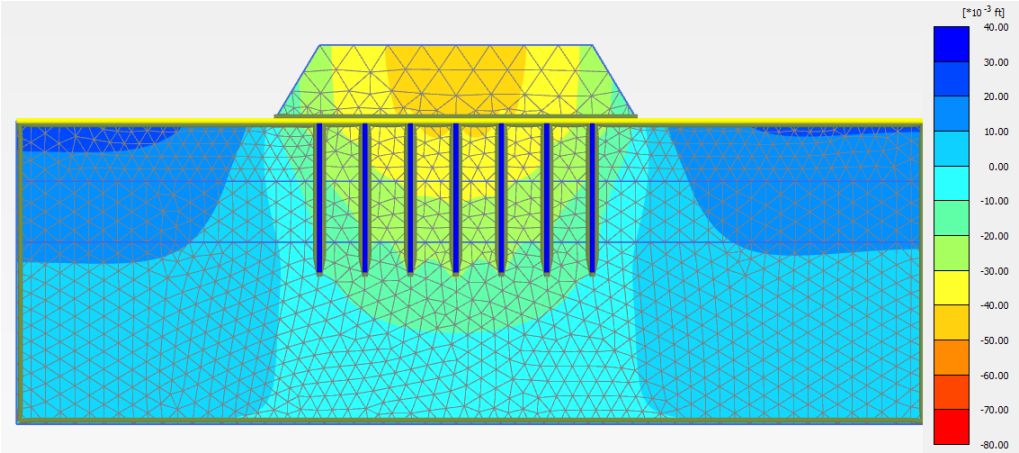

(b)

Figure 5.4 Contour diagram of vertical displacement (a) control section (b) RPP (6"x6" @ 0.9 m c/c) reinforced section.

The stress variation on RPPs and adjacent soil are presented in Figure 5.5. After the application for 1.8 m loading for the 6"×6" @ 0.6 m c/c RPP reinforced section, the maximum stress on RPPs was found 168 kPa. This vertical stress concentration occurs because the RPPs are stiffer than the surrounding soil media. This type of stress distribution was explained by van Eekelen et al. (2015). The analysis model presented by van Eekelen et al. (2015) refers to the triangular distribution of vertical stress, with a maximum part on the pile top and minor values on the region between piles. Zhao et al. (2019) published a similar case study about a widened highway embankment project,

in which prestressed tubular piles and geogrids were used to reinforce the embankment foundation. The in-situ measurements of earth pressures were reported. The resulting embankment load was 91.2 kPa, and the average earth pressure on top of the pile was 279.7 kPa, which is 207% higher than the embankment load. For this study, the obtained stresses on RPPs implied that the RPPs experienced about 342% higher load than the embankment load. The higher value of load sharing indicates that RPP, in combination with LTP, is more effective in distributing the embankment load to stiffer strata.

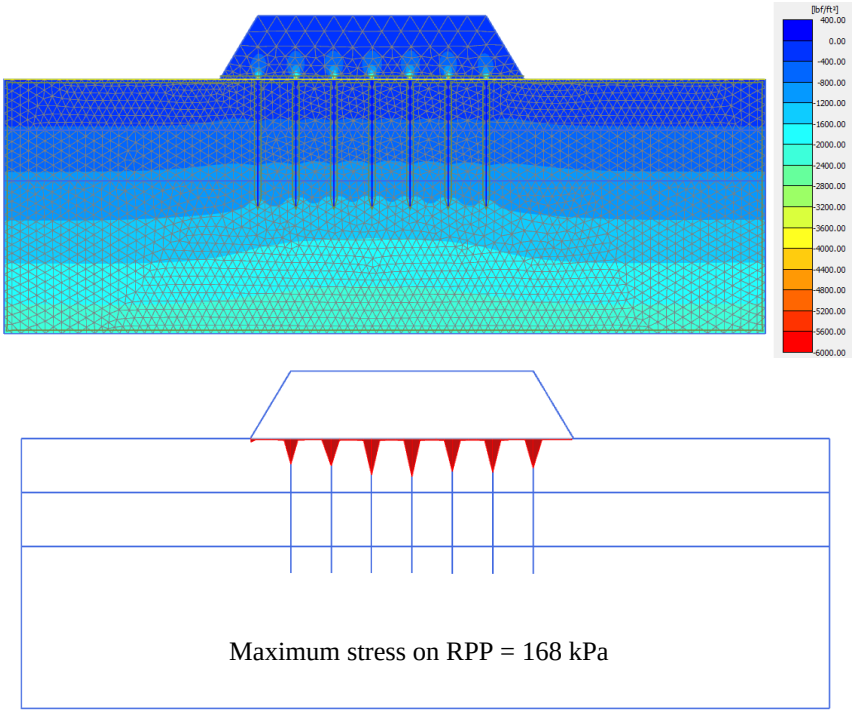

Figure 5.5 Stress diagram for 6"×6" @ 0.9 m c/c RPP reinforced section

5.3.1.1 *Maximum settlement*

A relative comparison plot of settlement between control and reinforced test sections (4"×4", 6"×6", 10"×10" RPP) observed from the calibrated models are presented in Figure 5.6. Based on the model-predicted results, the control section collapsed for an embankment height of 4.3 m. The reinforced sections were analyzed up to an embankment height of 5.2 m and were performing well;

however, the settlement increased with the increase of the height of the embankment. A significant difference in the settlement was found between the control section and the reinforced sections. The settlement reductions of the 4"×4", 6"×6", 10"×10" RPP reinforced sections for 2.4 m embankment height were about 24.2%, 43.9%, and 69.7%, respectively compared to the unreinforced section. Also, among the reinforced sections, the difference in the settlement was found to be gradually increasing with increasing embankment height.

Han and Gabr (2002) conducted a numerical study to evaluate the performance of geosynthetic reinforced pile-supported embankment for different fill heights. The authors found that the unreinforced embankment experienced a larger settlement compared to the reinforced embankment. Geogrid was used as the load transfer element, which ensures load mobilization to the piles. Similar conclusive results were observed from the current numerical analysis (Figure 5.4). RPP reinforced section showed considerably lower settlement compared to the unreinforced section. Also, with increasing RPP size, the settlement was found to be reduced.

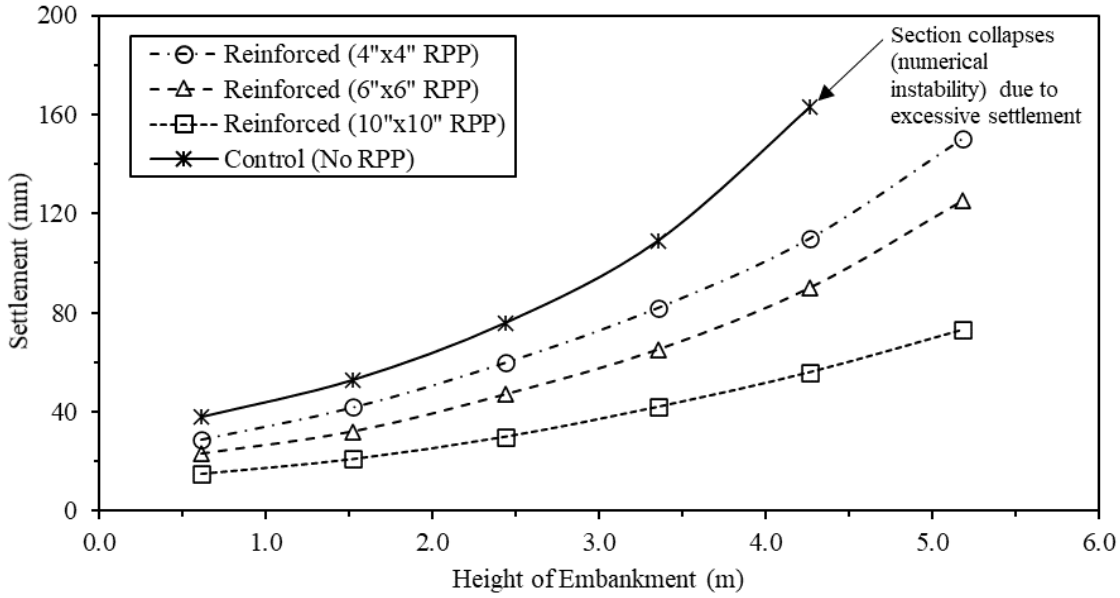

Figure 5.6 Maximum settlement results of control and reinforced section (at 0.9 m center to center spacing) for different embankment height

5.3.1.2 *Differential settlement*

Figure 5.7 shows the comparative settlement of the test sections at different points of the embankment base from the edge to the center of the embankment. It was observed that for the control section, settlement increased smoothly with the distance to the center of the embankment, while for the reinforced sections, settlement varied abruptly due to the inclusion of geosynthetic and RPP reinforcement. The settlement was higher between the RPPs because of the flexibility of the geogrid platform. The deformed shape of geogrids helped to transfer more load to RPPs by the soil-arching mechanism. At the point of RPPs, the settlement is comparatively less as the RPPs are stiffer and have relatively fixed support at their toe within the underlying firm soil layer.

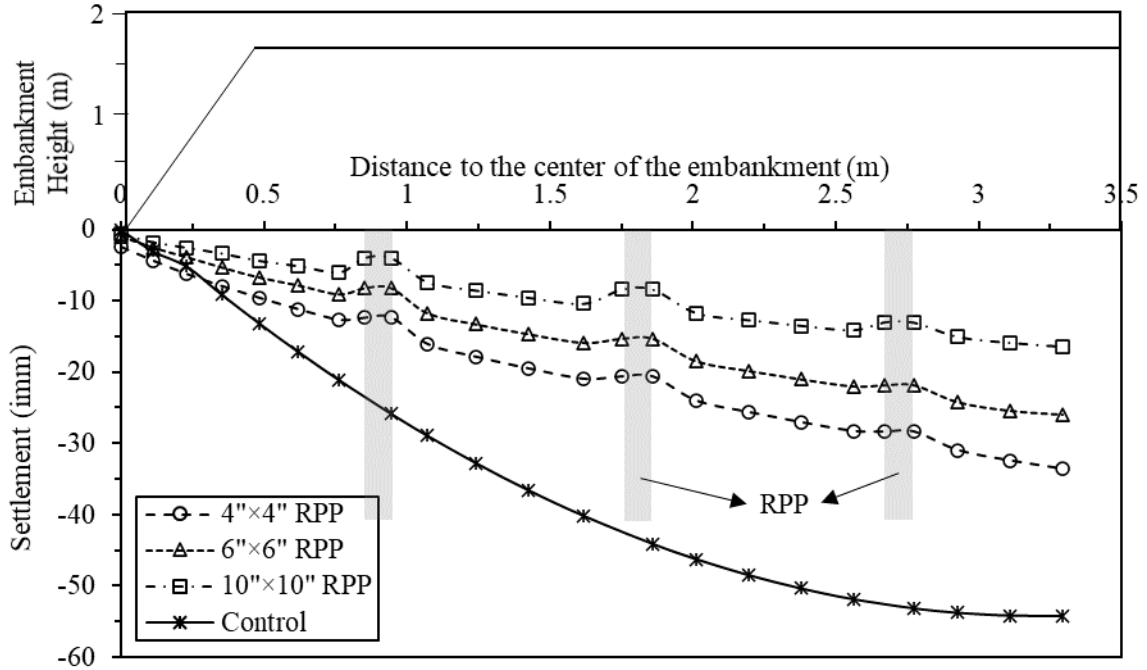

Figure 5.7 Settlement comparison between the control and reinforced test sections from the toe to the center of the embankment.

Jenck et al. (2009) observed similar results from a numerical study conducted for concrete pile-supported embankment, where the piles were considered to be completely rigid, therefore

insignificant settlement was observed at the top of piles. Maximum settlements for the 4"×4", 6"×6", 10"×10" RPP reinforced sections for 1.8 m embankment height were found to be 33.6 mm, 25.9 mm, and 16.4 mm, respectively; which corresponds to a settlement reduction of about 38%, 52.2%, and 60% respectively compared to the unreinforced section.

The variation of maximum differential settlement with embankment height and spacing to width ratio (s/b) is shown in Figure 8. The differential settlement is expressed as the settlement difference between the top of the RPP and the adjacent soil between RPPs. It can be observed that the differential settlement for the control section is much higher than the reinforced sections. The differential settlement significantly decreases with the inclusion of RPPs. The rate of increase of differential settlement decreased after an embankment height of 2.4 m. A similar trend was observed by Oh and Shin (2007) where they reported that the increment of differential settlement with the height of the embankment decreased due to the geogrid reinforcement. Han and Gabr (2002) observed a similar pattern of differential settlement for the geosynthetic reinforced piled embankment. On the other hand, at higher embankment height, the maximum total settlement increased at a higher rate (Figure 5.6).

Furthermore, the differential settlement increases with the increase of the spacing to width ratio. Oh and Shin (2007) concluded that when the pile spacing to diameter ratio is greater than 5, the reduction of differential settlement is relatively small. From Figure 5.8, it can be observed that the differential settlement is much higher for s/b ratio 6 compared to 3.6. At 5.2 m embankment height, the increase in the differential settlement is 10% from s/b ratio 9 to 6, and 24% for s/b ratio 6 to 3.6. Oh and Shin (2007) obtained an increase in differential settlement 2.3% for s/b ratio 4.0 to

5.5, and 12.2% for s/b ratio 3.0 to 4.0. The results of the present study are in good agreement with the results obtained from Oh and Shin (2007).

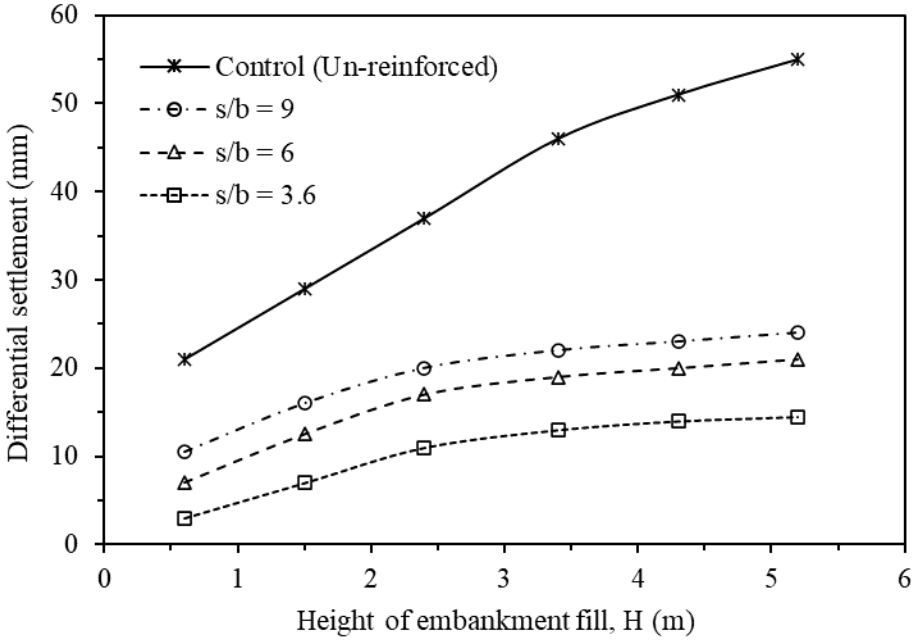

Figure 5.8 Differential settlement with embankment height

5.3.1.3 *Vertical stress and arching effect*

The pressures on RPP and adjacent soil between RPPs were obtained from the numerical modeling. The average vertical stress on RPP was calculated by dividing the axial force with the cross-sectional area of the RPP. The performance of RPP supported embankment can be evaluated based on the soil arching ratio, ρ and Stress Concentration Ratio, SCR (Han and Gabr 2002; Oh and Shin 2007). To understand the load transfer efficiency on RPP, both soil arching ratio and stress concentration ratio were calculated for different combinations.

The soil arching ratio can be defined as the ratio of the stress on the soil to the total surcharge load and can be expressed as follows:

$$\rho = \frac{\sigma_s}{\gamma H + q_0} \tag{5.1}$$

where, ρ = soil arching ratio; σ_s = stress on soil in between RPPs; γ = unit weight of embankment fill; H = height of embankment; q_0 = surcharge load.

The SCR is defined as the ratio of measured vertical stress acting on the top of the RPP (σ_p) to that acting at the ground surface between the RPPs (σ_s), expressed as:

$$SCR = \frac{\sigma_p}{\sigma_s} \tag{5.2}$$

The stress above LTP is mainly induced by the soil arching while the stress beneath the LTP is induced by both soil arching and the component of tension from the geosynthetic. The variation of soil arching ratio with embankment height is shown in Figure 5.9. It can be observed that the soil arching ratio decreases with an increase in the embankment height. This trend is found consistent with the results obtained by McNulty (1965) where he experimented with a trapdoor model to study the arching effect. At a low embankment height, the soil arching is not active due to the low shear resistance in the embankment fill. However, with the increase of the embankment fill, more shear resistance accumulates for enhancing the development of soil arching. It is found that the soil arching ratio approaches towards a constant value with the increase of embankment height. Han and Gabr (2002) also reported a similar trend with a numerical study on geosynthetic reinforced and pile-supported embankment.

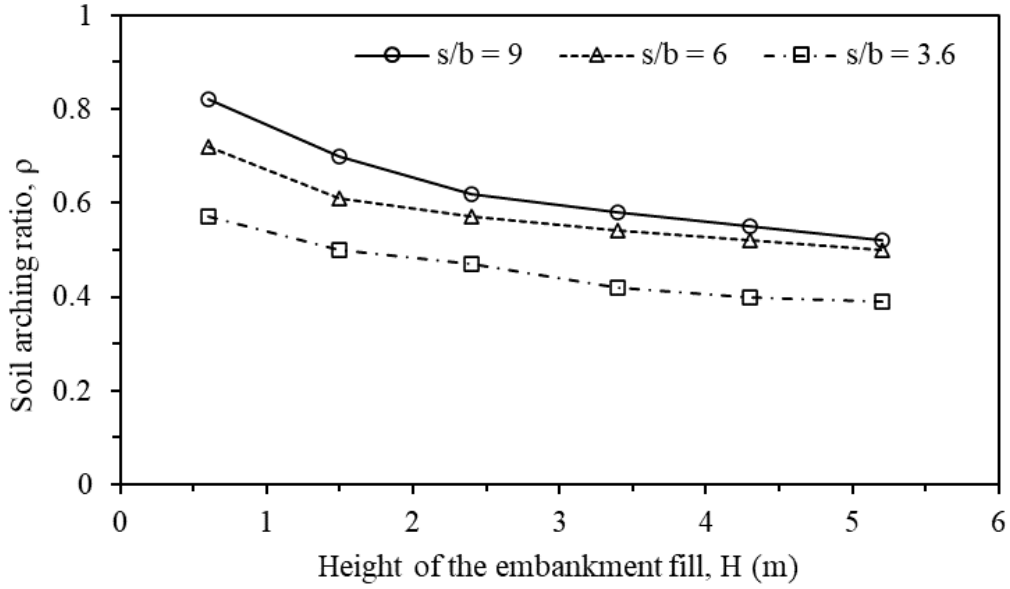

Figure 5.9 Variation of arching ratio with embankment height for different s/b ratio

The load transfer mechanism can be quantified with the values of SCR. A high value of SCR indicates the most effective load transfer from the embankment to the RPPs. The comparisons of SCR for different LTPs with other field studies are shown in Figure 5.10. It can be observed that the SCR value decreases with the increase of normalized embankment height (ratio of embankment height to spacing; H/s). The minimum SCR value was found as 4.7 for LTP-1, while the maximum value of SCR was found to be 7.8 for LTP-3. The high values of SCR indicate more load is transferred to the RPP rather than soil. Therefore, RPP, in combination with LTP, is effective for the stability of an embankment.

The obtained values of SCR are in good agreement with the results from Liu et al. (2007) and Zhao et al. (2019). Liu et al. (2007) conducted a field-scale study on geogrid-reinforced and pile-supported highway embankment over soft clay. The LTP was constructed with one layer of geogrid sandwiched between gravel layers. The SCR value from this study is slightly higher than Liu et al. (2007), with a difference of only 10%. Zhao et al. (2019) conducted a similar study of the PTC

pile-supported embankment and found the value of SCR 6.6, which is slightly higher than the values obtained from the present study. However, the results from Oh and Shin (2007) provided much lower SCR values than the present study, where they used only one layer of geogrid without any aggregate layer.

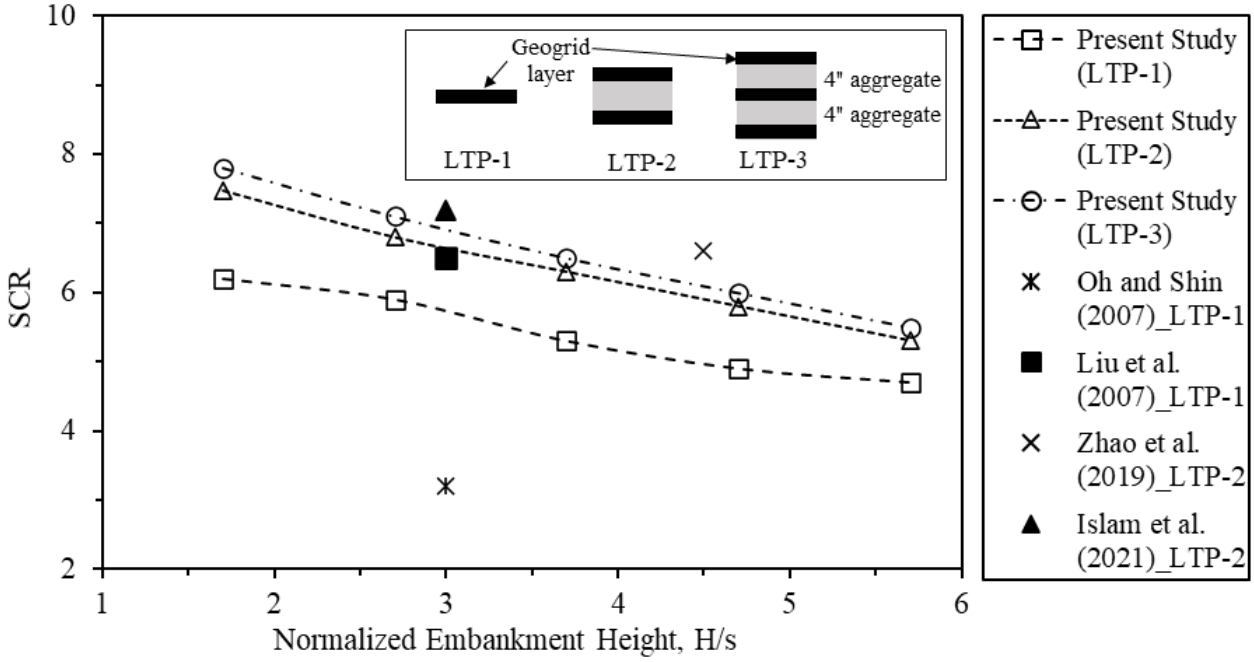

Figure 5.10 Comparison of SCR between this study and other literatures

5.3.1.4 *Performance efficacies*

The load efficacy and the differential settlement efficacy can be measured as an indicator of the overall LTP effectiveness. The load efficacy (E_p) can be defined as a ratio to the total vertical load carried by the piles to the total embankment load (W) and surcharge load (Q) (Ye et al. 2020) and can be expressed as follows:

$$E_p = \frac{F_p}{W + Q} \times 100\% \tag{5.3}$$

The differential settlement efficacy can be defined as a proportion of the difference between the maximum differential settlement on the top of the LTP ($\Delta S_{\max\_top}$) and at the base of the LTP ($\Delta S_{\max\_bott}$) to the maximum differential settlement at the base of the LTP (Girout et al. 2014) and can be expressed as follows:

$$E_s = \left(1 - \frac{\Delta S_{\max\_top}}{\Delta S_{\max\_bott}}\right) \times 100\% \quad (5.4)$$

Here, E_p and E_s are the load efficacies and differential settlement efficacies, respectively; F_P (kN) is the total load transferred onto the RPPs; W (kN) is the total embankment load; Q (kN) is the surcharge load; $\Delta S_{\max\_top}$ and $\Delta S_{\max\_bott}$ are the differential settlements between piles and subsoil at the top and at the base of the LTP, respectively. The greater values of load efficacy and/or the differential settlement efficacy indicate that the LTP can more effectively transfer the load to RPPs.

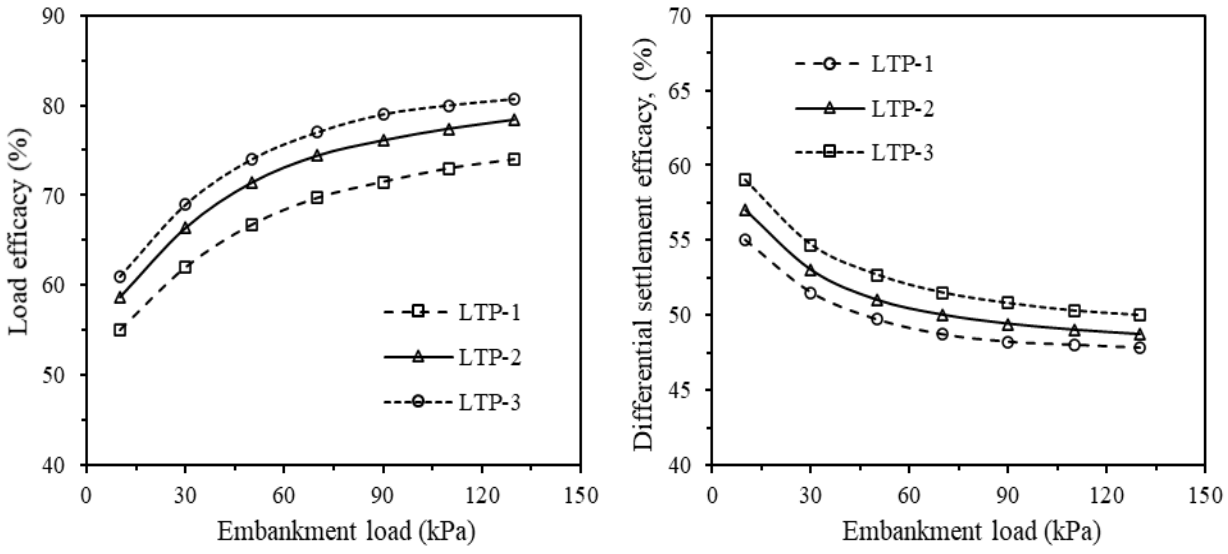

(a) (b)

Figure 5.11 Variation of efficacy with embankment load: (a) load efficacy; (b) differential settlement efficacy

The variations of the load efficacy and the differential settlement efficacy with embankment load are shown in Figure 5.11. It can be observed that both the efficacies are found increasing with the

increase of embankment load. The models with more layers of geosynthetics (LTP-3) has a higher efficacies compared to the single layer of geosynthetics. At 130 kPa embankment load, the load efficacy increased 5.9% (LTP-2) and 9.1% (LTP-3) compared to the LTP-1. The increase of load efficacy due to the increase of number of geosynthetic layers were not significant which is consistent with the findings from Chevalier et al. (2010). It was also observed that, the lower layer of geosynthetic was more important in transferring the embankment loads than the geosynthetics at higher elevation.

Similar observations were found for the differential settlement efficacies. Increasing the surcharge load led to a progressive decrease in the differential settlement efficacy. Differential settlement efficacy increased proportionately with the increase of number of geosynthetic layers. Badakhshan et al. (2019) and Ye et al. (2020) reported similar findings. They also concluded that differential settlement efficacy was reduced slightly by the closer spatial spacing between geosynthetic layers.

5.3.2 Parametric study

This section focuses on the parametric study of RPP supported embankment. The analyses have been conducted over a range of values to investigate the effect of several parameters on the load-deflection behavior of RPP supported embankment. The parameters considered in the analysis are RPP size, spacing, area ratio, types of the load transfer platform, embankment height, shear strength parameters of fill soil, and geosynthetic tensile stiffness. The influence of each parameter is evaluated through the consolidation settlement. In this parametric study, the design of the embankment and soil properties were considered from the calibrated model. Soil properties shown in Table 2 are considered as baseline case values. In the following sections, these values are used throughout unless otherwise specified.

5.3.2.1 *Influence of RPP size and spacing*

The present numerical study of the reinforced section was further evaluated using a parametric study. The parametric analysis was conducted to evaluate the effect of loading height of the reinforced section, the effect of different sizes, and the spacing of RPP on the settlement of the foundation soil. RPPs at 0.9 m center to center spacing are commonly used for slope stabilization or ground improvement projects (Hossain et al. 2017; Zaman 2019). For embankment design over soft soil, 0.6 m to 0.9 m spacing can be considered (Islam et al. 2021a). Therefore, in the current parametric study, along with the 0.9 m spacing, 0.61 m and 1.2 m RPP spacings were also considered.

Figure 5.12 shows the maximum consolidation settlements at the center of the embankment for different sizes and spacing of RPPs. Spacing between RPPs has a significant effect on settlement. With reduced spacing, a noticeable reduction in the settlement was observed for all sizes of RPPs. It is observed that the maximum settlement was found for 4"×4" with 1.2 m spacing, whereas the minimum settlement was found for 10"×10" with 0.9 m spacing. Reinforced section with 0.6 m spacing reduces settlement up to 35% compared to 1.2 m spacing section.

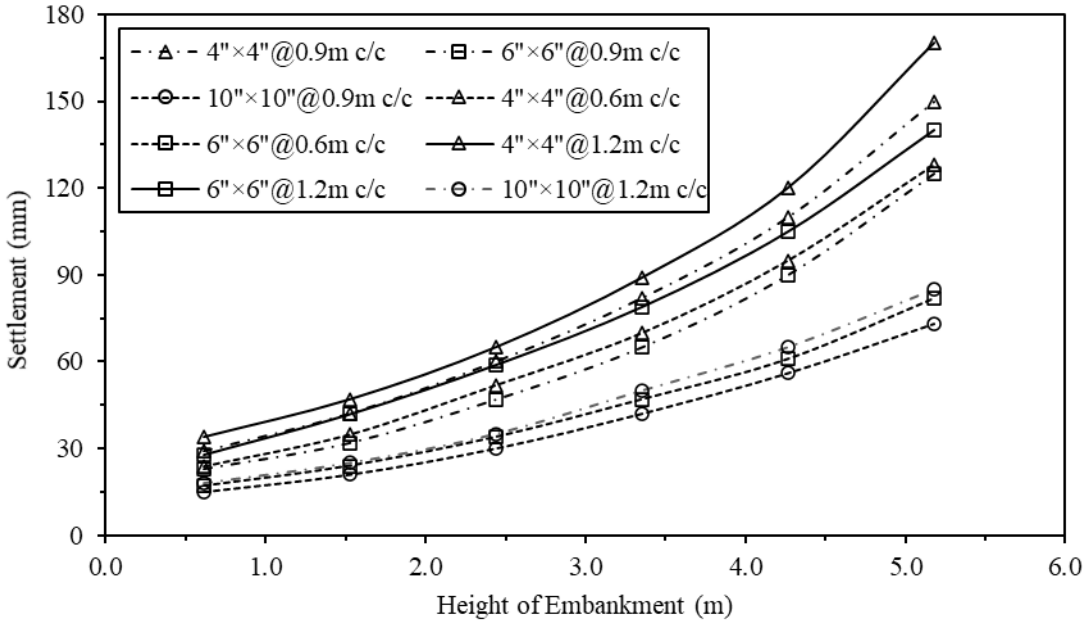

Figure 5.12 Settlement results for different sizes and spacings of RPP.

The settlement results largely depend on the percentage of area covered by RPPs. Increasing RPP size reduced settlement by providing additional support. The 4"×4" with 0.6 m spacing and 6"×6" with 0.9 m spacing layouts provided similar settlement results due to the same area ratio (2.8% of total area). The 10"×10" RPPs can reduce settlement up to 55% compared to the 4"×4" RPP section.

5.3.2.2 *Influence of area replacement ratio*

The area replacement ratio, A_r can be defined as the ratio between the total area of RPP to the loaded area. This parameter is important for an effective and economic design in the improvement of soft soil. Settlement improvement factor, n can be defined as the ratio between the settlement of the control section and the settlement of the reinforced section. Figure 12 shows the relationship between the settlement improvement factor and the area replacement ratio inverse. It can be

observed that the settlement improvement factor has a high value at low embankment height, and it decreases with the increase of embankment height.

The settlement improvement factor decreases with the increase of the area replacement ratio inverse. From Figure 5.13, it can be observed that, at the higher area replacement ratio, the change of settlement improvement factor is significant. For the values of inverted area ratio higher than 40, the decrease of settlement improvement factor is negligible.

Similar results were obtained by Elsawy and El-Garhy (2017) where the authors conducted a numerical study on granular pile improved soft ground under raft foundation. They reported that the decrease in settlement improvement factor decreases at a smaller rate while the inverted area replacement ratio was higher than 10. The trend of the curves is in good agreement with the present study.

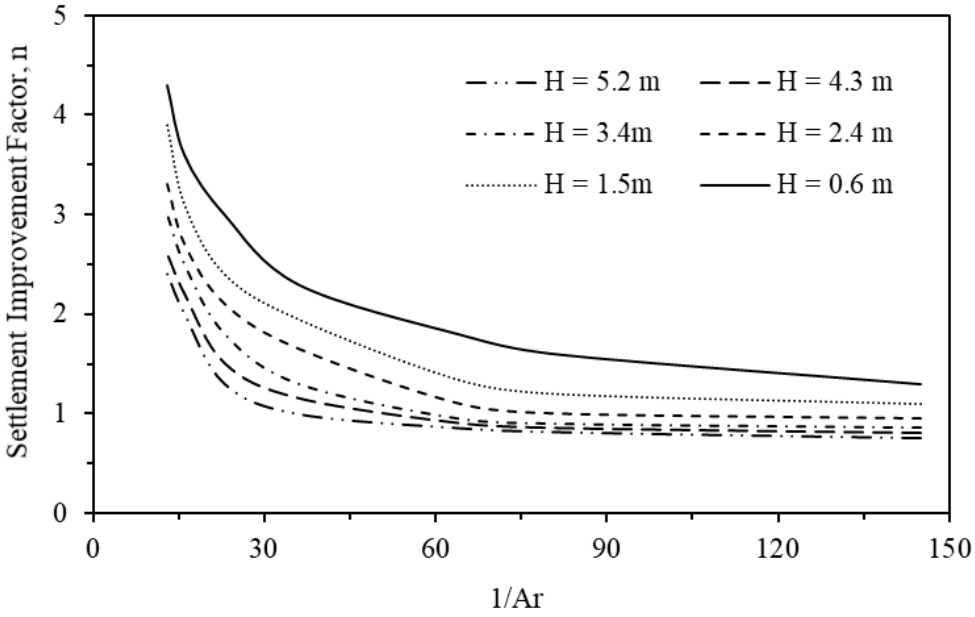

Figure 5.13 Relationship between settlement improvement ratio and the area replacement ratio inverse for different embankment heights

5.3.2.3 *Influence of geosynthetic tensile stiffness*

The effect of geosynthetic stiffness for different embankment heights is investigated by varying the stiffness from 250 kN/m to 9000 kN/m. The maximum settlements and tensile strength of geosynthetics were obtained at the end of the consolidation period. Figure 5.14 shows that the maximum settlement decreases and maximum tension in geosynthetics increase with the increase of geosynthetic stiffness. As the geosynthetic gets stiffer, the membrane action of the geosynthetic reinforcement becomes stronger which results in lower geosynthetic deflection. The increase in geosynthetic stiffness promotes more mobilization of geosynthetic strength which helps the soil arching and reduces maximum settlement. It can be noted that the values approach a limiting value at higher stiffness of geosynthetic (6000 kN/m). Therefore, after a certain stiffness value, increasing stiffness may not be effective for reducing settlement. A similar pattern was observed by Halder and Sing (2016) where they reported the effectiveness of increasing geosynthetic stiffness up to 5000 kN/m.

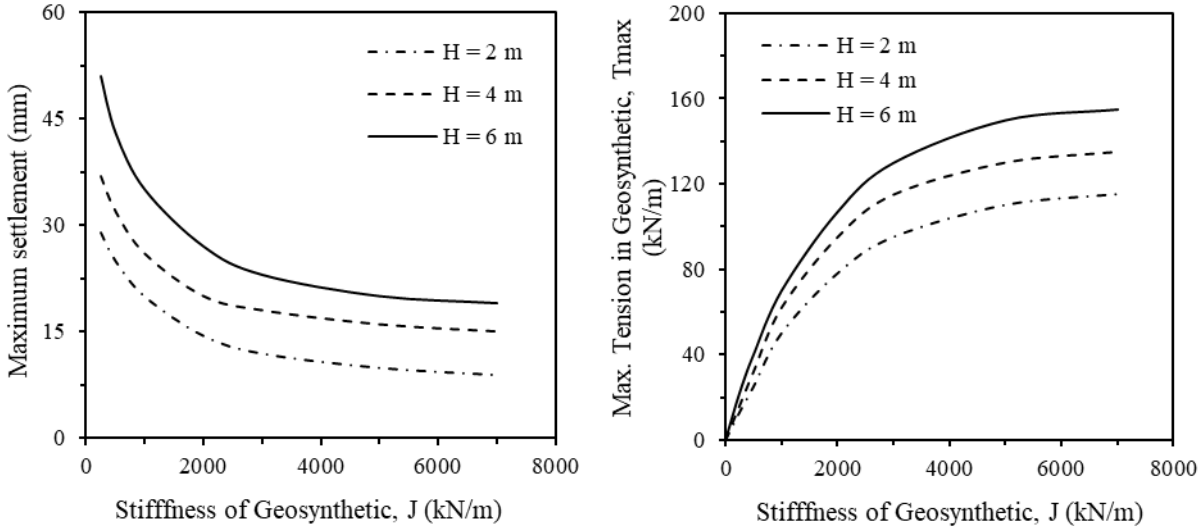

(a) (b)

Figure 5.14 Influence of geosynthetic stiffness on (a) maximum settlement and (b) maximum tension in geosynthetic for different embankment height

5.3.2.4 *Influence of load transfer platform*

In this study, three types of LTP were considered: LTP-1 (one layer of geogrid), LTP-2 (two layers of geogrid; aggregate layer in between), and LTP-3 (three layers of geogrid; aggregate layer in between). The aggregate layer was 100 mm thick, which was idealized with the Mohr-Coulomb model with friction angle as 40º, modulus of elasticity as 40.5 MPa, and Poisson's ratio as 0.25. The LTP types were selected based on the field study performed by Briancon and Simon (2012) and Abdullah and Edil (2007). The parametric study was conducted using different LTP types and embankment loads for the 4"×4" RPP reinforced section.

Figure 5.15 shows the variation of settlement with embankment height for different types of LTP. It is observed that LTP-3 provided minimum settlement due to its higher stiffness compared to the other types of LTP. The total settlement of LTP-2 and LTP-3 supported reinforced sections reduced up to 45% and 66%, respectively, compared to LTP-1. Furthermore, the percent decrease in settlement of LTP-3 is slightly higher than LTP-2. A similar trend of results was also observed for the axial force values. The maximum axial force on RPP was found for LTP-3 supported reinforced section since the load transfer is more effective because of higher stiffness. Moreover, the percent increase of axial force from LTP-1 to LTP-2 is more than the percent increase from LTP-2 to LTP-3. The obtained maximum axial forces remain below the average compressive strength capacity 16 MPa of RPP, as reported by Bowders et al. (2003).

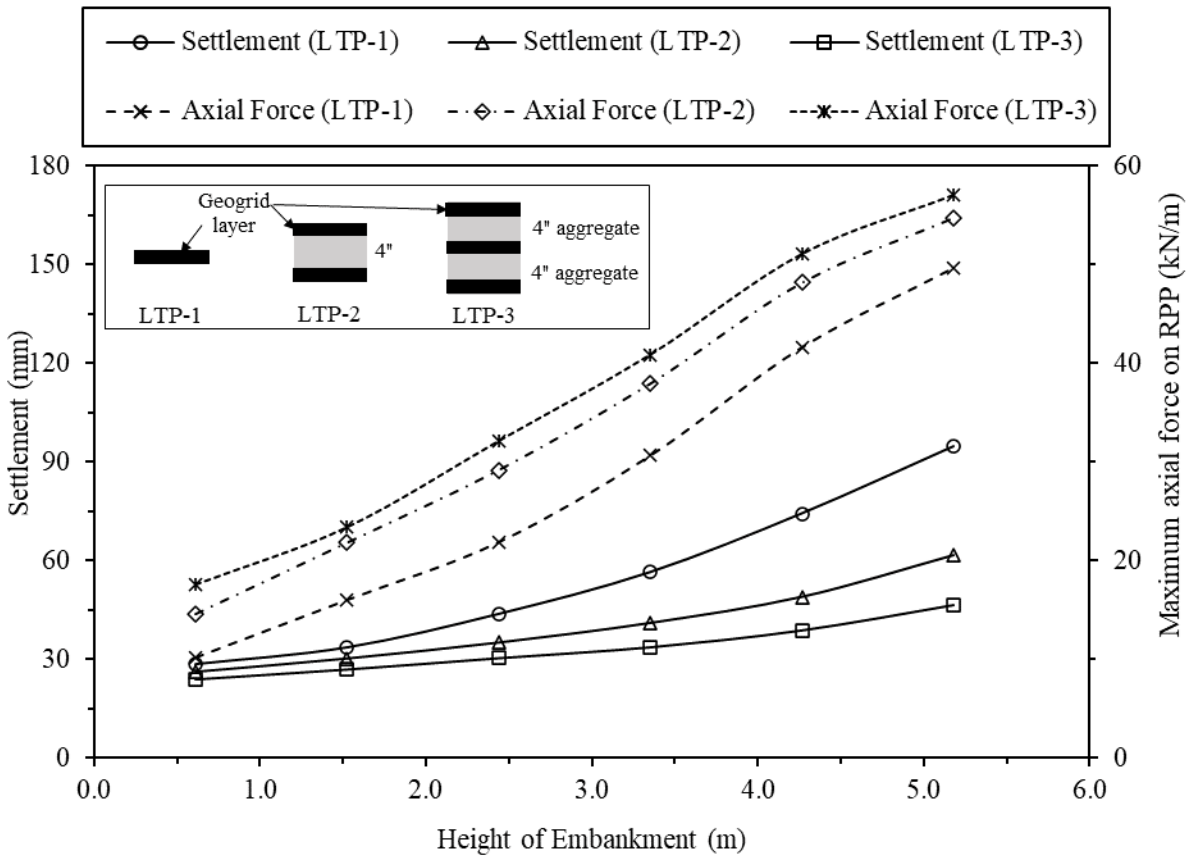

Figure 5.15 Variation of settlement and axial force for different LTP types.

5.3.2.5 *Influence of shear strength parameters of embankment fill*

The shear strength of embankment fill is one of the most important parameters which has a significant effect on the soil arching. The influence of shear strength parameters of embankment fill on the settlement behavior of RPP supported embankment is investigated both by varying the cohesion and by varying the friction angle. The cohesion was varied from 10 kPa to 150 kPa while the other parameters were assumed to be constant. The variation of maximum settlement with different embankment heights for different values of cohesion is shown in Figure 5.16 (a). The settlement increases with the increase of embankment height and with the decrease of cohesion.

The maximum reduction of the settlement was found 52% when the cohesion increased from 10 kPa to 150 kPa.

Figure 5.16 (b) shows the influence of friction angle on the settlement behavior of RPP supported embankment. The friction angle was varied from 10° to 40° while the other parameters were kept constant. The maximum settlement is found to decrease with the increase of friction angle. The maximum reduction of settlement was found 23.5% when the friction angle increased from 10° to 40°. It is apparent that the effect of increasing cohesion is more effective than that of increasing friction angle. Especially in the bridging layer of the LTP, higher cohesion not only transfers more load to piles but also reduces differential settlement (Liu et al. 2017). Therefore, the traditional granular embankment fill can be replaced with materials having excellent mechanical properties, such as cement-treated soil or lime. A similar conclusive judgment is also reported by He et al. (2006), Dias et al. (2010) and Liu et al. (2017).

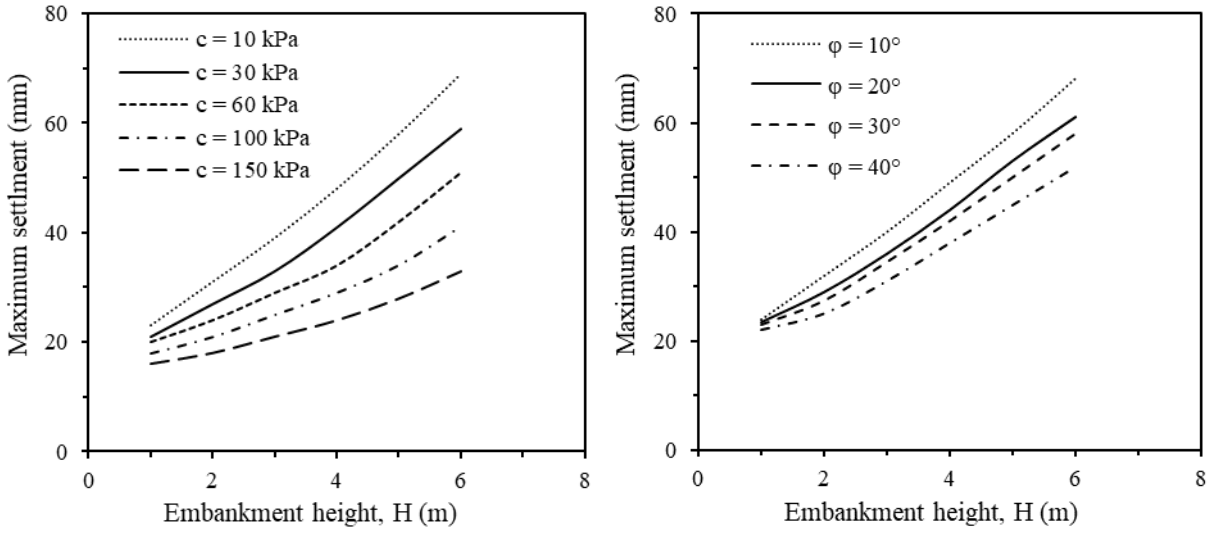

(a) (b)

Figure 5.16 Influence of shear strength parameters on the maximum settlement (a) cohesion, (b) friction angle

5.4 Conclusion

The current research showed the effectiveness of using RPPs along with LTP to improve the soft foundation soil supporting embankments. The main results and conclusion can be summarized as follows:

- The RPPs in combination with LTP are found more effective in distributing the embankment load to stiffer strata.
- The settlement reductions of the 4"×4", 6"×6", 10"×10" RPP reinforced sections for 2.4 m embankment height were about 24.2%, 43.9%, and 69.7%, respectively compared to the unreinforced section.
- The differential settlement increases with the increase of the spacing to width ratio. At 5.2 m embankment height, the increase in the differential settlement is 10% from s/b ratio 9 to 6, and 24% for s/b ratio 6 to 3.6.
- The soil arching ratio decreases with an increase in the embankment height and approaches towards a constant value at higher embankment heights.
- The stress concentration ratio decreases with the increase of normalized embankment height. The minimum SCR value was found as 4.7 for LTP-1, while the maximum value of SCR was found to be 7.8 for LTP-3.
- The settlement improvement factor decreases with the increase of the area replacement ratio inverse. For the values of inverted area ratio higher than 30, the decrease of settlement improvement factor is found negligible.
- The maximum settlement decreases and maximum tension in geosynthetics increase with the increase of geosynthetic stiffness. The maximum settlement and maximum tension in

the geosynthetics approach towards a limiting value which indicates that the efficacy of the RPP supported embankment may be insignificant with the increase of geosynthetic stiffness after 6000 kN/m.

- The performance of geogrid, along with the aggregate layer, was found better when compared to the geogrid-only LTP section. The settlement reduction was found higher in LTP-2 and LTP-3 compared to LTP-1. LTP-2 provided more percent reduction in settlement compared to LTP-1, however, the reduction in the settlement between LTP-2 and LTP-3 was less.
- The cohesion rather than the friction angle of embankment fill was found more influential in transferring the embankment load to RPPs through shear stress. Therefore, the traditional granular embankment fill can be replaced with materials having excellent mechanical properties, such as cement-treated soil or lime.

CHAPTER 6

SUMMARY AND CONCLUSIONS

6.1 Introduction

Excessive settlement and bearing capacity failure are common problems in areas where structures (e.g. embankments, roadways, highways etc.) are constructed on soft soil. The scenario of soft foundation soil is pretty common in north Texas area which could result in construction delays and in extreme cases, failure of the infrastructure. The major concerns regarding construction over soft foundation soil includes bearing capacity failure, excessive total as well as differential settlement of footing, lateral pressure and instability. The lack of good quality soil in the areas where infrastructures will be constructed, require the implementation of improvement techniques for the soft soil. The most common technique followed by TxDOT to counter such problem is remove and replacement of the weak soil with appropriate fill material. However, because of its high cost and being time consuming, a suitable remedial measure is required to address the soft foundation soil problem. Several research showed vertical stiff piles being effective, fast and does not require replacement of the existing soil. However, concrete and steel piles are costly and steel piles are also prone to corrosion; on the other hand, timber piles are prone to degradation. Therefore, a sustainable, effective yet economic solution to the inadequate bearing scenario of soft soil is required. The main objective of this study was to evaluate the performance of RPPs for improving the soft foundation soil.

6.2 Summary and Conclusions

The current study summarized an innovative, economic and sustainable solution to the inadequate bearing capacity and excessive settlement scenario of the soft foundation soil under structural loading. For this purpose, a field scale study has been conducted by replicating the scenario of structures constructed on weak foundation soil. An area inside Hunter Ferrell Landfill in Irving, Texas was chosen based on the soft soil layer for the field study. Two identical test sections were constructed, each having an effective test area of 6.1 m × 4.6 m. One section served as control section and the other section had RPP installed at the base of the structures to compare and evaluate the effectiveness of RPP. A total of 64 Nos of RPPs were installed in the reinforced section with 0.6 m c/c spacing. A load transfer platform was placed on top of the RPPs for improving the soil arching mechanism. The field performance of the test sections was monitored using horizontal inclinometers installed at the base of the test section. In addition, pressure plates, inclinometers and piezometers are also instrumented in the test sections. Embankment load was applied in three phases and the settlements and pressure variations were monitored for almost two years.

Along with the filed study, an analytical solution was developed for the RPP supported embankments with load transfer platform. In the analytical study, the load transfer mechanism accounted for soil arching and tensioned membrane effects were comprehensively studied. Finally, the effectiveness of RPP in combination with geosynthetics was investigated in a numerical environment using PLAXIS 2D. The measured field results from the test sections were used to calibrate and validate the model. The performance of the RPP supported embankment was evaluated with maximum consolidation settlement, differential settlement, and soil arching effect.

Furthermore, an extensive parametric study was performed to evaluate the effect of RPP size, and spacing, load transfer platform, stiffness of geosynthetics, and shear strength of embankment fill.

Based on the current study the main results and conclusions are summarized as follows:

6.2.1 Field test sections

a) After the application of phase-3 loading, the maximum settlement in the control section was 67 mm, whereas, in the reinforced section, the maximum settlement was 30 mm. The decrease in settlement of the reinforced section was 55% compared to the control section.
b) The excess pore water pressure in the control section was higher than in the reinforced section. For all the loadings, the dissipation of excess pore water pressure was faster in the control section compared to the reinforced section resulting in more consolidation settlement in the control section.
c) The measured consolidation settlement of the test sections was compared with analytical methods and excess pore water pressure data. The settlement profile for the control shows the best agreement with the computed values. However, the computed settlement from the analytical study of Zhuang and Wang (2017) overestimates the settlement prediction with a maximum difference of 51%.
d) The pressure on RPPs was found higher compared to the pressure on the soil, which indicates an effective load transfer mechanism to RPPs. The increase of the average pressure on the RPPs compared to adjacent soil was found to be 103%, 737%, and 874% for phase-1, phase-2, and phase-3 loading, respectively.
e) The average value of SRR and SCR was 0.45 and 8.3, respectively, which indicated a higher efficiency of load transfer compared to other field studies.

f) Three analytical methods for soil arching - EBGEO (2011), adapted Terzaghi method, and modified BS8006 method, were compared to evaluate the SRR. Among them, the adapted Terzaghi method was in good agreement with the obtained SRR values.

6.2.2 Analytical study

a) The results demonstrate that the proposed analytical solution can provide dependable and consistent results for the differential settlement, SCR, and SRR.

b) The current method was also compared with another similar field study and some standard design methods. In all the cases, the predicted results are in good agreement with other methods.

c) A parametric study is also performed to investigate the effect of different design parameters such as RPP size, spacing, tensile stiffness of geosynthetics, and friction angle of LTP on load transfer mechanism.

d) It was found that with an increase in the size of RPP installed at closer spacing, SCR will increase and SRR will decrease. Furthermore, the application of high strength geosynthetics in combination with compacted aggregate will increase the efficiency of the load transfer platform.

6.2.3 Numerical modeling

a) The settlement reductions of the 4"×4", 6"×6", 10"×10" RPP reinforced sections for 2.4 m embankment height were about 24.2%, 43.9%, and 69.7%, respectively compared to the unreinforced section.

b) The differential settlement increases with the increase of the spacing to width ratio. At 5.2 m embankment height, the increase in the differential settlement is 10% from s/b ratio 9 to 6, and 24% for s/b ratio 6 to 3.6.

c) The soil arching ratio decreases with an increase in the embankment height and approaches towards a constant value at higher embankment heights.

d) The stress concentration ratio decreases with the increase of normalized embankment height. The minimum SCR value was found as 4.7 for LTP-1, while the maximum value of SCR was found to be 7.8 for LTP-3.

e) The settlement improvement factor decreases with the increase of the area replacement ratio inverse. For the values of inverted area ratio higher than 30, the decrease of settlement improvement factor is found negligible.

f) The maximum settlement decreases and maximum tension in geosynthetics increase with the increase of geosynthetic stiffness. The maximum settlement and maximum tension in the geosynthetics approach towards a limiting value which indicates that the efficacy of the RPP supported embankment may be insignificant with the increase of geosynthetic stiffness after 6000 kN/m.

g) The LTP plays an important role in improving the effectiveness of RPP supported embankment. The LTP with aggregate layer in between reduces settlement significantly compared to the one layer of geosynthetics.

h) The cohesion rather than the friction angle of embankment fill was found more influential in transferring the embankment load to RPPs through shear stress. Therefore, the traditional granular embankment fill can be replaced with materials having excellent mechanical properties, such as cement-treated soil or lime.

Therefore, the present study can be useful for any embankment construction over soft soil, including bridge approaches and widening of any highway where the foundation soil is unsuitable for regular construction.

6.3 Recommendations for Future Studies

Based on the current study, the following recommendations are proposed for future studies:

- The study presented a field scale demonstration for embankment loading of two test sections. However, no large-scale actual ground improvement study was performed. Therefore, it is highly recommended to conduct a study on actual embankment constructed over soft soil and supported with RPP.
- The maximum embankment height of the present study was 2.4 m. Future field studies could consider taller embankment heights which better can reflect actual real life scenario. Furthermore, the failure scenario can be observed by increasing the embankment heights.
- Even though the current study presented performance monitoring of more than two years, a longer study could indicate the long-term effectiveness of the RPP reinforcement mechanism.
- Laboratory scale study with varying different influential parameters should be conducted to have a better understanding of the reinforcing mechanism of RPP.
- During the current study, RPP of only rectangular cross sections was utilized. There are other shapes (e.g. circular, H-pile etc.) that are commercially available which can be used to perform another study to determine effect of different shapes of RPP.
- The proposed analytical method can be further improved by considering more variable parameters for reliable and accurate prediction.

- In this study, two-dimensional numerical modelling was conducted using finite element software PLAXIS 2D. Sometimes, the 2D analysis may not perfectly simulate field scenario. Better and more reliable results can be obtained if a three-dimensional study is undertaken.
- Finite element studies on the effects of climatic or environmental loading, such as rainfall and water pressure, can be performed.
- Based on the performance monitoring data, extensive modelling should be performed to develop a design method for ground improvement using RPP.

REFERENCES

Abdullah, C. H., & Edil, T. B. (2007). Behaviour of geogrid-reinforced load transfer platforms for embankment on rammed aggregate piers. Geosynthetics International, 14(3), 141–153. https://doi.org/10.1680/gein.2007.14.3.141

Ahmed, A., Khan, S., Hossain, S., Sadigov, T., & Bhandari, P. (2020). Safety prediction model for reinforced highway slope using a machine learning method. *Transportation research record*, *2674*(8), 761-773.

Ahmed, A., and Islam, M. A. (2020). Effect of Using Geosynthetics in Mitigation of Freeze-Thaw through Numerical Analysis. *Proc., Geo-Congress 2020*, ASCE, Reston, VA, 463-445, https://doi.org/10.1061/9780784482810.046

Ahmed, A., Alam, M. J. B., Islam, M. A., & Hossain, M. S. (2021). Comparison of numerical modeling results from laboratory and field obtained unsaturated flow parameters. In *MATEC Web of Conferences* (Vol. 337, p. 02008). EDP Sciences. https://doi.org/10.1051/matecconf/202133702008

Ahmed, F. S. (2012). Engineering Characteristics of recycled plastic pin, lumber and bamboo for soil slope stabilization. University of Texas at Arlington.

Badakhshan, E., Noorzad, A., Bouazza, A., Zameni, S., & King, L. (2020). A 3D-DEM investigation of the mechanism of arching within geosynthetic-reinforced piled embankment. *International Journal of Solids and Structures*, 187, 58-74.

Badhon, F. F., Islam, M. S., & Islam, M. A. (2021). Contribution of Vetiver Root on the Improvement of Slope Stability. *Indian Geotechnical Journal*, 1-12. https://doi.org/10.1007/s40098-021-00557-0

Badhon, F. F., Islam, M. S., Islam, M. A., & Arif, M. Z. U. (2021). A simple approach for estimating contribution of vetiver roots in shear strength of a soil–root system. *Innovative Infrastructure Solutions*, *6*(2), 1-13. https://doi.org/10.1007/s41062-021-00469-1

Badhon F.F., Zaman, M.N.B., Bhandari, P., Islam, M.A., Hossain, M.S. (2021). Performance of Recycled Plastic Pins (RPP) for Improving the Bearing Capacity of MSE Wall Foundation. *International Foundations Congress & Equipment Expo,* Dallas, Texas, 521-259. https://doi.org/10.1061/9780784483411.049

Barends, F. (2011). Introduction to Soft Soil Geotechnique Content, Context and Application. Amsterdam, Netherlands: IOS Press.

Bergado, D.T., N. Phienwej, P. Jamasawang, G.V. Ramana, S. S. Lin, and H. M. Abuel-Naga. 2009. Settlement Characteristics of Full Scale Test Embankment on Soft Bangkok Clay Improved with Thermo-PVD and Stiffened Deep Cement Mixing Piles, In *Proc., 17th Int. Conf. Soil Mech. Geotech. Eng.*, 1969-1972. Alexandria, Egypt: ISSMGE.

Bhandari, P. (2021). *Evaluation of recycled plastic pins as shear keys in MSE wall base*, Doctoral Dissertation, Department of Civil Engineering, The University of Texas at Arlington, Texas, USA.

Bhandari, P., Zaman, M. N. B., Islam, M. A., Badhon, F. F., & Hossain, M. S. (2021). Increasing shearing resistance of MSE wall base using recycled plastic pins. In *International Foundations Congress & Equipment Expo,* Dallas, Texas, 44-54. https://doi.org/10.1061/9780784483411.005

Bowders, J. J., Loehr, J. E., Salim, H., & Chen, C. (2003). Engineering Properties of Recycled Plastic Pins for Slope Stabilization. *Transportation Research Record*, 1849(1), 39–46.

Bowles, J. E. (1988). Foundation analysis and design.

Briançon, L., and B. Simon. (2012). Performance of pile-supported embankment over soft soil: full-scale experiment. *Journal of Geotechnical and Geoenvironmental Engineering*, 138(4), 551-561. https://doi.org/10.1061/(ASCE)GT.1943-5606.0000561

BS 8006 (1995). Code of Practice for strengthened/reinforced soils and other fills. *British Standards Institution*, London.

BSI (British Standards Institution). (2010). *Code of practice for strengthened/reinforced soils and other fills*. BS8006-1, London.

Carlsson, B. (1987). "Armerad jord – berakningspriniper för – banakar pa palar". *Linköpig: Terrarema AB.*

Chen, C.-W., Salim, H., Bowders, J. J., Loehr, J. E., & Owen, J. (2007). Creep Behavior of Recycled Plastic Lumber in Slope Stabilization Applications. Journal of Materials in Civil Engineering, 19(2), 130–138. https://doi.org/10.1061/(asce)0899-1561(2007)19:2(130)

Chen, B. G., Zheng, J. J., Abusharar, S. W., & Chen, J. (2008a). Theoretical and Numerical Analysis on Geosynthetic-Reinforced and Pile Wall-Supported Embankment. In *Geosynthetics in Civil and Environmental Engineering* (pp. 709-717). Springer, Berlin, Heidelberg.

Chen, R. P., Chen, Y. M., Han, J., & Xu, Z. Z. (2008b). A theoretical solution for pile-supported embankments on soft soils under one-dimensional compression. *Canadian Geotechnical Journal*, *45*(5), 611-623.

Chen, R. P., Z. Z. Xu, Y. M. Chen, D. S. Ling, and B. Zhu. (2010). Field tests on pile-supported embankments over soft ground. *Journal of Geotechnical and Geoenvironmental Engineering*, 136(6), 777-785. https://doi.org/10.1061/(ASCE)GT.1943-5606.0000295

Chevalier, B., Villard, P., & Combe, G. (2011). Investigation of load-transfer mechanisms in geotechnical earth structures with thin fill platforms reinforced by rigid inclusions. *International Journal of Geomechanics*, 11(3), 239-250.

Collin, J. G., Watson, C. H., & Han, J. (2005). Column-Supported Embankment Solves Time Constraint For New Road Construction. GSP 131 Contemporary Issues in Foundation Engineering, (724), 1–25.

Davis, E. H., and G. P. Raymond. (1965). A non-linear theory of consolidation. *Geotechnique*, 15(2): 161-173. https://doi.org/10.1680/geot.1965.15.2.161

Das, B. M. (2015). *Principles of Foundation Engineering*. Cengage Learning.

Deb, K. (2010). A mathematical model to study the soil arching effect in stone column-supported embankment resting on soft foundation soil. *Applied Mathematical Modelling*, *34*(12), 3871-3883.

Demir, A., M. Laman, A. Yildiz, and M. Ornek. (2013). Large scale field tests on geogrid-reinforced granular fill underlain by clay soil. *Geotextile and Geomembrane*, 38, 1-15. https://doi.org/10.1016/j.geotexmem.2012.05.007

Dobie, M., Lees, A., & Khanardnid, J. (2018). Case study : performance of a geogrid stabilised working platform constructed over extremely soft dredged silt. 11th International Conference on Geosyntherics, (September). Seoul, Korea.

EBGEO. (2011). Recommendations for design and analysis of earth structures using geosynthetic reinforcements—EBGEO. German Geotechnical Society, Berlin.

Elsawy, M. B., and B. El-Garhy. (2017). Performance of Granular Piles-Improved Soft Ground Under Raft Foundation: A Numerical Study. *Int. J. Geosyn. Ground Eng.*, 3(4), 36. https://doi.org/10.1007/s40891-017-0113-7

Filz, G. M., & Smith, M. E. (2007). Net vertical loads on geosynthetic reinforcement in column-supported embankments. In *Soil Improvement*, 1-10.

Fluet, J. E., Christopher, B. R., and Slaters, A. R. (1986). Geosynthetic stressstrain response under embankment loading conditions. Proc. *3rd Int. Conf. on Geotextiles, Austrian Association of Engineers and Architects*, Vienna, Austria, 1, 175-180.

Ghosh, B., Fatahi, B., & Khabbaz, H. (2017). Analytical solution to analyze LTP on column-improved soft soil considering soil nonlinearity. *International Journal of Geomechanics*, *17*(3), 04016082.

Girout, R., Blanc, M., Dias, D., & Thorel, L. (2014). Numerical analysis of a geosynthetic-reinforced piled load transfer platform–validation on centrifuge test. *Geotextiles and Geomembranes*, 42(5), 525-539.

Guido, V. A., Kneuppel, J. D., & Sweeney, M. A. (1987). Plate loading tests on geogrid-reinforced earth slabs. Geosynthetic ’87 Conference, 216–225. New Orleans, USA.

Halder, P., & Singh, B. (2016) Effect of Geosynthetic Reinforcement on Pile-Supported Embankment Constructed on Soft Soils. *Journal of Civil Engineering and Environmental Technology*, 3(7), 596-601.

Han, G. X., Gong, Q. M., and Zhou, S. H. (2015). “Soil arching in a piled embankment under dynamic load.” *Inter. J. Geomech.*, *15*(6), 04014094.

Han, J., & Gabr, M. (2002). Numerical Analysis of Geosynthetic-Reinforced and Pile-Supported Earth Platforms over Soft Soil. *Journal of Geotechnical and Geoenvironmental Engineering*, 128(1), 44–53. https://doi.org/10.1061/(ASCE)1090-0241(2002)128:1(44)

He, L. D., Chen, Z. F., & Xu, Z. Z. (2006). Experimental study on load-bearing characteristics for single PTC pile with cap and composite foundation with PTC (prestressed thin-wall concrete) piles. *Rock and Soil Mechanics-Wuhan-*, *27*(3), 435.

Hewlett, W. J., & Randolph, M. F. (1988). Analysis of piled embankments. Ground Engineering, 21(3), 12–18.

Hong, W.P., J. Lee. and S. Hong. (2014). Full-scale tests on embankments founded on piled beams.” *Journal of Geotechnical and Geoenvironmental Engineering* 140(12): 04014067. https://doi.org/10.1061/(ASCE)GT.1943-5606.0001145

Horgan, G. J., and Sarsby, R. W. (2002). “The arching effect of soils over voids and piles incorporating geosynthetic reinforcement”. *Proc. 7th ICG*, Delmas, Gourc & Girard (eds), Lisse: Swets & Zetilinger, pp 373-378.

Hossain, S., Khan, S., & Kibria, G. (2017). *Sustainable Slope Stabilisation using Recycled Plastic Pins*, CRC Press.

Imtiaz T, A. Ahmed, S. Hossain and M. Faysal. (2020). Microstructure Analysis and Strength Characterization of Recycled Base and Sub-Base Materials Using Scanning Electron Microscope. *Infrastructures*., 5(9), 70.

Islam MA, Hossain S, Badhon FF, Bhandari P. (2021a) Performance Evaluation of Recycled-Plastic-Pin-Supported Embankment over Soft Soil. Journal of Geotechnical and Geoenvironmental Engineering; 147(6), 04021032. https://doi.org/10.1061/(ASCE)GT.1943-5606.0002528

Islam MA, Zaman, MNB, Badhon FF, Bhandari P, Hossain S. (2021b) Numerical Modeling of Recycled Plastic Pin Reinforced Embankment over Soft Soils. *International Foundations Congress & Equipment Expo*, Dallas, Texas, 541-550. https://doi.org/10.1061/9780784483411.051

Islam, M.A., Gupta, A., Gupta, N., & Islam, T. (2021c) Laboratory Investigation of Soil Plugs in Open Ended Model Piles Driven into Sand. In *IFCEE 2021* (pp. 108-118). **https://doi.org/10.1061/9780784483404.010**

Islam, M. A., Islam, M. S., Chowdhury, M. E., & Badhon, F. F. (2021). Influence of vetiver grass (*Chrysopogon zizanioides*) on infiltration and erosion control of hill slopes under simulated extreme rainfall condition in Bangladesh. *Arabian Journal of Geosciences*, *14*(2), 1-14. https://doi.org/10.1007/s12517-020-06338-y

Islam, M. A., Islam, M. S., & Elahi, T. E. (2020, February). Effectiveness of vetiver grass on stabilizing hill slopes: a numerical approach. In *Geo-Congress 2020: Engineering, Monitoring, and Management of Geotechnical Infrastructure* (pp. 106-115). Reston, VA: American Society of Civil Engineers. **https://doi.org/10.1061/9780784482797.011**

Jenck, O., Dias, D., and Kastner, R. (2009). "Three-dimensional numerical modeling of a piled embankment." *Inter. J. Geomech.*, *9*(3), 102-112.

Khan, M. S., S. Hossain, and G. Kibria. (2016). Slope stabilization using recycled plastic pins. *Journal of Performance of Constructed Facilities*, 30(3): 04015054. https://doi.org/10.1061/(ASCE)CF.1943-5509.0000809

Kibria, G., Hossain, M. S., & Khan, M. S. (2014). Influence of soil reinforcement on horizontal displacement of MSE wall. *International Journal of Geomechanics*, *14*(1), 130-141.

King, D. J., Bouazza, A., Gniel, J. R., Rowe, R. K., & Bui, H. H. (2017). Serviceability design for geosynthetic reinforced column supported embankments. Geotextiles and Geomembranes, 45(4), 261–279. https://doi.org/10.1016/j.geotexmem.2017.02.006

Lampo, R., & Nosker, T. J. (1997). Development and testing of plastic lumber materials for construction applications.

Liu, H.L., C.W. Ng, and K., Fei. (2007). Performance of a geogrid-reinforced and pile-supported highway embankment over soft clay: case study. *Journal of Geotechnical and Geoenvironmental Engineering*, 133(12), 1483-1493.

Liu, S. Y., Y. J. Du, Y. L. Yi, & A. J. Puppala. (2012.) Field investigations on performance of T-shaped deep mixed soil cement column–supported embankments over soft ground. *Journal of Geotechnical and Geoenvironmental Engineering*, 138(6), 718-727. https://doi.org/10.1061/(ASCE)GT.1943-5606.0000625

Liu, W., Qu, S., Zhang, H., & Nie, Z. (2017). An integrated method for analyzing load transfer in geosynthetic-reinforced and pile-supported embankment. *KSCE Journal of Civil Engineering*, 21(3), 687–702. https://doi.org/10.1007/s12205-016-0605-3

Loehr, J. E., Bowders, J. J., Owen, J., Sommers, L., and Liew, W. (2000). Stabilization of slopes using recycled plastic pins. *J. Trans. Res. B.,* 1714, 1-8. National Academy Press. Loehr, J. E., & Bowders, J. J. (2007). Slope Stabilization Using Recycled Plastic Pins – Phase III. In RI98-007D.

Low, B. K., S. K. Tang, and V. Choa. (1994). Arching in piled embankments. *J. Geotec. Eng.*, 120(11), 1917-1938. https://doi.org/10.1061/(ASCE)0733-9410(1994)120:11(1917)

Malcolm, G. M. (1995). Recycled Plastic Lumber and shapes design and specifications. Structural Congress, 2–5.

McNulty, J. W. (1965). *An experimental study of arching in sand* (No. 1). University of Illinois at Urbana-Champaign.

Michalowski, R. L., Asce, F., Wojtasik, A., Duda, A., Florkiewicz, A., Park, D., & Asce, S. M. (2018). Failure and Remedy of Column-Supported Embankment : Case Study. Journal of Geotechnical and Geoenvironmental Engineering, 144(3), 1–14. https://doi.org/10.1061/(ASCE)GT.1943-5606.0001839.

Pham, T. A. (2020a). Analysis of geosynthetic-reinforced pile-supported embankment with soil-structure interaction models. *Computers and Geotechnics, 121*, 103438.

Pham, T. A. (2020b). Load-deformation of piled embankments considering geosynthetic membrane effect and interface friction. *Geosynthetics International*, *27*(3), 275-300.

Oh, Y. I., & Shin, E. C. (2007). Reinforcement and arching effect of geogrid-reinforced and pile-supported embankment on marine soft ground. Marine Georesources and Geotechnology, 25(2), 97–118. https://doi.org/10.1080/10641190701359591

Okyay, U. S., & Dias, D. (2010). Use of lime and cement treated soils as pile supported load transfer platform. *Engineering Geology*, *114*(1-2), 34-44.

Ong, R., & Dobie, M. J. D. (2013). Working platform for heavy tracked plant constructed using geogrid over soft ground. 978–981. https://doi.org/10.3850/978-981-07-4948-4

Ozdemir, M. A. (2016). Improvement in Bearing Capacity of a Soft Soil by Addition of Fly Ash. Procedia Engineering, 143, 498–505.

Plaxis, B. V. (2020). PLAXIS 2D reference manual. *The Netherlands*.

Rowe, R. K., and Liu, K. W. (2015). "Three-dimensional finite element modelling of a full-scale geosynthetic-reinforced, pile-supported embankment." *Can. Geotech. J.*, *52*(12), 2041-2054, 10.1139/cgj-2014-0506.

Russell, D., and N. Pierpoint. (1997). An assessment of design methods for piled embankments. *Ground Engineering*, 30(10).

Russell, D., Naughton, P.J. and G. Kempton, G. (2003) A new design procedure for piled embankments. Proceedings of the 56th Canadian Geotechnical

Sherwood, P. (1993). Soil Stabilization with Cement and Lime.

Skempton, A. W. (1953). The post-glacial clays of Thames estuary at Tilbury and Shell-haven. 3rd ICSMFE, 302–308.

Terzaghi, K. (1925). *Erdbaumechanik auf bodenphysikalischer Grundlage*. Deuticke, Vienna.

Terzaghi, K. (1936). Stress distribution in dry and in saturated sand above a yielding trapdoor. *Proc. 1st International Conference on Soil Mechanics and Foundation Engineering*, Cambridge, Mass., Vol. 1, pp 307-311.

Terzaghi, K. (1943). Theoratical Soil Mechanics. New York: Wiley.

Ujankar, M. G., and Krishna, P. H. (2020). *Use of Waste Polypropylene Plastic in Geotechnical Applications*. In *Advances in Geotechnical and Transportation Engineering 2020*. Springer, Singapore.

Van Eekelen, S. J., Bezuijen, A., & Oung, O. (2003). Arching in piled embankments; experiments and design calculations. In BGA International Conference on Foundations: Innovations, observations, design and practice: Proceedings of the international conference organised by British Geotechnical Association and held in Dundee, Scotland on 2–5th September 2003 (pp. 885-894). Thomas Telford Publishing.

Van Impe, W. F. (1989). Soil improvement techniques and their evolution. Balkema, Rotterdam, the Netherlands, 110-111.

Watts, K., & Jenner, C. G. (2008). Large-scale laboratory assessment of geogrids to reinforce granular working platforms. EuroGeo4: 4th European Geosynthetics Conference. Scotland, UK.

Xu, C., Song, S., and Han, J. (2016). Scaled model tests on influence factors of full geosynthetic-reinforced pile-supported embankments. *Geosynthetics International*, *23*(2), 140-153.

Ye, G. B., Wang, M., Zhang, Z., Han, J., & Xu, C. (2020). Geosynthetic-reinforced pile-supported embankments with caps in a triangular pattern over soft clay. *Geotextiles and Geomembranes*, 48(1), 52-61.

Yun-Min, C., C. Wei-Ping, and C. Ren-Peng. (2008). An experimental investigation of soil arching within basal reinforced and unreinforced piled embankments." *Geotextile and Geomembrane*, 26(2), 164-174.

Zaman, N. B. (2019). *Sustainable Ground Improvement Method Using Recycled Plastic Pins*. Doctoral Dissertation, The University of Texas at Arlington, Texas, USA.

Zhuang, Y., & Wang, K. (2017). Analytical solution for reinforced piled embankments on elastoplastic consolidated soil. *International Journal of Geomechanics*, *17*(9), 06017010.

Zhao, M., Liu, C., El-Korchi, T., Song, H., and Tao, M. (2019). "Performance of Geogrid-Reinforced and PTC Pile-Supported Embankment in a Highway Widening Project over Soft Soils." *J. Geotech. Geoenviron. Eng.*, 145(11): 06019014.

Zhou, C., Yin, J. H., & Ming, J. P. (2002). Bearing capacity and settlement of weak fly ash ground improved using lime fly ash or stone columns. Canadian Geotechnical Journal, 39(3), 585–596.

APPENDIX A

Bore log details

LOGO UTA

BORING NUMBER BH-1

CLIENT Texas Department of Transportation (TxDOT)
PROJECT NAME Utilization of RPP for improving B/C of soft soil
PROJECT NUMBER
PROJECT LOCATION The City of Irving Landfill
DATE STARTED 4/22/19 **COMPLETED** 4/22/19
GROUND ELEVATION **HOLE SIZE** 6 inches
DRILLING CONTRACTOR West DRILLING
GROUND WATER LEVELS:
DRILLING METHOD HSA
AT TIME OF DRILLING ---
LOGGED BY Md Aziful Islam **CHECKED BY** Faria Fahim Badhon
AT END OF DRILLING --- No GWT found
NOTES Location: Outside the levee
AFTER DRILLING ---

DEPTH (ft)	GRAPHIC LOG	MATERIAL DESCRIPTION	SAMPLE TYPE NUMBER	RECOVERY % (RQD)	BLOW COUNTS (N VALUE)	POCKET PEN. (tsf)	DRY UNIT WT. (pcf)	MOISTURE CONTENT (%)	ATTERBERG LIMITS			FINES CONTENT (%)
									LIQUID LIMIT	PLASTIC LIMIT	PLASTICITY INDEX	
0		**SANDY LEAN CLAY (CL);**Color: Gray	SPT		3-4 (7)			16				71
		SANDY LEAN CLAY (CL); Color: Brownish Gray										
5		**FAT CLAY (CH);**Color: Dark Gray	SPT		4-6 (10)		112	12	38	15	23	53
10			ST									
			SPT		5-7 (12)			17	51	11	40	97
15		**SANDY SILT (ML);**Color: Gray	ST				101	22	35	29	6	62
		FAT CLAY (CH);Color: Brown										
20			SPT		5-8 (13)			16	55	23	32	96

Bottom of borehole at 20.0 feet.

GEOTECH BH COLUMNS - GINT STD US LAB.GDT - 8/27/19 16:04 - C:\USERS\TX1101\GOOGLE DRIVE\PHD THESIS\BORE LOG TEST RESULTS\SOFT BORING GINT\SOFT SOIL PROJECT BORING.GPJ

LOGO UTA

BORING NUMBER BH-2

CLIENT Texas Department of Transportation (TxDOT) **PROJECT NAME** Utilization of RPP for improving B/C of soft soil

PROJECT NUMBER **PROJECT LOCATION** The City of Irving Landfill

DATE STARTED 4/22/19 **COMPLETED** 4/22/19 **GROUND ELEVATION** **HOLE SIZE** 6 inches

DRILLING CONTRACTOR West DRILLING **GROUND WATER LEVELS:**

DRILLING METHOD HSA **AT TIME OF DRILLING** ---

LOGGED BY Md Azijul Islam **CHECKED BY** Faria Fahim Badhon **AT END OF DRILLING** ---

NOTES Location: Inside the levee (near ponding) **AFTER DRILLING** 3.00 ft

DEPTH (ft)	GRAPHIC LOG	MATERIAL DESCRIPTION	SAMPLE TYPE NUMBER	RECOVERY % (RQD)	BLOW COUNTS (N VALUE)	POCKET PEN. (tsf)	DRY UNIT WT. (pcf)	MOISTURE CONTENT (%)	ATTERBERG LIMITS			FINES CONTENT (%)
									LIQUID LIMIT	PLASTIC LIMIT	PLASTICITY INDEX	
0		**Lean Clay (CL);** Loose fill material, very soft; Color: Grey										
			SPT		1-1 (2)			14	22	12	10	92
		Sandy Lean Clay (CL); Color: Dark Brown										
5		**Lean Clay (CL);** Color: Brown	ST				105	25	32	15	17	64
			SPT		2-2 (4)				42	17	25	89
		Eagle Ford Shale; Color: Dark Grey										
10			ST				108	20	60	30	30	96
			SPT		18-23 (41)							
15								27	65	32	33	91
20												

Bottom of borehole at 20.0 feet.

GEOTECH BH COLUMNS - GINT STD US LAB.GDT - 8/27/19 16:04 - C:\USERS\TXI1101\GOOGLE DRIVE\PHD THESIS\BORE LOG TEST RESULTS\SOFT BORING GINT\SOFT SOIL PROJECT BORING.GPJ

LOGO UTA

BORING NUMBER BH-3

CLIENT Texas Department of Transportation (TxDOT)
PROJECT NAME Utilization of RPP for improving B/C of soft soil
PROJECT NUMBER
PROJECT LOCATION The City of Irving Landfill
DATE STARTED 4/22/19 **COMPLETED** 4/22/19
GROUND ELEVATION **HOLE SIZE** 6 inches
DRILLING CONTRACTOR West DRILLING
GROUND WATER LEVELS:
DRILLING METHOD HSA
AT TIME OF DRILLING ---
LOGGED BY Md Azijul Islam **CHECKED BY** Faria Fahim Badhon
AT END OF DRILLING ---
NOTES Location: Inside the levee
AFTER DRILLING 3.00 ft

DEPTH (ft)	GRAPHIC LOG	MATERIAL DESCRIPTION	SAMPLE TYPE NUMBER	RECOVERY % (RQD)	BLOW COUNTS (N VALUE)	POCKET PEN. (tsf)	DRY UNIT WT. (pcf)	MOISTURE CONTENT (%)	ATTERBERG LIMITS			FINES CONTENT (%)
									LIQUID LIMIT	PLASTIC LIMIT	PLASTICITY INDEX	
0		**Lean Clay (CL);** Loose fill material, very soft; Color: Grey										
			SPT		1-0 (1)			15	30	14	16	70
		Sandy Lean Clay (CL); Color: Brownish Grey										
			ST				102	24	35	12	23	65
5			SPT		2-3 (5)							
		Eagle Ford Shale; Color: Dark Grey										
			ST				110	21	65	30	35	97
10			SPT		3-4 (7)							
								25	66	28	38	96
15			SPT		7-14 (21)							
20												

Bottom of borehole at 20.0 feet.

GEOTECH BH COLUMNS - GINT STD US LAB.GDT - 8/27/19 16:04 - C:\USERS\TX11011\GOOGLE DRIVE\PHD THESIS\BORE LOG TEST RESULTS\SOFT BORING GINTSOFT SOIL PROJECT BORING.GPJ

APPENDIX B

Site Investigation and Installation

(a)

(b)

(c)

(d)

(e)

(f)

Figure B.1 Drilling for soft location (a) Geoprobe 6610 DT machine (b) Drilling rig set up (c) Collection of remolded sample (d) Bore hole after drilling with ground water table (e) Extruding undisturbed sample (f) Collection of undisturbed Shelby tube samples

(a)

(b)

(c)

(d)

(e)

(f)

Figure B.2 Installation of inclinometer casing (a) digging a uniform trench of 6 inch deep and 6 inch wide; (b) joining inclinometer casings to 80 ft long; (c) placement of inclinometer casing in the trench (d) fixing one end with concreting; (e) backfilling the trench with sand (f) backfilling the rest of the trench with in-situ soil and levelling the trench with EGL

(a) (b)

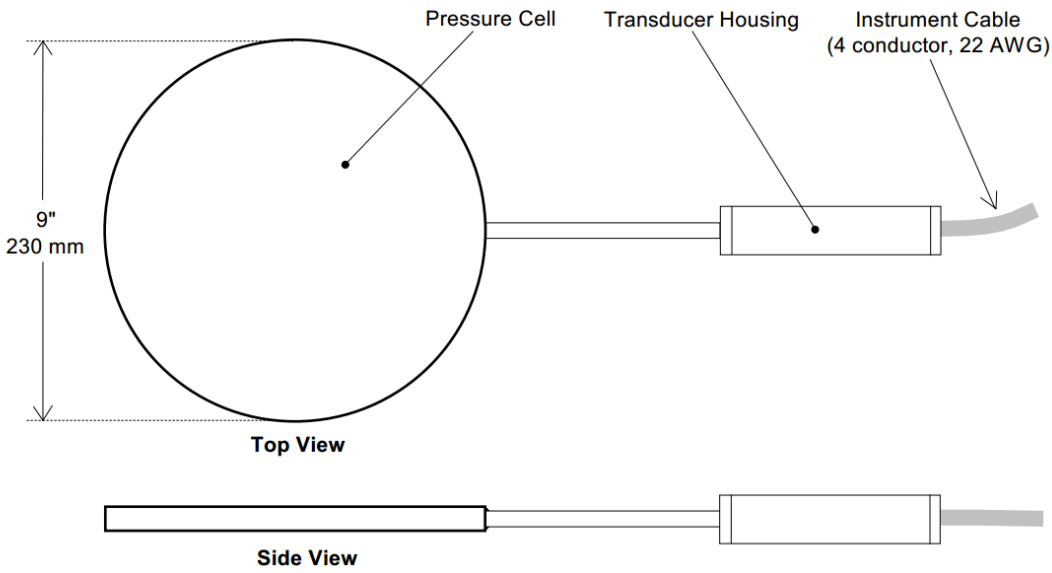

(c)

Figure B.3 (a) placement of pressure plate above RPP (b) covering the top and bottom part of the pressure plate with sand for damage protection; (c) schematic diagram of Model 4800 circular earth pressure cell (GEOKON PTE. LTD)

(a) (b) (c)

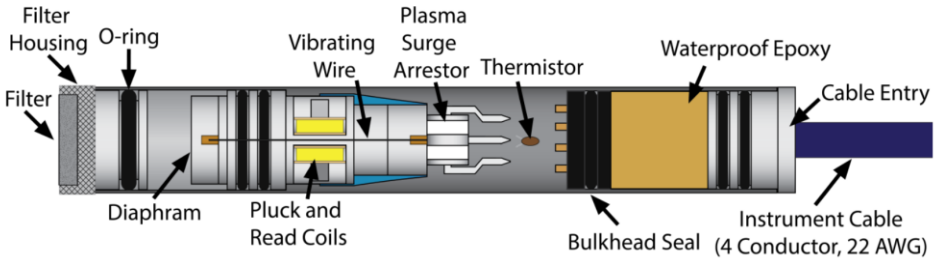

(d)

Figure B.4 Installation of piezometer (a) placing the inclinometer under small height of water for saturation and calibration of the piezometer (b) inserting piezometer through the borehole; (c) measuring depth of the piezometer under the ground surface; (d) Details of vibrating wire piezometer from GEOKON PTE. LTD.

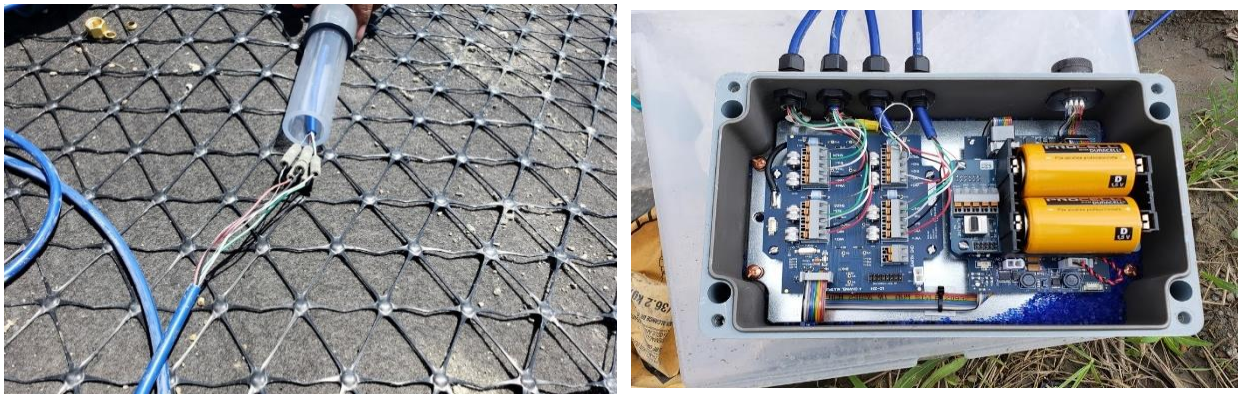

(a) (b)

Figure B.5 Instrumentation of the sensors (a) splicing for connecting extension cable with the sensors (b) Data logger setup

(a)

(b)

(c)

(d)

(e)

(f)

Figure B.6 Installation of load transfer platform (a) placement of first layer of geogrid (b) placement of geocomposite (c) Filling the top of the section with 4 inch thick recycled concrete aggregate (RCA) (d) levelling the RCA uniformly (e) placement of second layer of geogrid (f) completion of the load transfer platform

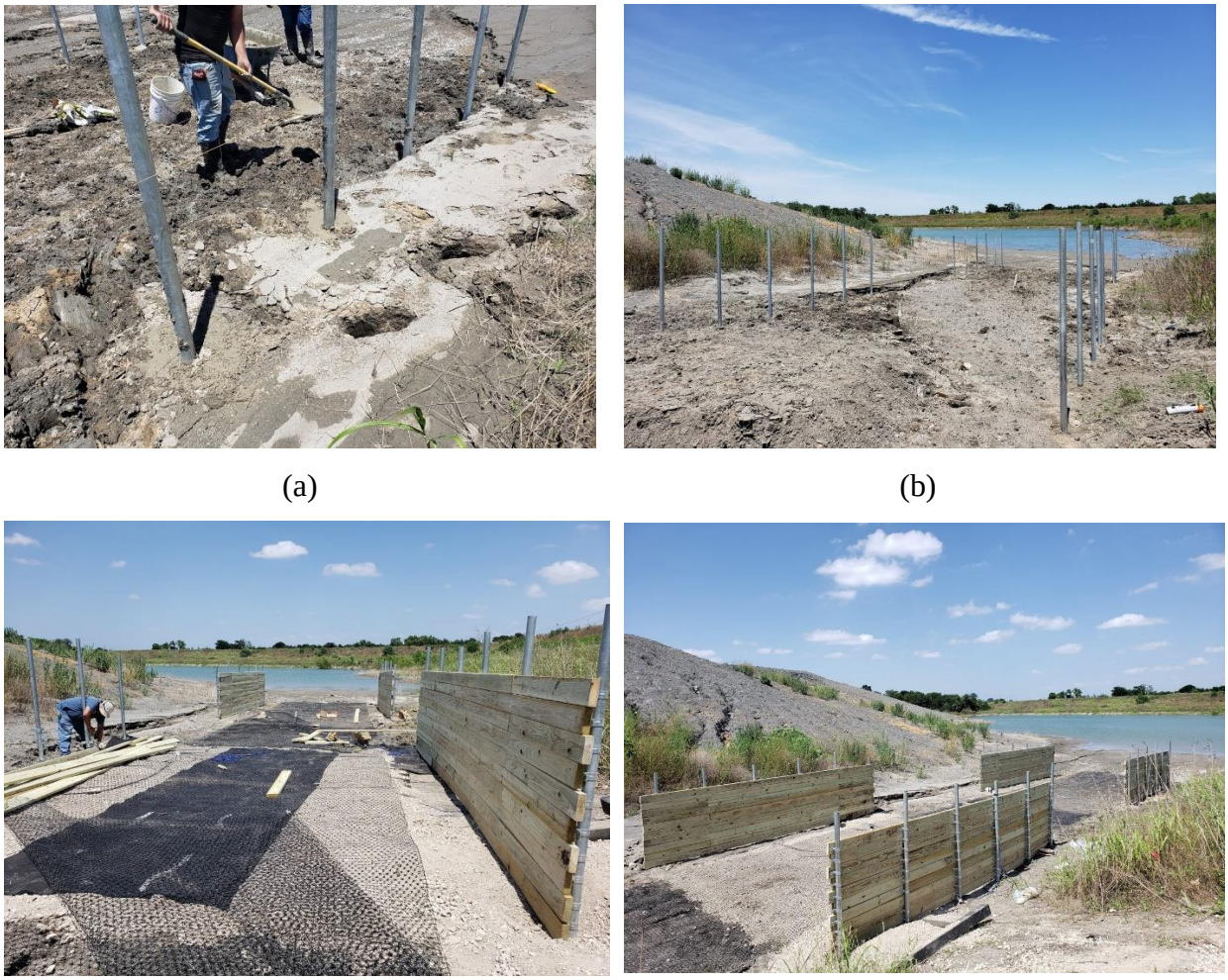

(a) (b)

(c) (d)

Figure B.7 Construction of fence on the two side of the sections (a) installation of steel post with base of about 3 ft deep concrete; (b) erection of all posts and connecting wooden planks with the posts; (c) construction of side walls with pressure treated planks; (d) after construction of the fence

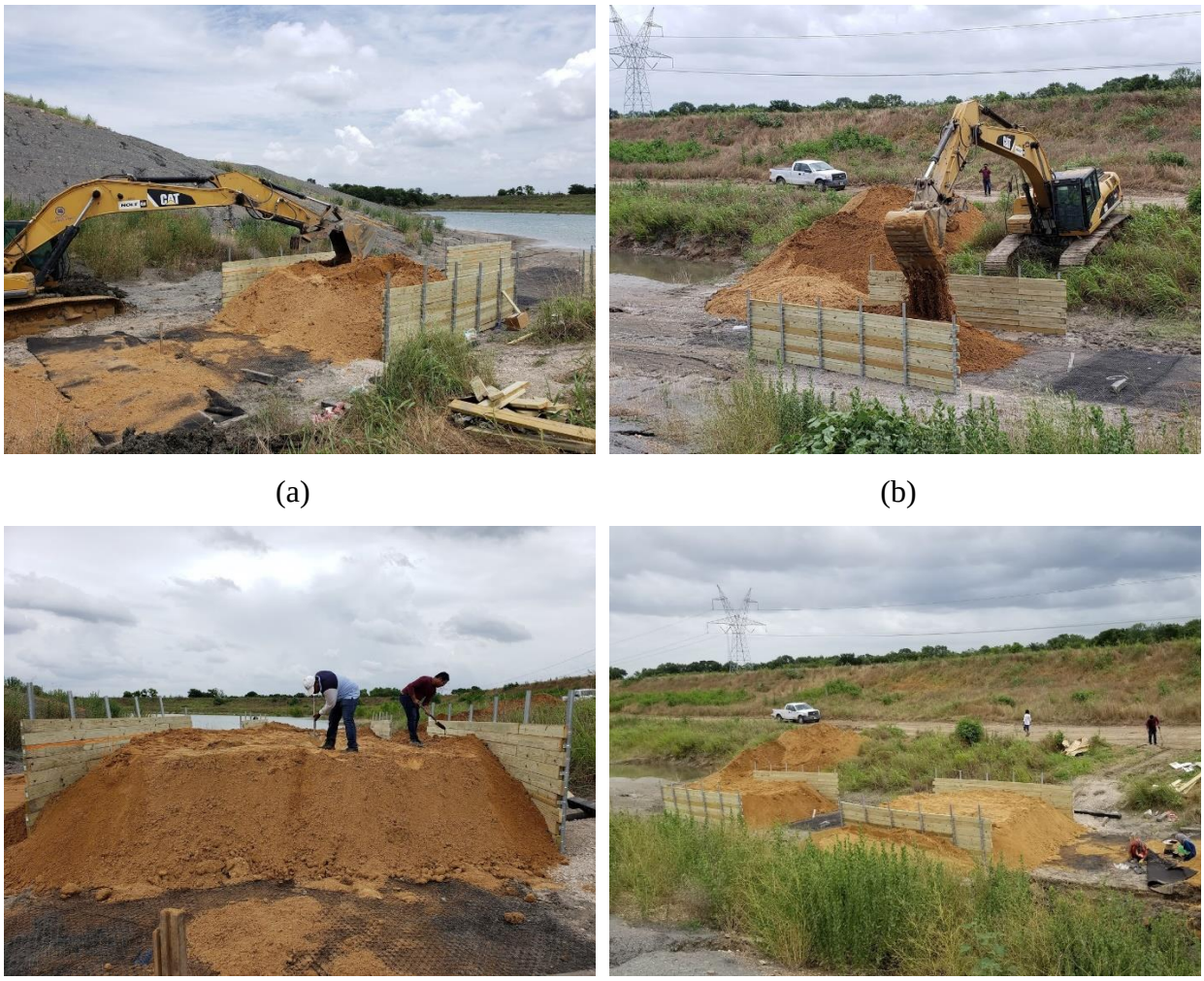

(a) (b)

(c) (d)

Figure B. 8 Application of surcharge load (a) backfilling of sand in RPP reinforced section (b) backfilling of sand in control section (c) leveling and making slope by hand (d) completion of the surcharge load

BIOGRAPHY

Mr. Md Azijul Islam was born in Dinajpur, Bangladesh. He completed his B.Sc. and M.Sc. in Civil Engineering from Bangladesh University of Engineering and Technology (BUET) in 2015 and 2018, respectively. He worked as a lecturer and later as an assistant professor at the Department of Civil Engineering, BUET from 2015 to 2018. During his undergraduate study, he ranked 1st among 195 students at BUET. Mr. Islam joined the University of Texas at Arlington in Fall 2018 to pursue Ph.D. in Civil and Geotechnical Engineering under the supervision of Dr. MD Sahadat Hossain. Mr. Azijul has more than 5 (five) years of professional, teaching and research experience in geotechnical and geo-environmental engineering. His research interests include nut are not limited to ground improvement, foundation engineering, pavement materials, slope stability analysis and landslide prevention, and disaster management. Mr. Islam has published in reputed international journals and conference proceedings. He has been serving as a reviewer in several international journals. He achieved "*Outstanding Civil Engineering Ph.D. Student Award*" in three consecutive years of 2018-19, 2019-20, and 2020-21 at UTA. He was also awarded "*Summer 2021 Dissertation Fellowship*" from UTA in recognition of his excellent performance through the doctoral program. Mr. Islam was the speaker and organizer of the ISWA-SWIS Winter School 2020. He is a student member of American Society of Civil Engineers (ASCE) and Deep Foundation Institute (DFI) and is an engineer-in-training (E.I.T.) in the State of Texas. He aims to be a part of the research and development area in the geotechnical engineering sector. Apart from academic and research works, Mr. Islam loves to play FIFA games.